Improving the management of lung cancer using mass spectrometry and spectroscopy techniques

Thesis submitted for the degree of

Doctor of Philosophy

Abigail Victoria Rutter

June 2016

Faculty of Medicine and Health Sciences

Keele University

Contents

Abstract

Lung cancer is a worldwide health problem associated with poor prognosis. The survival at 5 years remains between 5% and 15% in spite of the development of new drugs. One of the main reasons for this is the disease being diagnosed in late stages when curative treatments might not be available. Therefore, some of the most important factors within improving prognosis are both refining diagnostic techniques for early detection, and better assessing tumour response to treatment. Here lies a need for novel diagnostic tools for lung cancer. Spectroscopic and spectrometric analysis of the molecular underpinnings of the disease may provide biochemical signatures for use in diagnostics. Selected Ion Flow Tube – Mass Spectrometry (SIFT-MS) and Fourier Transform Infrared (FTIR) Spectroscopy may provide the gold standard of diagnostic assessment that is needed. Given both techniques previous contributions and technological advancements, their clinical requirements are being increasingly met. This is leading towards the opportunity for the study of lung cancer to benefit from the rapid, non-destructive and sensitive qualities they have to offer. In this thesis, both techniques have been used with the aim of improving the diagnosis and management of lung cancer.

List of Figures

List of Tables

List of Abbreviations

2D:	2 Dimensional
3D:	3 Dimensional
ADH:	Alcohol dehydrogenase
ALDH:	Acetaldehyde dehydrogenase
BCC:	Basal cell carcinoma
CP:	Control patient
CT:	Computerised tomography
DAPI:	4',6-diamidino-2-phenylindole
DMEM:	Dulbecco's modified Eagle medium
ECM:	Extracellular matrix
EGF:	Epidermal growth factor
EGFR:	Epidermal growth factor receptor
EMSC:	Extended multiplicative signal correction
FBS:	Foetal bovine serum
FNA:	Fine needle aspirations
FTIR:	Fourier transform infrared
GC-MS:	Gas chromatography – mass spectrometry
H&E:	Haematoxylin and eosin
HBEcC:	Bronchial epithelial sample
hFB:	Human fibroblasts
HP:	Healthy control participant
IL-8:	Interleukin-8
KRAS:	Kirsten rat sarcoma viral oncogene
LC:	Lung cancer patient
LD:	Lethal doses
MIM:	Multi-ion monitoring mode
MRI:	Magnetic resonance imagining
NAD^+:	Nicotinamide adenine dinucleotide

NSCLC:	Non small cell lung cancer
OCT:	Optimum cutting temperature
PC:	Pyruvate carboxylation
PCs:	Principle components
PCA:	Principle component analysis
PAP:	Papanicolaou
PBS:	Phosphate buffered saline
PET:	Positron emission tomography
PFA:	Paraformaldehyde
PI:	Propidium iodide
PPBV:	Part-per-billion-by-volume
PPM:	Parts-per-million
RH:	Relative humidity
SCC:	Squamous cell carcinoma
SD:	Standard deviation
SHMT:	Serine hydroxymethyltransferase
SIFT-MS:	Selected ion flow tube – mass spectrometry
SNV:	Standard normal variate
SPME:	Solid-phase microextraction
VOCs:	Volatile organic compounds
TA:	Threonine aldolase

Acknowledgements

I would like to thank my supervisor Dr Josep Sulé-Suso, for his tireless help and support throughout my PhD. Dr Sulé-Suso has not only contributed scientific and medical guidance towards my work but has also helped enormously in the development of my career as a researcher. Having given me many opportunities to travel during my studies, he has also enabled me to develop as a person. As my PhD has come to an end, I would like to thank him for being a wonderful supervisor and also a wonderful friend.

I would also like to thank my co-supervisor Dr Ying Yang who has supported me from the beginning of my scientific studies. From my Masters, Ying has not only advised me but also given me confidence in my experimental work.

I would like to express my gratitude for those that have helped me with SIFT-MS studies. Professor D. Smith, Professor Patrik Španěl and Dr Thomas Chippendale. It is with particular thanks that I am grateful to Professor Španěl, who was kind enough to accommodate me at the J. Heyrovský Institute, Prague.

I am also grateful to the Diamond Light Source MIRIAM B22 beamline staff; Dr Gianfelice Cinque, Dr Mark Frogley, Dr Katia Wehbe and Dr Jacob Filik for their collaboration and support. I would also like to thank the beam line staff at Soleil Synchrotron, Dr Paul Dumas and Dr Christophe Sandt (who regularly goes above and beyond to share knowledge and the joys of France with us.)

I would also like to thank Professor Hugh Byrne and Dr Frank Bonnier for accommodating me at FOCAS, the Dublin Institute of Science and Technology. I'd like to thank them both for the sharing their knowledge and also for the many hours of laughter at conferences.

I would like to extend my gratitude to the many people I have worked with at the ISTM, who created a wonderful working environment. In particular, I'd like to give thanks to Dr Deepak Kumar for his advice and help with this thesis, Tina Dale for her limitless knowledge, Dr Hareklea Markides for her tireless encouragement, Dr Richard Webb for his help with software and Rashid Siddique for his support.

I would like to give a big thank to my mum and dad for their help and love in my academic pursuits, without whom I would not have achieved any of them. Finally, I would like to give a special thank you to James Roberts for his tremendous support for the last 3 years, for being a source of support, laughter and love.

I would like to acknowledge Diamond Light Source for partially funding this thesis along with Keele Acorn Fund and the London Community Foundation (Slater & Gordon Health Projects & Research Fund/14/15 Round 1/A344896).

List of Outputs

Publications

1. **Rutter. A. V.,** Siddique. M. R., Filik. J., Sandt. C., Dumas. P., Sockalingum. G. D., Yang. Y. and Sulé-Suso. J. (2014) Study of Gemcitabine Sensitive/Resistant Cancer Cells by Cell Cloning and Synchrotron FTIR Microspectroscopy. Cytometry, Part A, 85(8), 688-697.

2. **Rutter A. V.**, Chippendale T., Yang Y., Španěl P., Smith D., and Sulé-Suso J. (2013) Quantification by SIFT-MS of acetaldehyde released by lung cells in a 3D model Analyst 138(1), 91-95.

3. Pijanka. J. K., Stone, N., **Rutter, A. V.,** Forsyth, N., Sockalingum, G. D., Yang, Y., and Sulé-Suso, J. (2013). Identification of different subsets of lung cells using Raman microspectroscopy and whole cell nucleus isolation. Analyst, 138 (17), 5052-5058.

4. Filik J., **Rutter A.V.**, Sulé-Suso J. and Cinque G. (2012) Morphological analysis of vibrational hyperspectral imaging data. Analyst, 137(24), 5723-5729.

Oral presentations

1. Synchrotron Based FTIR Spectroscopy as a Tool to Detect Embryonic Stem Cell Differentiation. SPEC2012, Chiang Mai, Thailand; November, 2012. Studentship awarded.
2. A Study of Chemotherapy Sensitive/Resistant Cancer Cells by Cell cloning and Synchrotron FTIR Microspectroscopy. Diamond Light Source Science Away Day, Williams F1 Conference Centre, Oxford; June, 2015.

Posters

1. **Abigail V. Rutter**, Muhammad R. Siddique, Jacob Filik, Christophe Sandt, Paul Dumas, Gianfelice Cinque, Ganesh D. Sockalingum, Ying Yang, and Josep Sulé-Suso. Synchrotron Based FTIR Spectroscopy as a Tool to Detect Sensitive/Resistant Cloned Populations of Cancer Cells. Diamond Light Source Scientific Away Day, Diamond Light Source, Oxford; June, 2013.
2. **A. V. Rutter,** V. Untereiner, N. Forsyth, G. D. Sockalingum, and J. Sulé-Suso. Raman Spectroscopy of Lung Cells Using a Glass Substrate Raman spectroscopy of lung cells using a glass substrate. Spec2014, Krakow, Poland; August, 2014.
3. **A. V. Rutter**, V. Untereiner, N. Forsyth, G. D. Sockalingum, and J. Sulé-Suso. Raman spectroscopy of lung cells using a glass substrate. CLIRSPEC Summer School, Windermere, UK; July, 2015.
4. **A. V. Rutter**, M. R. Siddique, Y. Yang, N. Forsyth, P. Španěl, D. Smith, and J. Sulé-Suso. The role of culture conditions on the release of volatile organic compounds by lung cells measured with the Selected Ion Flow Tube Mass Spectrometry technique. IABR Summit, Breath 2015, Vienna, Austria; September, 2015.
5. J. Sulé-Suso, **A. V. Rutter**, M. R. Siddique, S. Gilani, N Watson, A. Jegannathen, A. M. Brunt, J. Belcher, Y. Yang, P. Španěl, and D. Smith . Volatile Organic Compounds in breath of lung cancer patients measured with the Selected Ion Flow Tube Mass Spectrometry technique. IABR Summit, Breath 2015, Vienna, Austria; September, 2015.
6. M. R. Siddique, **A. V. Rutter**, G. Cinque, Y. Yang, G. Bellisola, and J. Sulé-Suso. Synchrotron based IR microspectroscopy of leukaemia cells in 2D and 3D models. Spec2014, Krakow, Poland; August, 2014.

Prizes

Poster Prize awarded by Clinical Infrared and Raman Spectroscopy CLIRSPEC Summer School, Windermere, UK; July, 2015.Summer School 10/06/15.

Press interview

The Sunday Times interview on Lung Cancer Research and synchrotron based FTIR microspectroscopy; 7th September, 2015.

Chapter 1 Introduction

1.1 Lung Cancer

Worldwide, lung cancer was estimated to be responsible for a staggering 1.8×10^6 accounts in 2012, with an estimated 1.59×10^6 people dying from the disease in the same year. In the UK, 44.5×10^3 new cases were diagnosed and 35.4×10^3 people died from the disease the same year (Cancer Research UK). Lung cancer can be divided in 2 main subgroups, non small cell lung cancer (NSCLC) and small cell lung cancer (SCLC) (Appendix 1). The former accounts for around 87% of lung cancer cases and the latter for around 12% (Cancer Research UK). Staging of lung cancer has been summarised in Appendix 2.

1.1.1 Incidence

Globally, lung cancer is the most predominantly occurring cancer site in males affecting 17% of those diagnosed with cancer. It also accounts for 23% of total male cancer deaths (Jemal, B. 2011). In economically developed countries, lung cancer is responsible for the highest number of male cancers, except for prostate cancer.

In the global female population, 8.5% of new cases of cancer were lung cancer in 2008. Among females, the mortality burden of lung cancer in developing countries accounts for 11% of total female cancer deaths – on par with cervical cancer (Jemal, B. 2011, Siegel, N. 2013). Within developed countries however, lung cancer rates are two to five times higher, perhaps due to improved diagnosis and lifestyle choices (Jemal, B. 2011).

1.1.2 Tobacco/non-tobacco

"More people smoke today than at any other time in human history. One person dies every ten seconds due to smoking-related diseases"

- (Tabish, S.A. 2007).

The association of smoking with lung cancer has been established since the 1950s, pioneered by Sir Richard Doll who first established a relationship between smoking and increased risk of heart disease and lung cancer. The risk of dying from lung cancer is associated with particulars of cigarette smoking, which are the duration, regularity, tar concentration and age of initiation (Ostroff, R. M. 2010). It therefore comes as a surprise to find that despite the lower prevalence of smoking among Chinese women, at less than 4 % of adult smokers within the population, Chinese females have higher lung cancer rates than those within European countries (Mackay, J. 2004). Thus, we cannot attribute all lung cancer occurrences to smoking alone.

Other risk factors are clearly at play if we are to consider the unusual rates amongst populations that do not have high numbers of smokers. In the case of Chinese women it has been thought to reflect the presence of indoor air pollution caused by poorly ventilated coal stoves (Lam, W.K. 2004). Further sources of risk include occupational and environmental hazards; such as asbestos, arsenic, radon and polycyclic aromatic hydrocarbons (Boffetta, P. 2003). Boffetta et al. (2003) conclude and warn that whilst there is a relatively small risk of cancer following direct exposure to environmental carcinogens, they are not to be ignored. Given a causal relationship, a large number of cases would be caused as a result of high level prevalence of exposure.

Lam et al. (2004) comment that despite other etiological factors identified as having a relationship with lung cancer, the effect of tobacco smoke on incidence is overwhelming, calling for a concerted effort against tobacco use and a drive for scientific research into lung cancer. Global statistics back up Lam et al.'s conclusions; 80% of the lung cancer burden in males and 50% in females is attributed to smoking (Ezzati, M. 2003). Understanding the root of lung cancer may hold the key to overcoming the disease. Despite the obvious risks of smoking, and as Tabish et. al. (2007) has stated, more people smoke today than ever, meaning that lung cancer will be a growing problem to be tackled by scientists and clinicians for years to come.

1.1.3 Lung Cancer Diagnosis

Kendall et al. (2009) state that the most important factor in the prevention of the disease's progression is early detection, and identifying and removing the pre-malignant cells before systematic invasion.

If a patient presents with suspected lung cancer (through cough, breathlessness, haemoptysis –coughing up blood-, and pain), they are sent for an evaluation using imaging techniques. This is a vital stage as the diagnosis of the tumour type and stage will affect the treatment strategy applied and inevitably the prognosis of the disease. The first stage is typically imaging, through chest x-ray, computerised tomography (CT) scan, and positron emission tomography (PET).

The CT scan remains the main technique used to stage tumours and for post therapeutic evaluation, assessing location, size and anatomical characteristics. The widely recognised limitations of the CT scan are the uncertainty of detecting metastasis within normal sized lymph nodes and the difficulty in differentiating between tumour adhesion and tumour infiltration (Schrevens, L. 2004). The assessment of pulmonary nodules is conducted using PET, which is considered significantly more accurate than CT scan (Schrevens, L. 2004). Both methods have been used in tandem to overcome the movement of tumours with breathing motion, creating a 4D scan (Wolthaus, J.W.H. 2005). An alternative to CT and PET scans is magnetic resonance imaging (MRI). However, despite recent advantages in MRI, using the technique to assess the staging of tumours remains limited. This is because MRI is susceptible to motion artefacts and the lung parenchyma (there is a poor signal here due to low proton density) (Schaefer-Prokop, C. 2002)(Figures 1A an1B).

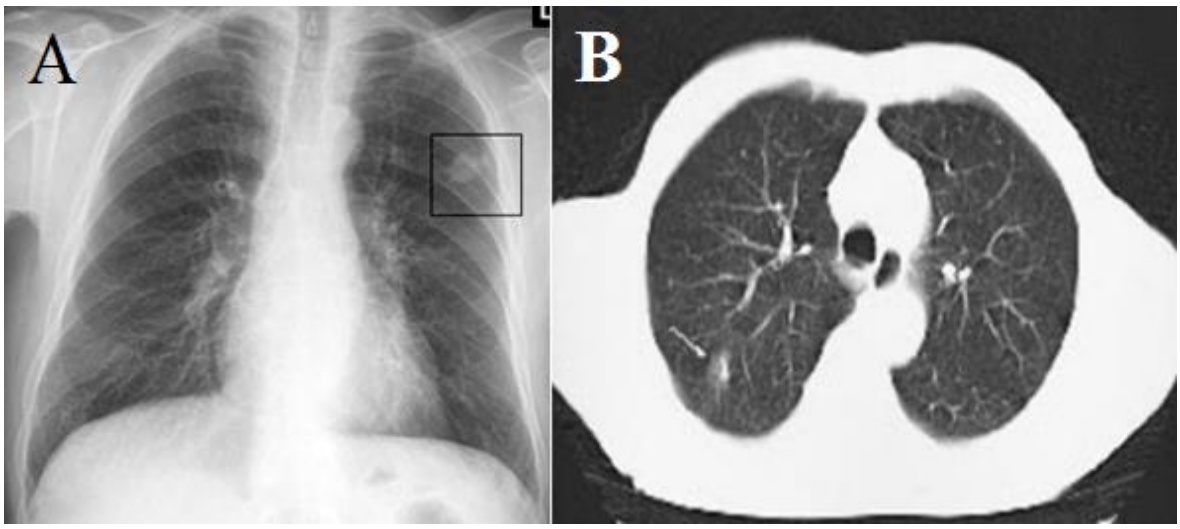

Figure 1. (A) Chest x-ray and (B) CT scan of chest.

The images in Figures 1A and 1B are of a chest x-ray and a CT scan, respectively. They demonstrate the difficulty in using these techniques to make a firm diagnosis. Figure 1A

depicts a tumour in the left upper lobe while Figure 1B illustrates a faint nodule in the right lung. The inability to image the entire lung with a resolution high enough to detect pre-invasive tumours and the lack of biochemical information about the disease is holding current imaging techniques back (Wardwell Jr. N.R. 2005). By the time the tumour is visible using conventional diagnostic techniques, the cancer might be diagnosed in advanced stages (Kendall, C. 2009). Following imaging, the tumour needs to be confirmed through tissue diagnosis. This can be done through sputum cytology, thoracentesis, lymph node biopsy, bronchoscopy, transthoracic needle aspiration (also known as fine needle aspiration) and video assisted thoracoscopy (Collins, L.G. 2007).

1.1.4 Cytology

Sputum cytology has been shown to lead to the early detection of lung cancer and improve the 5 year survival rate (Miller, L.M. 2005). The nature of obtaining the sputum, which can be done through application of a saline mist (induced sputum) and aspiration of forced coughing, is recommended for patients who may not be suitable candidates for invasive methods. The largest drawback to sputum cytology is that it is dependent on the quality of the sample obtained, which in some circumstances can be minimal due to size and location of the tumour (Collins, L.G. 2007). Despite this, sputum cytology could hold promise with the refinement of monolayering, preserving the preparations, and improving the automation of staining (Miller, L.M. 2005).

Sputum cytology provides several advantages over surgical specimens other than the obvious lack of invasive procedure. Firstly, the application of Papanicolaou (Pap) staining-

which is routine. Secondly, the stain has a high sensitivity for keratinization which aids the distinction between squamous cell carcinoma and adenocarcinoma.

The distinction between the two forms of NSCLC has become increasingly important as advancements in personalised therapies have evolved to include the identification of Epidermal Growth Factor Receptor (EGFR) and Kirsten Rat Sarcoma Viral Oncogene Homolog (KRAS), which dictate management and treatment response. Recent studies suggest that cytology is keeping up with this advancement in oncology, supporting the identification of KRAS and EGFR to a high standard even within high-volume histopathology practices (Rekhtman, N. 2011). However, most of these studies ignore the issue of the identification of early stage carcinoma, focussing mostly on sub-typing rather than sensitivity of tumour detection. By its own admission, the above study states that the impact on survival of this new approach towards diagnosis has yet to be confirmed. On the other hand, the cytological diagnosis of cancer is still, up to certain extent, dependent on the subjective decision of the appropriate pathologist.

Further drawbacks to cytology (sputum and aspirated) based samples are the low cellularity of the specimens and the non-cancer cells within the suspension (French, C.A. 2009; Rekhtman, N. 2011) Figure 2 demonstrates the difficulty of cytology diagnosis, other non-cancer cells within the specimen is hindering a clear view of cells that may be cancerous.

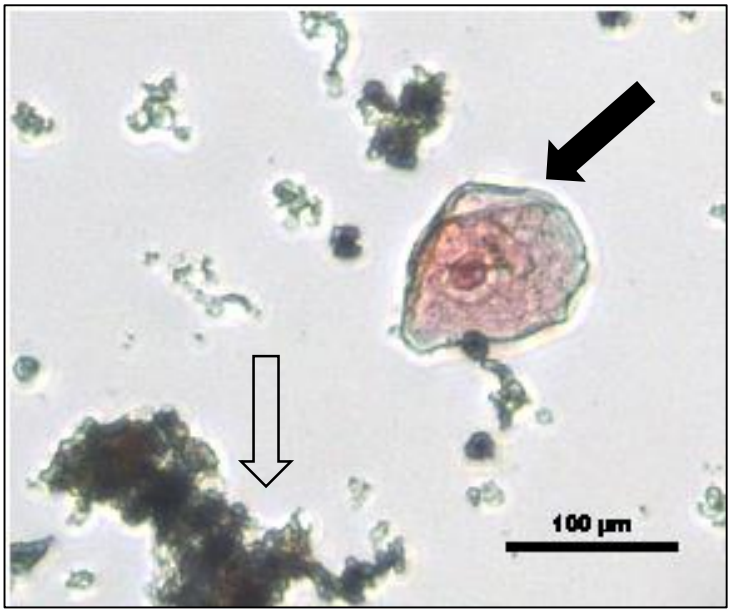

Figure 2. A cytological sample displaying an epithelial cell (pink, filled arrow) and lung cancer cells (blue, non-filled arrow) (bottom left).

1.1.5 Histopathology

Biopsy specimens (tissue samples) have been compared to fine needle aspirations (FNA) used for cytology diagnosis. Biopsy samples also yielded other biological constituents (such as clotted blood, lung/fibrous tissue) as well as the desired cellular components. Overall, biopsy and FNA yielded specimens with similar cell content (in 83% of cases), making neither sampling method particularly advantageous over the other for diagnostic purposes (Yazdi, H.M. 1987).

Once obtained, tissue samples are typically stained with Haematoxylin and Eosin (H&E). Haematoxylin colours the nuclei of cells, centrioles, fibrin, and red blood cells blue, and the Eosin colours protein based (eosinohilic) structures a red/pink/orange, including collagen, reticulin fibres and cartilage (Avwioro, G. 2011; Langer, C.J. 2010).

There is an ongoing dispute to the value of histology and cytology, and which one offers the highest levels of sensitivity and specificity, histology suffering from the same drawbacks as cytology with regard to sample quality and subjectivity applied to the diagnosis. When compared, it is often concluded that both cytological and histopathological tools should both be performed routinely in cases of suspected malignancy (Jones, A.M. 2001).

1.1.6 Diagnostic Conclusions

Overall, it is clear that the current diagnostic practises for lung cancer do not provide a comprehensive view of the disease and present with many problems, such as poor resolution, false negatives and the lack of biochemical information needed to detect cancerous cells. Both cytological and histopathological practises are reliant on the subjective diagnosis from a pathologist, again at a cost of sensitivity and specificity, with the risk of the patient having to undergo further biopsies to reach a conclusive result.

It is clear that further understanding of the molecular pathways, biochemical signals and behaviour of cancerous cells will only stand to benefit the study of the disease and help to refine the current diagnostic practises. This could be ascertained through *in vitro* studies that have already contributed to clinical practises and what we know about cancer today.

1.1.7 Treatment of Non-Small Cell Lung Cancer

The treatment of NSCLC can be split into four subgroups; surgery, radiation, chemotherapy and targeted treatments. Each group can be used in combination, cause different side effects and are used to teach NSCLC in different stages (Refer to Appendix 2 for staging guidelines). Surgery is used to treat stage I and stage II cancers. Chemotherapy can be applied after surgery to try to prevent the cancer from returning, this is known as

"adjuvant chemotherapy" and is particularly effective in those patients with stage II and stage IIIA disease. Radiation and chemotherapy treatment is often given in combination for stage III cancer that cannot be removed surgically. For stage IV cancer chemotherapy is used as the main treatment. Stage IV disease is treated with radiation, for palliative care (National Institute for Health and Care Excellence, 2011).

The chemotherapy drugs used in the treatment of lung cancer are often used in combination. Cisplatin, carboplatin, docetaxel, gemcitabine, paclitaxel, vinorelbine and pemetrexed are commonly used. Dependant on tumour response to the drugs, differing numbers of courses are prescribed for the patient (National Institute for Health and Care Excellence, 2011).

In some cases chemotherapy is used prior to other treatments, such as before surgery or radiotherapy, in the hope that the drug may shrink the tumour, this is known as neoadjuvant chemotherapy). Continued treatment with the same drug following the surgical procedure is more likely to aid in successful treatment (National Institute for Health and Care Excellence, 2011).

Targeted treatments refer to those treatments that specifically target lung cancer cells – differing from chemotherapy drugs which are not specific. Targeted therapies also differ in that they are cytostatic, blocking cancer cell proliferation instead of cytotoxic chemotherapy. Examples of targeted treatments for NSCLC are erlotinib, afatinib, gefitinib, bevacizumab, crizotinib and ceritinib. Such therapies are often used in combination with a chemotherapy drug (Cancer.org, 2016).

1.2 Lung Cancer *in Vitro:* 3D Cell Cultures

Most cell cultures are developed and maintained within a 2 Dimensional (2D), monolayer environment. Within the cellular engineering community there has now been a surge of

evidence substantial enough to demonstrate the advantages of cell culture within a 3D one. At face value, this has come as no surprise given that within mammalian tissues cells are supported and maintained within a 3D extracellular matrix (ECM), in populations that are functionally diverse. The populations also have a specific balance of functionality and spatial configuration in order to create healthy living tissue, with tissue engineers striving to mimic the natural environment as closely as possible; 3D scaffolds that mimic the ECM are therefore desirable. 3D cultures generally house the cells within a homogenous colony that is supplied with a nutrient rich medium and good gas exchange, allowing the diffusion of nutrients and waste products.

Whilst 2D environments still allow a substrate in which the cells may be able to develop the communication they require between each other, the culture may not be able to facilitate this in the same manner as they are able to in a 3D matrix. One obvious limitation of a 2D culture is the lack of representation of stroma, which has an important role to play within cancer development. The tumour stroma is comprised of non-malignant cells and extracellular matrix. Non-malignant cells are specialised mesenchymal cells (specific to tissue area), endothelial cells and pericytes. The extracellular matrix consists of the structural proteins collagen and elastin along with specialised proteins (fibronectin, fibrilin, elastin) and proteoglycans (Ronnov-Jessen, P. 1996).

It has been shown that the stroma provides a base in which tumours can create vascularisation. NSCLC cells have been found to release angiogenic factors leading to the creation of blood vessels. The interaction of these factors with the stroma is less well known about. Anderson et al. (2000) investigated the expression of interleukin-8 (IL-8) (a known

angiogenic factor secreted by cancer cells) and the role the stromal layer plays. Co-cultures of NSCLC cells and pulmonary fibroblasts were created. IL-8 was consistently induced within the fibroblastic culture (Anderson, I.C. 2000). The study highlights the importance of the cancer – stroma interaction and the high level of influence cancer cells have over their environment. As the preliminary data here suggests, there are unidentified soluble factors at play, influencing both the cancer cells and the cells within their surroundings. It is therefore vital to include a representation of the stromal layer within *in vitro* cultures or provide a scaffold which could go some way into encouraging a realistic interaction for cancer cells with their environment.

Cell adhesion and growth will also be affected by the differences in microenvironment between *in vivo* and *in vitro* studies (Xu, F. 2007). This is because receptors on the surface of cells (integrins) attach the cells to the substrate that they are on. Through integrins, cells also determine the biochemical information received from their immediate surroundings. Interpretation of such information determines cell behaviour such as differentiation, proliferation, apoptosis and metastatic capacity (Smalley, K.S.M. 2006).

Implementation of 3D cultures will inevitably produce more clinically relevant research, which is particularly relevant with regard to cancer studies. *In vivo,* tumours are comprised of a relatively complex structure consisting of dividing, hypoxic and necrotic tumour regions (Friedrich, M.J. 2003).

Studies looking at anti-tumour activity are strong examples of how the use of 3D cultures go some way to reflecting the impact of the structure of a tumour growth on experimentation,

over the use of previously conventional 2D cultures. In 2005 Bissell and LaBarge examined how the structure of a tissue would impact the resistance of malignant and non-malignant cells to chemotherapeutic agents. The results indicated that the structure of the tumour played an important role within the emergence of resistance to the chemotherapeutic agents alongside the genetic and growth factor signalling of the cells. Bissel and LaBarge conclude that no cell is able to function without instruction from its microenvironment, which *in vivo* is a product of the cell's own genetic instructions.

In vitro culture imposes an artificial microenvironment on the cells and so it comes as no surprise that earlier studies by Weaver et al. (1997) found that breast cancer cells changed behaviour, characteristic morphology and patterns of growth when grown on 3D constructs (Weaver, V.M. 1997). The study also utilised the inhibitory effects of beta 1-integrin antibody, illustrating that a cell's interaction with its microenvironment (via integrins) is significant enough to change a cell's phenotype. Reversal of the effects was created once the antibodies were removed, restoring the original cancerous phenotype (Weaver, V.M. 1997). Also, when dissociated from the 3D construct, that is mimicking the basement membrane, into a culture suspension, cell’s phenotype changed or suffered anoikis, (a form of apoptosis caused through lack of anchorage (Frisch, S.M. 2001).

Having defined a suitable environment to study lung cancer cultures, the next step in tackling the issues associated with the disease would be to look at the diagnosis process that hinders the overall outcome of patients. The 3D cultures could be implemented into the work of a new form of diagnosis. It is obvious from the data collected on lung cancer that the disease

is not being identified early enough. Could cell cultures provide any chemical information that could allow earlier identification within a clinical setting?

1.3 Spectrometry

1.3.1 SIFT-MS

One avenue in which to explore this challenging area is to look at the volatile metabolites that may be given off by cancer cells both *in vivo*; that is to examine the breath of patients with cancer, and *in vitro*; through examination of the volatile organic compounds (VOCs) that are given off from cell cultures. SIFT-MS allows such an examination, being a long established method of gaining insightful quantitative and qualitative information about the headspace of biological substances, having being developed primarily for real-time analysis of trace gases in breath/air (Smith, D. 2005). Despite emphasis of study being placed upon biological analysis, SIFT-MS was originally used to examine fundamental ion-molecule interaction at thermal energies (Adams, N.G. 1976), plasma reactions within the terrestrial atmosphere (Smith, D. 1980) and interstellar clouds (Smith, D. 1992). The instrument has made considerable progress since those early studies in capacity, sensitivity and transportability (Španěl, P. 2011). SIFT-MS can easily lend itself to the study of biological samples given the unusual capability of the machine to cope with the relatively large amount of water vapour often present in biological and breath samples. Although care should be taken to avoid direct contact of the SIFT-MS sampling arm with water.[1]

[1] Upon contact, the SIFT-MS sampling arm will draw water into the instrument, where it is kept under vacuum. Under vacuum, water boils rapidly (at ~20 mbar, the vapour pressure of water). As the vacuum reduces atmospheric pressure, the boiling point for water is reached at a much lower temperature. At this point the energy for boiling starts to come from water molecules, consequently its temperature reduces and so with a reducing pressure the water starts to freeze, becoming ice. Ice then blocking the instrument.

SIFT-MS relies on a chemical ionisation technique to determine the molecules present within a sample. Chemical ionisation is the process where new ionization species are created when gaseous molecules interact with ions. This involves electron, proton or other charged species transfer between the reactants. (IUPAC, 1997). Acidity is an example of how ionization takes place. Acids are chemical species that have the tendency of donating protons (Bronsted, J.N. 1923). Strong acids will completely dissociate into ions, completely ionizing, when placed in water. However weaker acids will only partially ionize. The degree of which an acid ionizes can be worked out using the acid ionization constant (K_a), this is the equilibrium constant for the ion dissociation in water (ie., The point in which the concentration of each chemical species does not change over time).

$$HA + H_2O \rightleftharpoons H_3O^+ + A^- \quad K_a = \frac{[H_3O^+][A^-]}{[HA]}$$

SIFT-MS works on similar principles, with the interaction of selected precursor ions, undergoing proton donation or a charge transfer process. That is reagent ions collide with the unknown analyte ions within the sample, the electrons present ionising the reagent gas molecules. In this case H_3O^+, NO^+ and O_2^+ reactant ions are used. H_3O^+ reactions follow proton transfer, H^+ is transferred from the H_3O^+ precursor ion to the analyte compound *M*. Product ions formed from this reaction also undergo hydration as the samples are humid, that is H_2O molecules will associate with the protonated MH^+. NO^+ reactions are charge transfer reactions, that is an electron is drawn from the analyte (our sample molecule), *M*, by the positively charged reactant ion neutralising the NO^+ ion to the neutral NO. As the samples are humid hydride ion transfer occurs; H^- is transferred from the analyte molecule to the precursor ion. O_2^+ reactions are also charge transfer reactions, like with NO^+, an electron is drawn from the analyte molecule and accepted by O_2^+ leaving an O molecule that is neutral. SIFT-MS utilizes the reaction of mass selected precursor ions with sample ions that are introduced into a flow tube via a helium gas carrier. The subsequent product ions

are then studied by a downstream mass spectrometer (See Figure three). Mass selected precursor ions are created using a microwave resonator, as mentioned, commonly selected ions are H_3O^+, NO^+ and O_2^+ ions, for the simple reason that they do not react readily with the common constituents of air (Španěl, P. 2011). A downstream mass spectrometer is then used to select the correct ions generated by the microwave generator. A series of pumps and sampling orifices are used to maintain the correct pressure and to focus the ions along the SIFT-MS. The downstream mass spectrometer operates at around 5-10 Torr, the proceeding flow tube operates at 0.5 Torr in order to achieve articulate gas reactions. Venturi inlets are used to sustain such changes in pressure but maintain a focussed flow of ions. Once a stream of defined precursor ions has been established the sample of interest is then injected into the flow tube through a helium carrier gas; the gas again being specific for this purpose due to its inert nature at a pressure of around 1 Torr. The introduced ion species from the sample of interest then reacts with the precursor ions (preselected by the upstream quadrupole) as they travel across the flow tube at high speed (Španěl, P. 2011). Product ions and precursor ions travel through a final sampling orifice where they are met by the downstream quadrupole. An electron multiplier then amplifies the signal given from the final quadrupole. In brief, a quadrupole mass analyser is compiled of four parallel rods, with associated positive and negative charges. They have fixed direct current (DC) and alternating radio frequency (RF) potentials applied to create an electric field that ions with a particular *m/z* are able to pass through. This is because the electric field only allows those ions with a stable trajectory to pass through to the detector. The alternating RF potential changes, functioning as a tool to focus ions with differing *m/z* into a stable trajectory and to be "in focus", therefore passing through the column of rods to the detector. As this potential changes, a mass spectrum can be built up of ions with differing *m/z* (Paul. W, 1983).

An on-line computer is then able to calculate the relative concentration of trace compounds from the reaction of product ions and sample gas (Smith, D. 2005; Španěl, P. 2011; Smith, D. 2011).

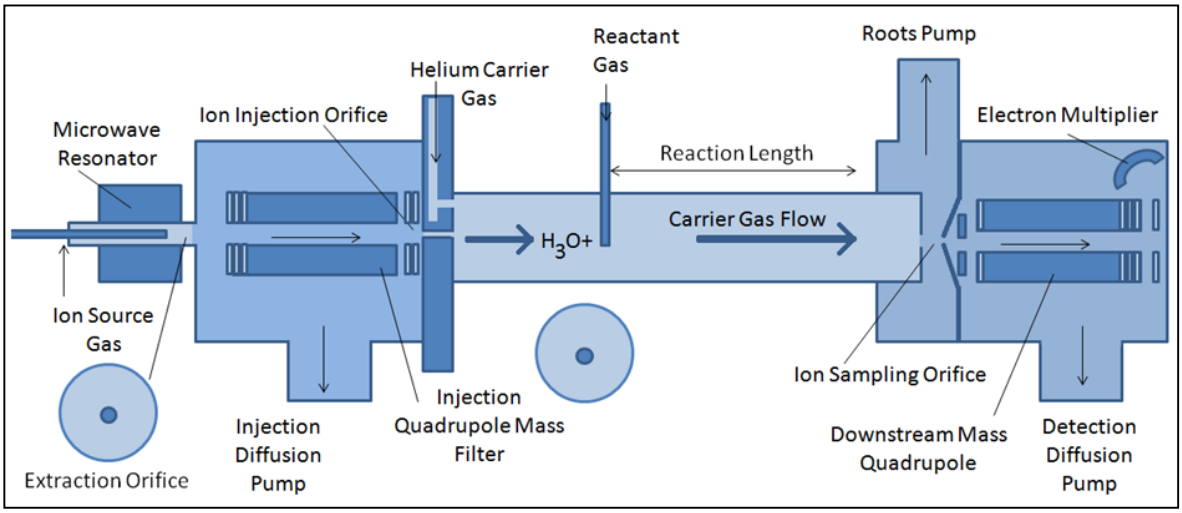

Figure 3. Schematic diagram of the SIFT-MS.

Given that the mass to charge ratio (m/z) of the precursor ions is known, along with flow rate and size of the flow tube (typically 5 cm in modern SIFT-MS instruments) it is possible, using this kinetic information, to determine the rate coefficient of product ions of the sample, in real-time, with a relatively large molecular weight range (10 m/z to 180 m/z) and a higher sensitivity (in *Profile 3* instruments) (Španěl, P. 2011), something that gives the SIFT-MS advantage over other forms of mass spectrometry also used to study cancer.

With regard to lung cancer, SIFT-MS studies can be split into two groups; firstly the study of breath from patients diagnosed with cancer (*ex vivo* studies) and secondly the study of cancerous and non-cancerous cell cultures (*in vitro* studies). In support of breath diagnosis, it is important to have a grasp of where potential volatile biomarkers of cancer could lie. *In vitro* studies are a good place to find a focus for this work.

Earlier studies of the lung cancer cell lines CALU-1 and SKMES, found that the release acetaldehyde VOC is proportional to the cell number within a two dimensional culture (Smith,D. 2003). The study was extended to include a comparison of lung cancer cell lines to normal lung epithelial cells, NL20 and 35FL121 (Tel+) lung fibroblastic cells (Sulé-Suso, J. 2009). Again, acetaldehyde was found to be produced in proportion to the cell numbers for CALU-1 and NL20. However, the 35FL121 cell line was seen to consume the compound. Interestingly, carbon dioxide was produced by respiration by the CALU-1 and 35FL121 cell lines as expected but in lower amounts by the NL20 cell line (Sulé-Suso, J. 2009), suggesting that the lower levels of CO_2 produced maybe due to an inhibited metabolism. There has also been some preliminary evidence to suggest that elevated acetic acid levels are produced by the CALU-1 cell line when cultured in acidic conditions (Smith, D. 2003). Given that the non-cancerous cell lines are also seen to produce acetaldehyde, the study provides insufficient evidence to identify acetaldehyde as a biomarker of cancer (Smith, D. 2003). Further exploration into the scale and nature of this production is needed to define the role acetaldehyde has to play within cancer metabolism.

Whilst 2D cultures have provided us with a spring board into the examination of lung cancer (the cells studied were all grown as a monolayer within a culture flask) it is important to endeavour to mimic human physiology as closely as possible. The development of collagen hydrogels within the tissue engineering community has provided a suitable scaffold in which cells are able to be expanded as a 3D tissue-like sample (Petersen, M.C. 2007). SIFT-MS would provide a strong comparison for how cancer cells behave in a traditional 2D *in vitro* setting compared to those grown within a 3D hydrogel construct. On a broader scale, SIFT-

MS could provide key knowledge about the interaction cells have in general for a widely used scaffold and the volatiles the scaffold gives off.

The interaction of *in vitro* cell culture studies and SIFT-MS poses some issues in itself that need to be overcome in the methodology. The conditions needed to maintain cell populations incorporate VOCs that may interfere with the identification of a biomarker. It has been found that foetal calf serum contained in the medium of the cell culture contributes to acetone and ethanol, (Sulé-Suso, J. 2009) and serves as a warning of the complexities brought with cell culture investigation. This also demonstrates the value of using SIFT-MS, which is addressing interactions within cultures between cells and the growth medium in real time.

In recent years there has been a strong shift towards the development of SIFT-MS as a clinically accessible bedside tool (Smith, D. 2010). This would have multiple advantages for a disease such as lung cancer. As mentioned before, the earlier lung cancer can be diagnosed the better the prognosis for the patient. Current diagnostic techniques need to be refined in order to fulfil this remit. Ideally, a new approach to lung cancer screening should also be developed. SIFT-MS has the potential to do so through the detection of early stage volatile biomarkers that cancerous cells may give off, as do other sources of analytical instruments that also measure breath volatiles; such as Gas Chromatography-Mass Spectrometry (GC-MS). There is a wealth of reviews that offer a summation of the work completed so far in an effort towards the improvement of lung cancer diagnosis (Amann, A. 2011; Poli, D. 2005; Smith, D. 2010); all come with speculation over some of the requirements that need to be met by breath testing and the analysis of volatile biomarkers if the challenges of this disease are to be met.

First and foremost is perhaps the sensitivity of such instrumentation. Can bedside analytical methods be sensitive enough to detect small early stage tumours that may only give off relatively minimal amounts of volatile compounds? Early stage SIFT-MS studies are promising, to the extent that analyses of single breath exhalations are able to generate sufficient sensitivity to detect VOCs in other diseases such as renal failure and cystic fibrosis .(Smith, D. 2010; Enderby, B. 2009; Davies, S. 1997; Gilchrist, F.J. 2012) However, GC-MS studies have revealed potential biomarkers such as alkanes, present at very low concentrations, in parts-per-trillion, in the breath of patients with primary lung cancer (Phillips, M. 1999; Phillips, M. 2003; Phillips, M. 2004), a challenging level for SIFT-MS instruments. With the identification of possible biomarkers at such a low level it is important to take into account the large levels of compounds that are present within the ambient air we breathe. A distinction must be made between endogenous compounds, produced by the body or cancerous tissues, and the exogenous compounds that are inhaled by the subject of interest. With further research and development, the SIFT-MS could offer insight into these questions (Smith, D. 2015; Smith, D. 2010)

In addition to sensitivity, SIFT-MS has also met the challenge of timing. Real-time analysis of single breath inhalations of dozens of patients have been analyzed in a single day, with immediate results (Smith, D. 2010). Calibration of the instrument is also extremely quick. Other analytical instruments often require time consuming and costly calibration methods that require the user to obtain commercially available standards, such as with the GC-MS.

SIFT-MS is improving all the time. The new *Profile 3* instrument (Instrument Science Limited) has an increased sensitivity when compared to previous models due to the fine tuning of the instrument. For example, the size of the flow tube (5 cm) (Španěl, P. 2011),

incorporating refined pump systems and dynamic quadrupoles. The use of alternate ion sources with the later SIFT-MS instruments has not only increased the sensitivity but has also brought with it the challenges of additional ion chemistry. One particular challenge to our studies is the adduct ions formed as a product of three-body reactions. A three-body reaction is a reaction that yields a single product from two reaction species and a third body to stabilize the product ion. Equations are being utilized within the kinetics library for each compound in order to give an increasingly realistic quantitative measurement that accounts for such ion interferences (Španěl, P. 2011).

So far, SIFT-MS has given us a glimpse of what to expect from the instrument as an analytical tool having already been used to identify VOCs in the headspace of bodily fluids. The urine of patients with bladder and prostate cancer was analysed, revealing that formaldehyde is clearly elevated in the urine of cancer sufferers over that of the healthy controls (Španěl, P. 1999). From breath samples we have gained insight into diabetes (Davies, S. 1997), where acetone levels were found to be ten times greater in diabetic individuals when compared to the rest of the population, even exceeding 5×10^3 part-per-billion-by-volume (ppbv) when under insulin control. The focus of the study was to monitor the breath of patients undergoing haemodialysis. The renal patients were found to have high ammonia levels in their breath (prior to dialysis) exceeding 10 parts-per-million (ppm) when compared to the healthy population that has around 1 ppm. SIFT-MS found that the levels of both ammonia and acetone fell during dialysis demonstrating how the instrument could be implemented in monitoring the efficiency of the treatment. This too could lend itself to the study of lung cancer – providing information about the efficiency of chemotherapy during the treatment process as opposed to the *post hoc* method.

1.3.2 GC-MS

GC-MS has proved a popular choice amongst the breath analysis community, having been used to identify VOCs secreted from gastric cancers and the bacteria associated with the disease (Buszewski, B. 2008). Solid-phase microextraction (SPME), which utilizes a sorbent fibre that captures the compounds of interest when exposed to the liquid or gaseous environment that they are in, has identified a higher amount of 1-propanol and carbon disulfide given off by cancerous stomach tissue when compared to non-cancerous stomach tissue (Buszewski, B. 2008). The study also found that bacteria *Helicobacter pylori*, associated with gastric cancer, may cause an increase in the concentration of these compounds released by the cancerous tissue. The same principles could be applied to the study of lung cancer – could certain compounds linked with smoking correlate with the VOCs given off by cancerous lung tissue?

Lung cancer has been the focus for many GC-MS studies. As early as 1985, GC-MS has demonstrated the detection of VOCs from the breath of lung cancer patients and compared them to the breath profiles of those without the disease. Despite a limited patient population and the production of one hundred and fifty peaks of VOCs, it has been found that the GC/MS was able to detect profiles of lung cancer distinct from those without lung cancer. The initial study found that acetone, methyl ethyl ketone and n-propanol were clinically significant compounds, providing a classification accuracy of 93% (Gordon, S M. 1985). Further studies also found that the analysis of breath was going to be complex due to the production of many compounds. O'Neill et al. (1988) found a myriad of VOCs within the eight patients they screened, with results containing up to 386 individual components. Conclusions were drawn to focus on the 45 components that occurred at a 75% occurrence level and the 28 components that were greater than 90% in occurrence level of the total

composition of expired air samples. The study also noted that compounds of interest were often representative of environmentally related pollutants, highlighting the complexity of this form of analysis (O'Neill, H.J. 1988).

Later studies compared the VOCs found in the breath of patients with lung cancer and the VOCs found to be given off by *in vitro* cell cultures. Some metabolic products did correlate between the 2 study groups, 11 VOCs from the breath of patients were identified as possible biomarkers of cancer (Chen, X. 2007). This previous study, that utilized samples taken directly from the breath of lung cancer patients, has so far used small sample populations, largely comprised of smokers, of 15 lung cancer sufferers (Chen, X. 2007) and so cannot offer a realistic prediction of what to expect from a clinically representative population.

In vitro studies, as already discussed, may offer an insight into lung cancer and provide a good platform for larger scale studies. The cell line CALU-1, a non-small cell lung epithelial carcinoma, was studied using the SPME method of GC-MS. An increase of 2, 3, 3-trimethylpentane, 2, 3, 5-trimethylhexane, 2, 4-dimethylheptane and 4-methyloctane was found in the headspace of the cell cultures. Interestingly, there was a decrease of acetaldehyde in the culture, which is in contrast to the VOCs found through SIFT-MS sampling. One explanation for this discrepancy could be the difference in culture methods. The studies utilising the SIFT-MS technique allowed for the attachment of the CALU-1 cells to a culture flask, an attachment that would mimic the natural environment of the tumour cells. However, the GC-MS examined cells that had been cultured within a fermenter where cells were kept in suspension (Filipiak, W. 2010). The cell line NCI-H2087, a non-small cell lung adenocarcinoma, was also cultured within a fermenter and was also found to consume acetaldehyde, 2-methylpropanal, 3-methylbutanal, 2-methylbutanal and butyl acetate

(Sponring, A. 2009). The difference across studies highlight the importance of a refinement of a suitable cell culture environment – do the cells give off VOCs according to different environmental status?

An expansion of the study of *in vitro* cell lines included A549, a lung adenocarcinoma cancer cell line, to be compared to two non-cancerous cell lines, HBEcC (a bronchial epithelial sample) and hFB (human fibroblasts). The VOCs detected from all cell lines exhibited a similar pattern of behaviour, that is an increase of 2-pentanone and 2, 4-dimethyl-1-heptene. Differences were seen with regard to branched hydrocarbons, that were principally given off by the non-cancerous cell lines. Of note, aldehydes were decreased within the headspace of the hFB and HBEcC when compared to the A549 cells, which may be more akin with the SIFT-MS results, despite also being grown within a fermenter (Sponring, A. 2009).

It is clear that further comparison across the different forms of mass spectrometry need to be facilitated if we are to be able to draw firm conclusions about the possible biomarkers of lung cancer. Sample populations also need to be significantly increased in size if we are to get an accurate grasp of what to expect from clinically relevant populations of cancer patients and control cases.

Mass spectrometry has a diverse range of contributions to make towards improving the diagnosis of lung cancer. Despite other methods such as the GC-MS providing a more comprehensive analysis of chemical compounds, the SIFT-MS is perhaps the most clinically relevant. As mentioned, the instrument functions in real time, with many user friendly applications – such as the on-board kinetics library. Given the absence of sample preparation and the portability of the instrument above the heavier GC-MS, the SIFT-MS is perhaps the

right choice for the bedside diagnostic tool. Other instrumentation is perhaps geared towards the laboratory setting – providing deeper knowledge into cancer cell behaviours but being less suitable for a hospital setting which requires the rapid turnover of many samples.

1.4 Vibrational Spectroscopy

Another tool that also offers both clinical and scientific application is vibrational spectroscopy. As a whole, vibrational spectroscopy has a number of potential advantages for the *ex vivo* assessment of lung cancer and to assist the current histopathological classification currently applied. The comprehensive studies are able to offer rapid, high resolution, non-destructive molecular examination without staining, possibly aiding prognostic information. (Kendall, C. 2009)

Within molecules, there are different vibrational modes as a result of the energy and nature of the bonding between each molecule (see Figure 4). This allows the atoms to move in dimensions, keeping the molecule in continuous movement. The energy of a given molecule is partitioned into 3N degrees of freedom that describe the molecule's 3 translational and 3 rotational motions. The degrees of freedom for vibrational modes of linear molecules is 3N-5 and for nonlinear molecules 3N-6, N being equal to the number of atoms within the molecule.

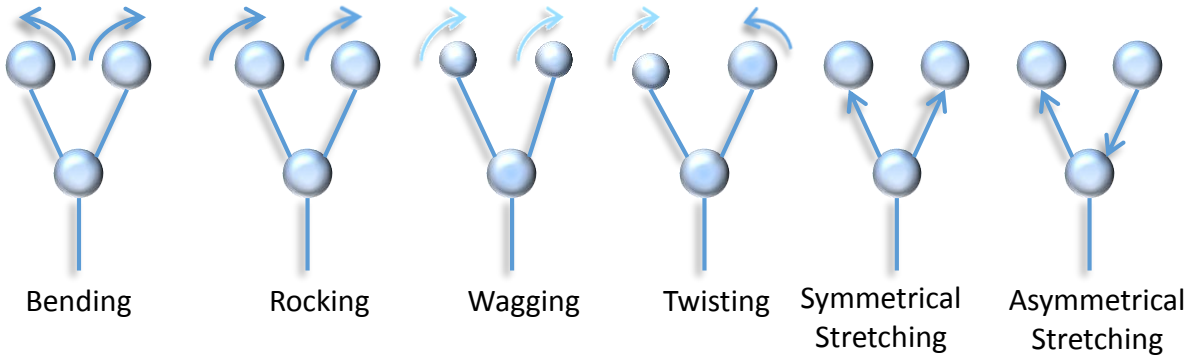

Figure 4. The different vibrational modes of molecules.

Photons (light energy) interact with the different vibrations via absorption or Raman scattering. The study of this interaction allows us to gain qualitative and quantitative information on the sample of interest within the portion of the light spectrum, in this case infrared spectrum. Infrared spectroscopy provides us with this information through measuring the loss of energy from a known frequency of incident light or the level of absorbance, once it has interacted with the molecule/molecules. Absorbance occurs if the energy of the incident radiation is the same size as the vibrational mechanism of the molecule it collides with. Raman spectroscopy utilises Raman scattering; the inelastic scattering of a photon, to observe the molecular vibrations (Griffiths, P. R. 2002). When monochromatic light makes contact with a molecule the cloud of electrons around the nuclei is polarised, forming a temporary virtual state. Most photons are elastically scattered from the atom/molecule, differing in only a very small frequency, with the same energy as the incident photons. This is called Rayleigh scattering. However, if the incident photons cause oscillating polarisation, energy is then transferred either from the incident photon to the molecule or from the molecule to the incident photon. This is dependent on whether the molecule was excited from the ground state or from a higher vibrational state (Figure 5). This inelastic scattering and the energy of the scattered radiation is different from that of the

incident photons. If during Raman scattering the scattered photon has a longer wavelength than the incident photon, the molecule has absorbed the energy and is promoted from the ground state to the first excited vibrational state. This is known as Raman stokes scattering. If during Raman scattering the molecule loses energy and the scattered photon has more energy than the incident photon, this is known as anti-stokes Raman scattering (Keresztury, G. 2002).

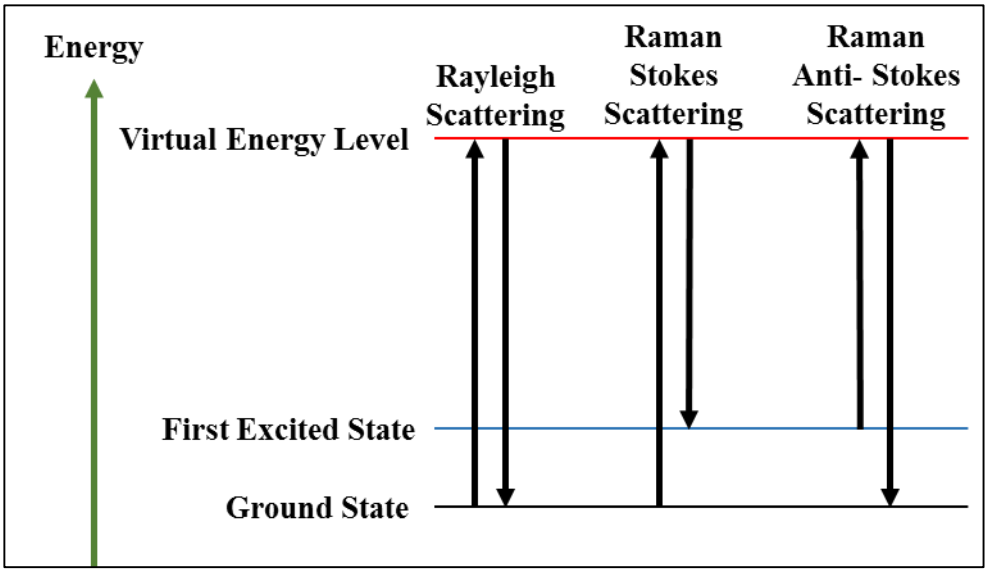

Figure 5 Diagram of Rayleigh and Raman scattering.

The infrared spectrum is a portion of the electromagnetic spectrum that is split into different regions; the mid-, near and far infrared. The spectrum itself is primarily organised along the x-axis, which is a frequency scale (in cm^{-1}) directly proportional to the energy of the vibrational bond within a molecule. The focus of this literature review will be on the mid-infrared region. This is because the wavelengths studied here are in the 4000-400 cm^{-1} wavenumber region, this corresponds to wavelengths of 2.5 to 25 μm, a relevant size when looking at cellular samples.

1.4.1 FTIR microspectroscopy to Study Biological Molecules

Fourier Transform Infrared (FTIR) microspectroscopy can be used to study components of biological structures, such as human tissue and cells. These samples are made of several crucial biomolecules; lipids, proteins, carbohydrates and nucleic acids. As mentioned before, each biomolecule will produce its own spectral signature based on the nature of the bonds within it and therefore each kind of cell will produce an individual spectrum. A typical spectrum of a biological sample can be seen below in Figure 6.

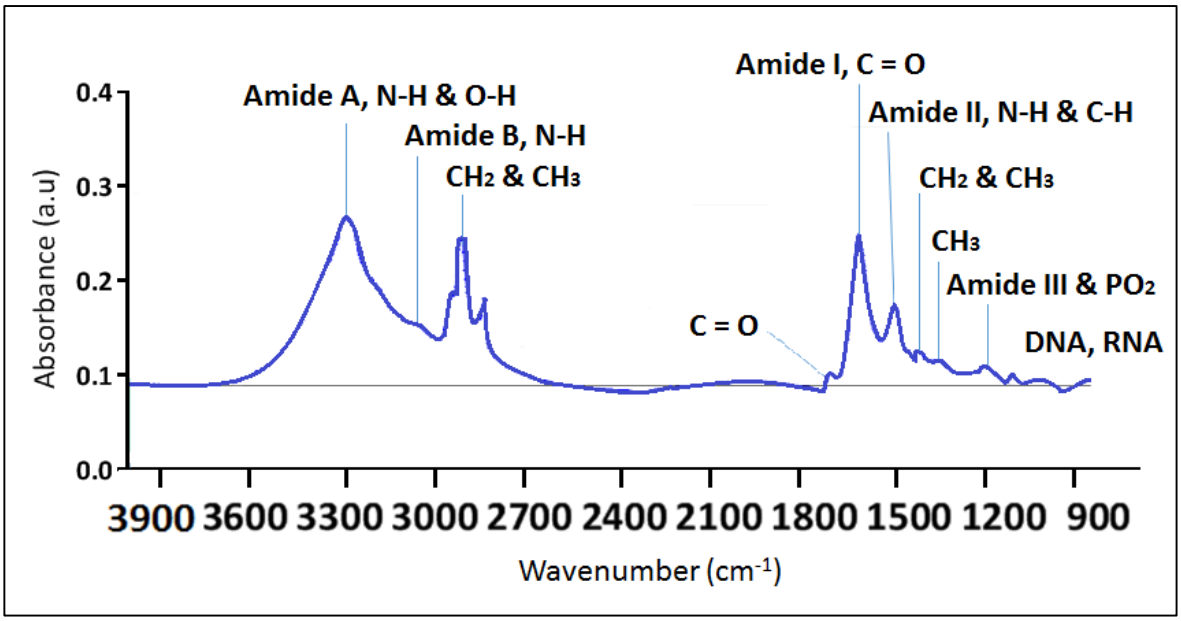

Figure 6. A typical FTIR spectrum of a cell. Biological bands of interest are labelled.

Lipid structures appear within the region between 3000-2800 cm^{-1} due to the C-H stretching vibrations (both asymmetric and symmetric) of the CH_3 and CH_2 groups of acyl chains as seen within the sample spectra above. C=O groups produce peaks at 1740 cm^{-1}, CH_2 at 1465 cm^{-1}, a range of strong bands at 1070 cm^{-1} – 1050 cm^{-1} and weaker bands at 1400-1250 cm^{-1} as a result of the C-O-C groups (Lewis, R.N.A.H. 2006).

Protein structures were first determined at atomic resolution in the 1950s using x-ray crystallography (Hodgkin, D.C. 1950). FTIR microspectroscopy can provide some detail into structure and function of proteins within human tissues. Proteins are comprised of amino acids and distinguished from each other by the number and order of amino acid units that they contain. The structure of a protein is folded into primary and three dimensional structures, secondary and tertiary. FTIR microspectroscopy is able to provide information about the secondary structure of proteins, that is the stretching vibrations of the C=O bond within the Amide I band and bending vibrations of the N-H bond with C-N stretching within Amide II. Amide I appears within the 1700-1600 cm^{-1} region of the mid-IR spectra, with an intense peak at 1650 cm^{-1} defined within the broader peak, whilst Amide II manifests itself within the 1530 cm^{-1} region. Proteins are also characterised by bands appearing at 3300 cm^{-1} – the Amide A band (N-H stretching). Amide III bands also occur as a result of intracellular proteins at 1400-1230 cm^{-1}. The peaks result from weaker protein vibrations from a combination of C-N stretching and N-H bending vibrations, like Amide I, but are dependent on the side chain structures of the protein between 1310 – 1450 cm^{1}. Proteins are a good example of the complex overlapping that can occur within FTIR spectra when trying to examine biomolecules (Gauglitz, G. 2014).

Carbohydrates produce broad bands around 3400-3380 cm^{-1} due to the OH stretching vibrations and another band at 2930-2900 cm^{-1} due to the presence of CH_2 groups and C-H stretching. Further peaks are seen at 1200-950 cm^{-1} from the C-O, C-C stretching and C-OH bending modes. At the lower end of the mid-IR spectrum, 950-700 cm^{-1} bending vibrations

produce peaks due to the presence of C-OH, C-CH, O-CH and C_1-H bending vibration (Kacurakova, M. 1996; Brandenburg, K. 2002).

How do the vibrational modes of a biomolecule result in peaks on an infrared spectrum? In order to absorb the photons a change within the dipole of the molecule must occur. During the activation of different vibrational modes (Figure 4), the dipole of the biomolecule is changed. The change in dipole is based on the nature or strength of the bonds between the groups so the stronger bonds with lighter atoms result in a higher frequency of vibration. The higher frequency in vibration will appear as a peak at the top end on the mid-IR spectrum. Within biomolecules we see a higher level of overlap between spectral bands due to the similar absorption of different molecules within the cell samples, as demonstrated by the description of peaks for each component.

The complicated interactions between the molecules and their vibrational modes results in a fingerprint spectra that could be used to identify, diagnose and explore biological samples for medical applications. Applying vibrational spectroscopy to the study of disease has been practised since the 1950s. Vibrational spectroscopy could help us to improve screening, diagnosis, our ability to predict a response to therapies, intraoperative monitoring and follow-up studies (Fisher, S. E. 2011). In order to fulfil this clinical remit, vibrational spectroscopy must be able to provide rapid, consistent and reliable techniques to a wide sample population. A technique that will be able to do this is FTIR spectroscopy. FTIR spectroscopy utilises a Michelson Interferometer (Figure 7) which splits the infrared light source (A) into 2 optical beams using an intermediate semi-transparent mirror. Half of the beam is directed towards Mirror 1 (B) which reflects the beam back, through the semi-

transparent mirror, to the detector. The other half of the beam (C) passes through the semi-transparent mirror to Mirror 2 where it is reflected back, joining beam B before being reflected back to the detector. Both beams undergo different surface reflections. Mirror 2 will be moveable and Mirror 1 is fixed, adjustments in the path of the beam caused by Mirror 2 create an interference which is then recorded by the detector. This movement also provides FTIR with a unique property, the ability to measure all infrared frequencies simultaneously (Griffiths, P. R. 2007). This is a major advantage of using FTIR spectroscopy for clinical applications – simultaneous measuring of frequency allows the instrument to make fast measurements.

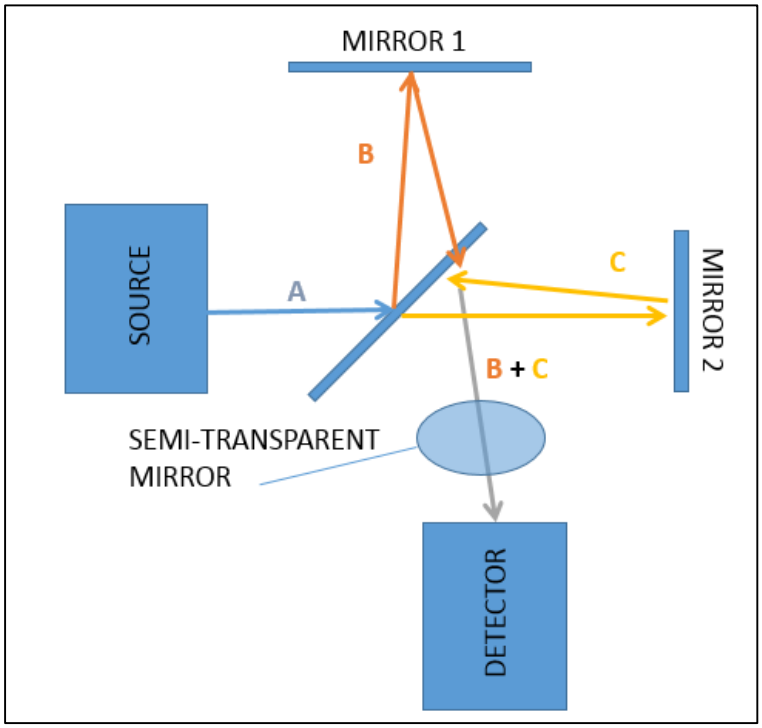

Figure 7. Michelson Interferometer.

The interferogram acquired will require further interpretation if the frequency spectrum is required. This decoding comes from a well-known technique called Fourier Transformation. This is usually completed digitally producing as outcome the IR spectrum we are familiar with.

1.4.2 Sources of Infrared

The first and perhaps most obvious reason to choose FTIR spectroscopy is the sensitivity of the instrument. Benchtop FTIR instrumentation has a Globar source; a silicon carbide rod, which is heated electronically to ~1300 °K. Such a high temperature reduces the signal to noise ratio within the spectrum, providing continuous mid-infrared radiation. The choice of a Globar as a source is a compromise – higher temperatures provide a reduced signal to noise ratio within the spectra but must also be kept stable within the local atmosphere, have a good lifespan and must limit saturating the detector. Commercially available Globars are cooled using water jackets to avoid the over-heating of electrical components within the system but are limited by this aspect of use. Despite the limiting factor, Globars have been used to divulge the chemical make-up of a variety of different materials, such as minerals, plant and animal tissues, polymers laminates and pharmaceuticals (Griffiths, P.R. 2007).

The main competitor of the Globar source of IR is Synchrotron radiation. The radiation is produced by electrons travelling in a synchrotron ring at relativistic velocity. The ring is created through the use of magnetic fields which bend the path of electrons into a focussed, closed orbit. This source size is around 100 μm in size, producing a light source with very high brightness (Carr, G.L. 1999). The brightness generated is 100-1000 times brighter than the Globar sources (Miller, L.M. 2005). The narrow range of angles for emission of the source is coupled with a small sample area (by the aperture), this in turn decreases the level of flux that will reach the detector and the signal to noise ratio is reduced. The advantage of using a synchrotron source is based around the 10-20 μm area. Miller et al. (2005) demonstrated that due to the high brightness, if an aperture is set to a throughput of 10 μm, 80% of the infrared light is still able to pass through reaching the detector. Smaller amount of Globar light is able to pass through at this aperture. However, at 70 μm, it is worth noting

that a synchrotron light source will lose its advantage given that the source produces no more power than a Globar (Diem, M. 2004).

Biological samples such as cellular components are therefore well suited to benefit from the synchrotron's brightness due to the small scale of these samples. Many studies have already started to utilize these advantages to examine the molecular chemistry of disease.

1.4.3 Lung Cancer Studies and FTIR spectroscopy

Previous studies have already applied FTIR spectroscopy to the study of cancers in various formats, such as colon and skin (Ly, E. 2008), leukaemia (Di Giambattist, L. 2010), oesophageal (Quaroni, L. 2009), prostate (Baker, M. J. 2009), breast; including lymph node mestastasis (Bird, B. 2009) and ovarian (Krishna, C.M. 2007) to name a few. Some, with a focus on the diagnostic applications, or to focus on the study of the effects of drugs on the cancers themselves. The same has been seen for the study of lung cancer,

Early studies into the structural changes associated with lung cancer within the pleural fluid were conducted using microscopic FTIR spectroscopy (Wang, H.P. 1997). The infrared spectra demonstrated differences between the normal, malignant and tuberculous cells within the pleural fluid, taken as a primary source from cancer patients. The significant findings were between the peak intensities of 1030 and 1080 cm^{-1} – mainly associated with the glycogen and phosphodiester groups. The work demonstrated an overall reduction of glycogen and hydrogen bonding of C-OH groups of amino acids (in proteins) in the abnormal cells and an increase of the hydrogen bonding of the phosphodiester groups of

nucleic acids, warranting that pleural fluid may be of some diagnostic value (Wang, H.P. 1997). Lobectomized lung specimens of squamous, adenocarcinomas and corresponding non-cancerous counterparts were directly analysed by FTIR spectroscopy. Again, glycogen was a feature within the analysis of the spectra. The analysis had a focus on the height of the peaks formed during the sampling, attributing a ratio of cholesterol and glycogen to be of most significance when identifying discriminatory factors of cancerous tissues (Yano, K. 2000). Microscopic mapping was also used to show areas of cancerous and non-cancerous tissue – providing information on the spatial distribution of the cancerous cells, FTIR spectroscopy being used in conjunction with other techniques for this method – although this would not be clinically necessary to make a diagnosis, this knowledge could be applied scientifically to further our knowledge about cancer behaviour.

Not all studies examine primary tissue sources, such as biopsy/lobectomized samples. FTIR spectroscopy has been used to assess a lung cancer cells' response to chemotherapy agents (Sulé-Suso, J. 2005). Gemcitabine was applied to the commercially available cell lines CALU-1 and A549 (both epithelial lung carcinoma). Following the addition of gemcitabine to the *in vitro* cultures, FTIR spectra produced changes within the 950-1150 cm^{-1} region. The ratio 1080/1050 cm^{-1} peaks, corresponding to the vibrations of PO_2 and C-O stretching associated with glycogen and carbohydrate moieties were found to increase with the levels of gemcitabine added. The data also determined information about the survival rates of the cells. At the lethal doses (LD) of 75 (for A549) and 50-75 (CALU-1) the ratio of interest reaches a plateau phase – correlating the changes in peaks with cell survival (Sulé-Suso, J. 2005).

So far the studies already mentioned utilised a Globar source radiation for FTIR spectroscopy. As already discussed, FTIR spectroscopy has now advanced into higher brightness capabilities using synchrotron IR radiation. So what does this mean for the diagnosis of lung cancer? Having already considered the problem of staining samples for diagnosis, it is also important to assess the contribution of the stain to any spectra produced by FTIR spectroscopy, especially if FTIR is to be used as a complementary service to this form of diagnosis. Clinical preparations of the cells should also be taken into account – are the specimens prepared using a cytospin or smear methods (such methods are currently used to apply samples to substrates for analysis, and are described in the methods sections of this thesis)? The effects of haematoxylin and eosin (H&E) and Papanicolau (Pap) stains were examined at single cell level. The aim of the study was to see if the stains interfered with the spectra and also to assess if the technique could still detect a difference between the cancerous and non-cancerous counterparts. Again, *in vitro* cell cultures of CALU-1 (epithelial carcinoma) and NL20 (normal lung epithelial cells) were used and indeed the FTIR spectra could detect differences between the two cell types. The staining showed changes within the lipid and amide II band regions but this did not impede the correct identification of the cancerous and non-cancerous cells. In one case, differences between cells stained at different centres were seen (Pijanka, J. 2010). Such application of FTIR technology, the assessment of clinical procedure, would have some value to the medical community in itself.

The study of cancer using synchrotron based FTIR microspectroscopy has also gone some way to evaluate one of the problems associated with FTIR spectroscopy. Mie scattering effects are an inevitable occurrence due to the size of sample and probe wavelength. S-FTIR microspectroscopy is able to look at the isolated cell nuclei due to its improved resolution.

A study examined the resulting spectra detailing the separation of optical (Mie) and chemical effects from the samples having compared single cell spectra and just the nuclei areas (Pijanka, J.K. 2009). Changes were seen within the lipids, proteins and DNA absorption bands, also demonstrating that the Mie effects were caused primarily by the nucleus of the cells. Unfortunately, although it was not the aim of the study, the authors did not include the normal lung cell counterparts to the cancerous ones, an aspect that should be included in further study in order to help characterize possible biomarkers for cancer diagnosis (Pijanka, J.K. 2009).

It is clear that FTIR spectroscopy (both Globar and synchrotron sourced) has a lot to offer to the study of lung cancer. Both within a scientific setting; to explore the mechanisms underpinning cancer cell behaviours but also within the clinical setting; for better diagnosis and the assessment of drug resistance. Therefore further work is needed; some biomarkers have been identified as having potential, such as glycogen, but no clear conclusions can be confirmed. The need for further ground work is obvious given the complex molecular activity within the cells but that is not to say that a useful clinical diagnostic tool is not within the capabilities of this technology which is able to offer a rapid, non-destructive and cost effective application to the study of lung cancer.

1.5 Conclusions

Spectroscopy could contribute greatly to the facilitation of a new gold standard diagnostic tool, which could exclude the current problems of subjectivity, cost effectiveness and poor resolution. The technique could potentially replace and/or complement currently available techniques to improve the management of those suffering with lung cancer. It is clear that

both FTIR spectroscopy and SIFT-MS have strong clinical applications, the first with a niche towards the support for histopathological diagnosis and the latter with the aim of breath diagnosis. Both provide obvious advancements to the scientific study of *in vitro* cultures and tumour response to cancer treatments, the value of which should not be underestimated to the study of lung cancer.

Chapter 2 Materials and Methods

2.1 Cell Culture Methods

2.1.1 Cells

The cell lines used in this thesis were:

A549 is a human lung adenocarcinoma cell line, (Figure 8A) derived from the epithelial lung tissue of a 58 year old Caucasian male. A549 was purchased from the European Collection of Cell Cultures (Salisbury, UK).

CALU-1 is a squamous lung cancer cell line, purchased from the European Collection of Cell Cultures Figure 8B). It was derived from a 47 year old Caucasian male with epidermoid cancer of the lung[2].

The different types of lung cancer have been listed in Appendix 1.

35FLP are parental, normal lung fibroblast cells, derived from a 35 year old female. 35FL121 cells are those derived from the parental 35FLP cells, immortalized via infection with a retrovirus containing hTERT[3], catalytic subunit of telomerase (Forsyth, N. 2003). Both cell lines were a gift from Dr Nicholas Forsyth (Figure 8c).

NL20 cells are a nontumorigenic cell line, consisting of immortalized human bronchial epithelial cells derived from a 20 year old Caucasian female. They were established through

[2] Squamous and epidermoid are terms used for the same type of cancer.
[3] Human Telomerase Reverse Transcriptase is a subunit of telomerase, the enzyme. It is used to prevent telomere shortening and overcome telomere-controlled senescence (Lee K. M., 2004).

the transfection of the replication-defective SV40 large T plasmid, p129 and purchased from the American Collection of Cell Culture (ATCC, CRL-2503) (Figure 8D).

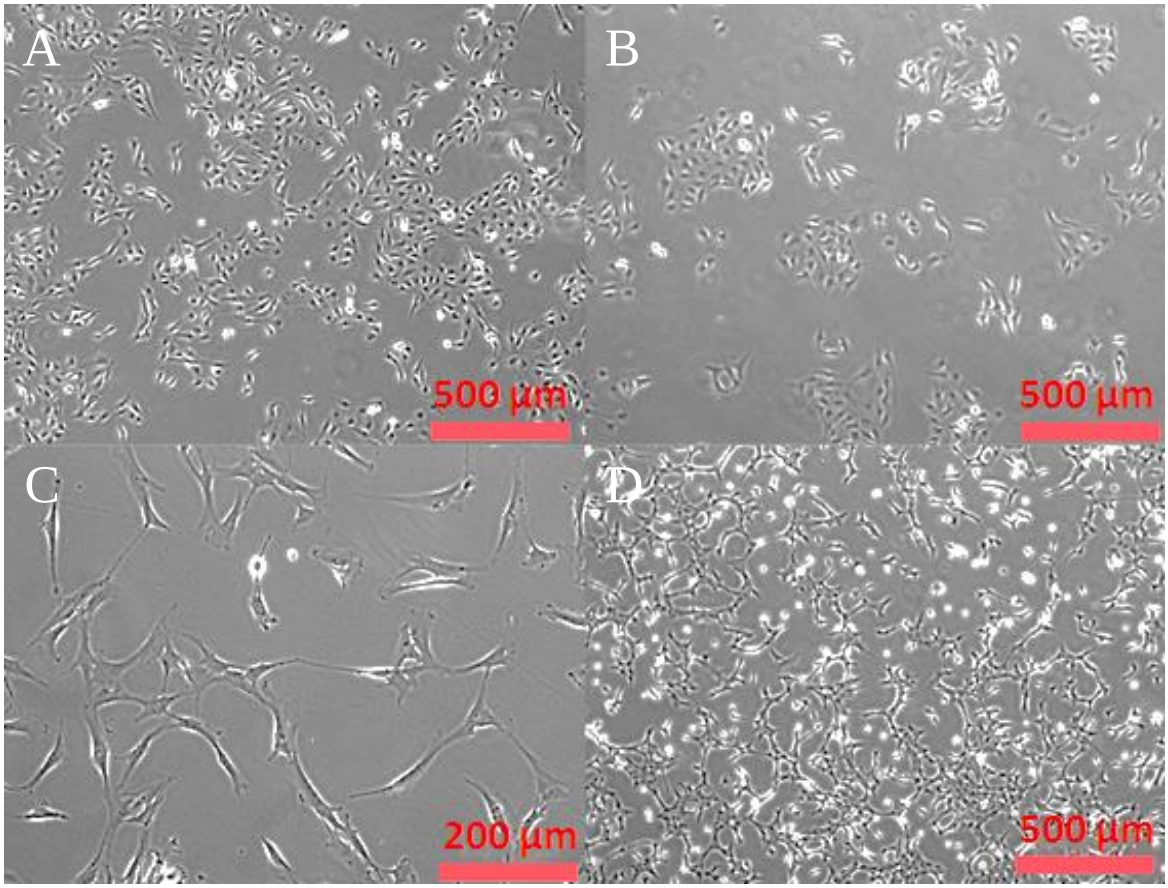

Figure 8. Light microscope images of (A) A549, (B) CALU-1, (C) 35FL121 and (D) NL20.

2.1.2 Culture Conditions

Below is a table of culture conditions for each cell line and media used. Each different culture condition is numbered for ease of identification throughout this thesis, particularly as media used on cell lines are interchanged across chapters for different experimental setups.

Table I Cell culture conditions.

Conditions	Cell Line (s)	Base Medium	Supplements	Dissociation Medium
Culture Conditions 1	A549/ CALU-1 /35FL121	DMEM, High Glucose 4.5 g/L	10% Foetal Bovine Serum (FBS) 1% Antibiotic/Antimycotic (100x) 1% L-Glutamine (200 nM) 1% Hepes Buffer Solution (1M) 1% Non-Essential Amino Acids (100x) 1% Sodium Pyruvate (100nM)	8:6 Trypsin - EDTA Solution (10x) : Phosphate Buffered Saline (1x)
	NL20	Ham's F12, Glucose 2.7 g/L	1.5 g/L $NaHCO_3$ 2 nM L-Glutamine (200 nM) 0.1 mM Non-Essential Amino Acids (100x) 5 µg/ mL Insulin (10 mg/ mL) 10 µg/ mL Epidermal Growth Factor (EGF) 1 µg/ mL Transferrin 0.5 µg/ mL Hydrocortisone 4% FBS 1% Antibiotic/Antimycotic (100x)	21 mg EDTA, 5.3 mL FBS, 100 mL Hank's Balanced Salt Solution (1x)

Conditions	Cell Line (s)	Base Medium	Supplements	Dissociation Medium
Culture Conditions 2	A549/ CALU-1 /35FL121	DMEM, without Glucose	10% Foetal Bovine Serum (FBS) 1% Antibiotic/Antimycotic (100x) 1% L-Glutamine (200 nM) 1% Hepes Buffer Solution (1M) 1% Non-Essential Amino Acids (100x) 1% Sodium Pyruvate (100nM) 4.5 g/L Glucose	8:6 Trypsin - EDTA Solution (10x) : Phosphate Buffered Saline (1x)
	NL20	DMEM, without Glucose	1.5 g/L $NaHCO_3$ 2 nM L-Glutamine (200 nM) 0.1 mM Non-Essential Amino Acids (100x) 5 µg/ mL Insulin (10 mg/ mL) 10 µg/ mL Epidermal Growth Factor (EGF) 1 µg/ mL Transferrin 0.5 µg/ mL Hydrocortisone 4% FBS 1% Antibiotic/Antimycotic (100x) 4.5 g/lL Glucose	8:6 Trypsin - EDTA Solution (10x) : Phosphate Buffered Saline (1x)

Cells were grown in T75/T175 cell culture flasks (Sarstedt, Leicester, UK) in the relevant media (Table I) in a 37 °C and 5% CO_2 incubator. The media was changed every 3-4 days and cells passaged before reaching confluence (typically weekly).

2.1.3 Clonal Isolation

Clonal isolation was accomplished using the CALU-1 cell line. Cells were passaged before reaching confluence from T75 cell culture flasks by adding trypsin-EDTA to flasks after removing culture media, and then incubating cells at 37 °C for 4 minutes. The trypsin-cell mixture is then quenched with culture medium and the suspension span at 1200 rpm for 4 minutes. The supernatant is then discarded and the cell pellet is resuspended in 5 mL of media and mixed thoroughly. Cells are then counted using the trypan blue exclusion assay. Cells were then seeded at 0.5 cells/well within a 96 flat bottomed well plate using a multichannel pipette and topped with 200 µL of culture medium. As an example, and for simplicity, for 100 wells, 50 cells were placed in 20 mL of medium and distributed evenly in these 100 wells. For each individual experiment, 5 x 96 well plates were setup. The plates were then wrapped in foil, to avoid dehydration, as they were then incubated for two weeks at 37 °C with 5% CO_2. A media change is completed after the first 7 days of this incubation time, by removing 180 µL of media to avoid the disruption of any clonal colonies that might be forming and replacing with 180 µL of fresh media. Following a 2 week incubation, the plates were then rigorously checked (by inspecting the wells daily with a microscope) for suitable clonal colonies, meaning those colonies that had formed within a single rounded population and those of a medium – large size. Other populations containing more than 1 clone or sparse number of cells were discarded, yielding on average 25-30 clones per experiment. Figure 9 shows a representative clone.

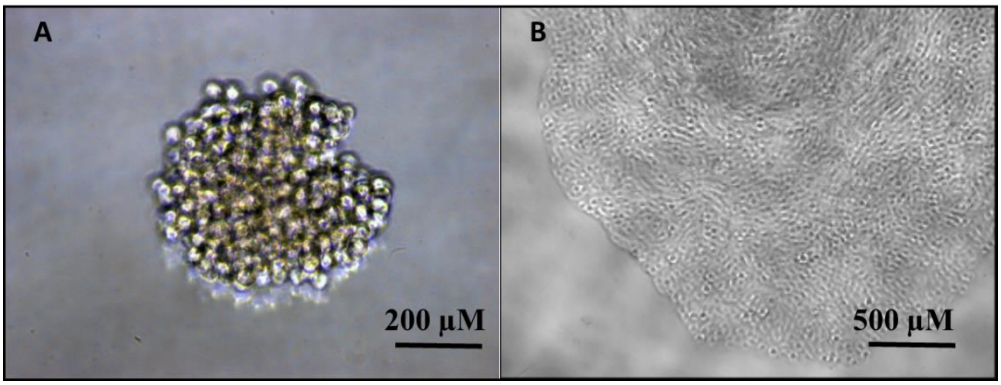

Figure 9. CALU-1 clonal cell populations after (A) 1 week in culture and (B) 2 weeks in culture.

2.1.4 The Post-Hoc Detection of Cells Sensitive/Resistant to Gemcitabine

The chemotherapy agent used within this study was the nucleoside analog[4] Gemcitabine (2' 2' – difluorodeoxycytidine) (Figure 10).

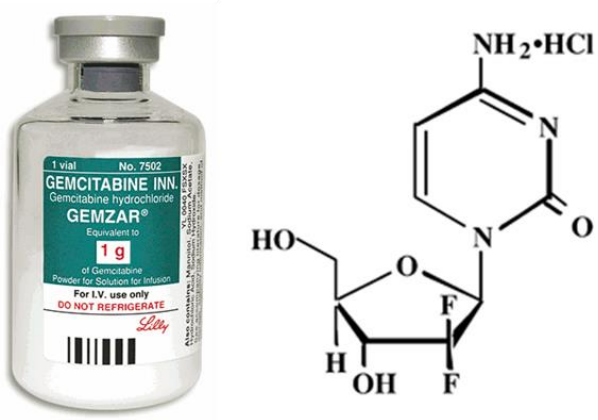

Figure 10. The chemotherapeutic drug Gemcitabine.

It was selected as it is a chemotherapy agent used in the management of lung cancer and as a locally sourced drug used within the University Hospital of North Midlands. Gemcitabine (Lilly, UK) was added to clonal populations of CALU-1 as follows: After the 2 week

[4] Nuceosides analogs are nucleosides that contain a nucleic acid analog and a sugar.

incubation period required to produce adequate size clones, each colony of cells was detached from its well using 10 µL of trypsin and incubated for 5 minutes at 37 °C. Following this, 190 µL of medium was added to each well and mixed thoroughly. Cells were collected and seeded proportionally into 5 wells of a flat bottomed 96 well plate, and topped to reach 200 µL of medium per well, then incubated for 24 hours. Gemcitabine was then added at four different concentrations; 25 nM, 50 nM, 75 nM and 100 nM, leaving a control well unexposed to the drug. The drug was added within 100 µL of fresh medium after 100 µL of medium was removed from each well, to reach the desired drug concentration. The control well having 100 µL media change with fresh medium alone. The cultures were then incubated for a further 5 days before sensitive and resistant populations could be identified. Sensitive clones were identified as those with low cell survival, characterised by wells with high amounts of debris and little cell attachment. Resistant cells were identified as cells that continued to proliferate and maintain a "healthy" population within the wells.

2.1.5 3D Culturing Techniques

3D matrices were implemented within the cell culture experiments given their ability to mimic *in vivo* tissue more accurately. The matrices were constructed from rat tail collagen type I (10.59 mg/ mL, BD Life Sciences). They were produced to form a gel with a final collagen concentration of 1.5 mg/mL, based on previously described work, (Yang, Y. 2005) and following the protocol described below (Figure 12). The collagen scaffold is prepared by combining, under ice, the neutralised solution of acetic acid extracted collagen with cell culture medium and cells. Once combined the gel is poured into a suitable vessel and incubated at 37° C in 5% CO_2. Neutralising and heating the gel causes the collagen to polymerise, forming a fine lattice of fibrils, 10-20 nm, that then trap the cells and fluid inside,

forming a hydrogel structure (Bell, E. 2014), Figure 11 depicts the collagen fibres that are present within a hydrogel structure.

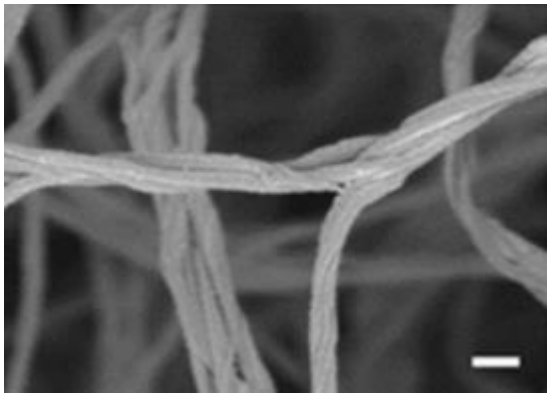

Figure 11 Scanning electron microscopy (SEM) image of the collagen fibres within a hydrogel. Scale bar corresponds to 200 nM (Moreno-Arotzena, O. 2015).

Determination of final volumes for collagen gelation procedure:

1.1 10x DMEM / 10x F12 / 10x PBS:

$$\frac{\text{Total Volume}}{10} = \text{mL 10x \{Media\}}$$

1.2 Final volume of collagen:

$$\frac{\text{Total Volume x Final Collagen Concentration in mg/mL}}{\text{Concentration of Collagen (Provided by Supplier)}} = \text{mL Collagen}$$

1.3 Final Volume of 1N NaOH:

Final Volume of Collagen x 0.023 mL = mL 1N NaOH

1.4 Final Volume of dH_2O:

(Total Volume) – (Final Volume of Collagen) – (Final Volume of 10x {Media}) – (Final Volume of 1N NaOH) = mL dH_2O

Figure 12. The determination of final volumes for 3D collagen model gelation protocol.

10x MEM (Gibco Life Technologies, UK) powder was reconstituted with 2.2 g of $NaHCO_3$ and mixed well with 100 ml dH_2O and sterile filtered with a 0.2 µ filter (Whatman, GE Healthcare Life Sciences). The process was repeated for 10x F12 (Gibco, Life Technologies,

UK) with 1.176 g of $NaHCO_3$ being added to the powder. 10x PBS (Oxoid, UK, BR0014G) was reconstituted in dH_2O according to the manufacturer's instructions.

Where cells were to be studied, the constituents that make up the gel were added first and mixed well. At this point, the pH of the mixture then becomes suitable not only for gelation but for cell growth. The cell population is counted and span down in order to remove any previous cell culture media that may alter the final setting conditions of the gel. The cell pellet is then added to the gel and mixed well, this is done rapidly to avoid the gel setting before the cell population is distributed equally. 3D constructs were given 24 hours minimum culture time in order for cells to get used to their new more physiological environment.

2.1.6 Survival Assays

2.1.6.1 Trypan Blue

Cell viability was determined using the trypan blue exclusion method. 0.4% trypan blue solution (Sigma Aldrich, T8154) was added 1:1 to 20 µL of cell suspension and mixed thoroughly. A haemocytometer was then loaded with the stained suspension. Healthy cells, those that appear bright and unstained are counted as live cells, those cells that take up the trypan blue, appearing dark blue under the microscope, are determined as non-viable.

2.1.6.2 Live/Dead

In order to assess cell survival in collagen scaffolds, a standard live/dead cell double staining kit (Sigma Aldrich) was used. The scaffolds were removed from the SIFT-MS bottles and

dissected into 0.5 cm^3 portions taken from different areas of the sample (6 sections/scaffold). The fluorescence double staining kit utilises calcein-AM to stain live cells green and propidium iodide (PI) to stain dead cells red. The stain was diluted according the provider's instructions in phosphate buffered saline (PBS) and applied directly to the scaffolds for 1 hour. Scaffolds were agitated every 15 minutes to ensure a thorough penetration of the stain within the sections. Sample imaging was performed using a FV300 confocal microscope (Olympus, Japan).

2.1.7 Extraction of Live Cells from Collagen Scaffolds

Scaled down versions of the 10 mL 3D Collagen gel matrices[5] (1 mL) were digested in order to assess the cell viability within the culture. Media from the top of each culture was removed and collagenase from *Clostridium histolyticum* (working concentration 1000 units/ mL, Sigma Aldrich, C6885) was added to each gel. The gels were mechanically sectioned using a pipette and incubated for 1 hour at 37 °C. Once the matrix had dissolved, the trypan blue exclusion method was used as described above.

2.1.8 Identification of Cells in fixed Collagen Scaffold

A DAPI stain (Vectashield Antifade Mounting Medium with DAPI, Vector Laboraties) was applied to cryosectioned samples of cells within collagen matrixes. The stain was applied for 1 minute, washing 3 times with dH_2O after. The samples were then air dried. This process was used to confirm the presence of cells within the matrix for S-FTIR analysis. Unfortunately, it was unpractical to identify cells by microscopy alone. DAPI was also

[5] The justification of downscaling collagen scaffolds is explained in the corresponding chapter.

applied to 2D cytospun samples, using the same method here, to confirm the absence of differences in the spectra produced by the cells.

2.2 Spectrometry

2.2.1 SIFT-MS

2.2.1.1 Instrumentation

Figure 13. The SIFT-MS *Profile 3* instrument.

The headspace of cell cultures was measured for VOCs using a *Profile 3* SIFT-MS instrument (Figure 13), from Instrument Science, UK. As described in the Introduction, selected reagent ions were produced from a microwave discharge ion source and sorted using a mass quadrupole (Figure 14). In this case, the selected ions were H_3O^+ and NO^+. They are injected into a stream of helium- the inert carrier gas for the reaction, thus obtaining an absolute concentration of product ions (10-180 m/z). The humid headspace of the cell cultures was taken via a heated sampling line, a hypodermic needle puncturing the septum

of the culture bottles connecting the headspace directly into the inlet port of the *Profile 3*. During the sampling, the cell culture bottles were maintained within a water bath at 37 °C.

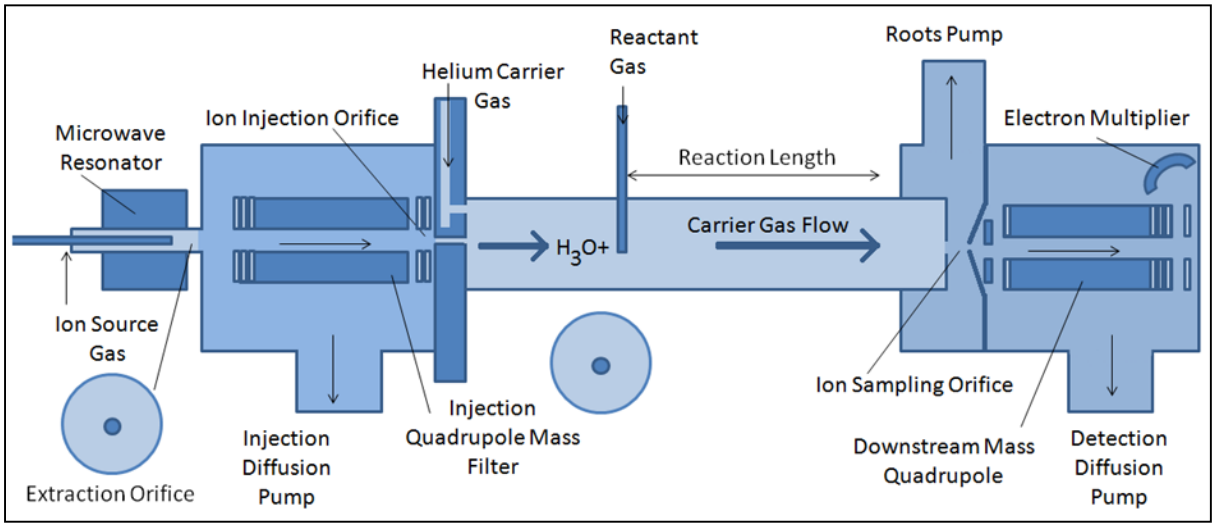

Figure 14. Schematic diagram of the SIFT-MS *Profile 3* instrument.

The headspace is met by the flow of reagent ions within the carrier gas and travels along the flow tube during a well-defined reaction time. The instrument was used in multi-ion monitoring mode (MIM), to study chosen analytes, or on full scan mode (FSM), to study analytes in the range between 10 -180 m/z. After mass analysis using a mass spectrometer, they are detected and counted by an electron multiplier/pulse counting system and the on-board computer immediately calculates the concentrations of the trace gases (metabolites) in the sample with the aid of a kinetics database library compiled from numerous studies of ion-molecule reactions.

2.2.1.2 Sample Preparation

In this thesis, the headspace to be examined with the SIFT-MS was obtained in 2 ways. Either a 3D cell culture created matrix, within a sealed glass bottle with septum (Figure 15A)

or breath samples that have been exhaled by participants directly into a Nalophan bag (Figure 15B).

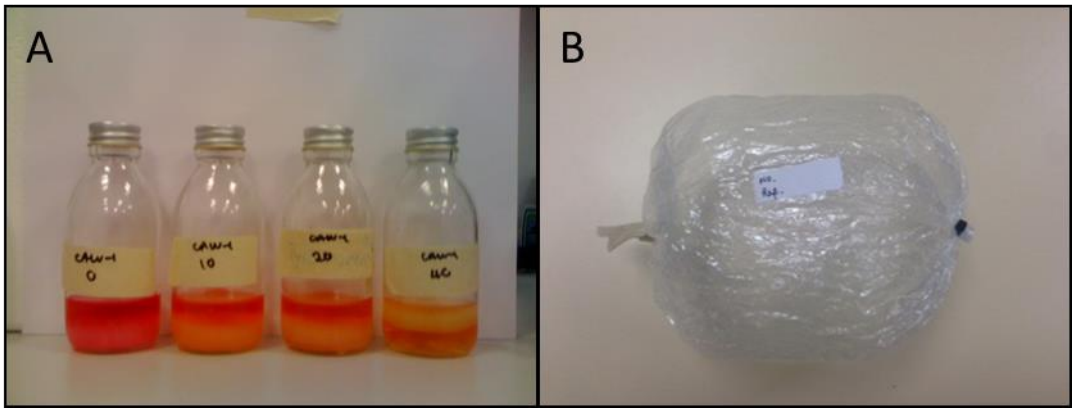

Figure 15. Sampling methods for the SIFT-MS (A) Bottle samples and (B) a bag sample.

For bottle samples, gels containing cells and control gels without cells were allowed to solidify by incubating them at 37 °C and 5% CO_2 with the lids open for 2 hours. After this incubation time, 10 mL of media were added to the top of the gels and incubated for a further 22 hours with the lids open. Following this incubation time, for a remaining 16 hours before SIFT-MS sampling in order to allow the headspace to develop, as previously described (Sulé-Suso, J. 2009). The lids contain a central rubber septum which can be punctured to study the headspace.

For bag sampling however the air is sampled immediately, the bags being punctured directly with the SIFT-MS sampling needle. Nalophan tube sheeting is cut into 30 cm length and a 3 cm poly-tubing length is inserted into one end, fixing into place with a cable tie before being sealed with parafilm. The opposite end is sealed using a cable tie and parafilm. Once the breath sample is collected, a syringe is used to seal the tube end of the sampling bag and

a further layer of parafilm is used to seal the connection. All participants were asked to fill each bag with at least 3 breaths, exhaling normally (ethical approval for this study had been obtained).

All samples, bottle and bag were stored at room temperature, under ambient conditions until they were to be sampled using the SIFT-MS. At this point samples were placed into a 37 °C water bath (for bottles) or incubator (bags) for 10 minutes, allowing them to reach that temperature and sampled from within these storage containers.

2.2.1.3 Data Processing

6% Water Correction

During the SIFT-MS measurements using H_3O^+ precursor ion, humidity of each sample and environment can differ (relative humidity and temperature). This has a relative effect on the quantification of compounds derived by the kinetic library. To overcome this variation a 6% water correction is used on measurements obtained using the H_3O^+ precursor. That is, each measurement is brought up to a standard 6% water level using the flow rate adjustment incorporated into the software. The kinetic library then quantifies the VOCs on this percentage of water (Smith, D. 2011).

2.2.1.4 Data Analysis

Data analysis was performed using the SIFT-MS software to produce an ASCII file that was then analysed within Microsoft Excel. PCA was performed to examine differences where

relevant using The Unscrambler software (Camo, Norway) and visualised using Graph Pad Prism 6.

2.3 Spectroscopy

2.3.1 S-FTIR Spectroscopy

S-FTIR data were obtained from two different synchrotron sources, Diamond Light Source (Oxford)(Figure 16A) and Soleil Synchrotron (France)(Figure 16B).

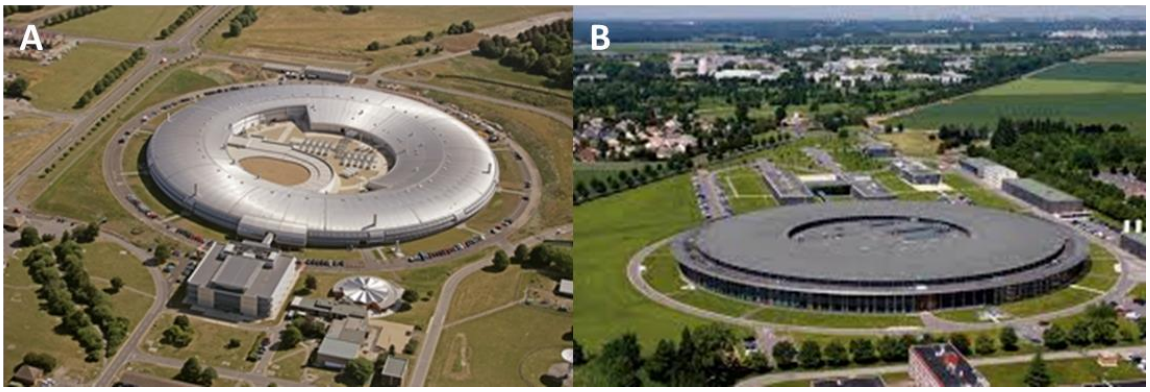

Figure 16. Synchrotron sites (A) Diamond Light Source, Oxford and (B) Soleil Synchrotron, France.

The SMIS station at Soleil Synchrotron was equipped with a Nicolet Continuum IR microscope and Nicolet Nexus FTIR spectrometer (Thermo Nicolet), with a MCT/A detector cooled with liquid nitrogen (Figure 16). Spectra and images were obtained via a 32x infinity corrected Schwarzchild objective, and managed by Omnic Software (Thermo, Omnic ver 8.2).

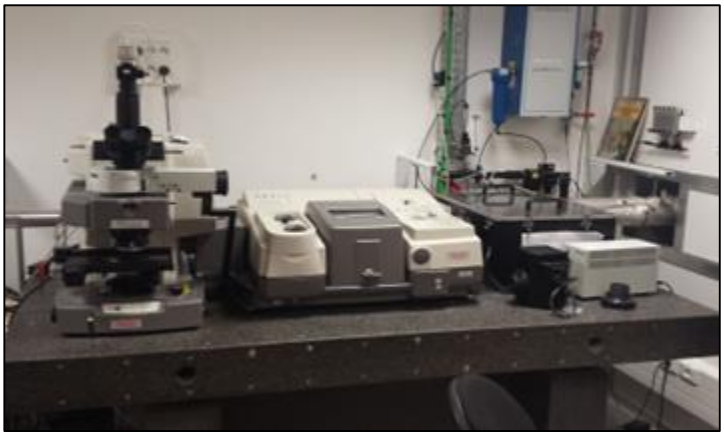

Figure 17. The end station at SMIS beamline, Soleil Synchrotron.

B22 or MIRIAM is the beamline station used within Diamond Light Source (Figure 18). The station is equipped with a Hyperion 3000 microscope (Bruker) and a Bruker 80V FTIR spectrometer, coupled with a liquid nitrogen managed 100 x 100μm^2 MCT/A detector. Spectra and images were obtained via a 36x Schwarzchild objective, managed by Opus software (Bruker).

Figure 18. The end station at B22, MIRIAM at Diamond Light Source.

For each sample, the size of the aperture was considered per experiment, and was dependant on sample size. Typically, cytospun cellular samples were measured using a 15x15 µm aperture, placing the beam centrally onto a cell. For some cell types that were difficult to identify within a collagen matrix a smaller, 12x12 µm aperture was used to focus on the centre of a cell.

Spectral parameters were ascertained following initial test measurements. Following these a standard resolution of 4 cm^{-1} was used, 128 co-added scans per cell spectrum taken and 256 scans for background measurements (a higher scanning number taken to minimise the signal to noise). Background measurements were taken every 15 cells, and taken from areas of substrate that were clear of any sample material. All measurements were taken in transmission mode, using a CaF_2 substrate, 0.5 mm thick (Crystan). Where possible with

time restraints and sample condition, between 50 - 70 cells were measured per sample. The maximum number of cells were taken for those samples lacking in population, such as those that had been exposed to higher doses of a chemotherapy drug.

2.3.2 Sample Preparation

2.3.2.1 Substrates

UV grade CaF_2 (Crystan) windows (0.5 mm thickness) were used for the S-FTIR work. CaF_2 windows were selected due to their suitability for S-FTIR transmission work.

2.3.2.2 Fixatives

All cell samples for spectroscopy were fixed using 4% paraformaldehyde (PFA) in 0.9% NaCl at room temperature for 20 minutes in the case of 2D samples and for 1 hour for 3D samples. This was followed by 3 washes with 0.9% NaCl and 1 wash with deionised water. 2D samples were then left to air dry under ambient conditions. 3D samples were then cryosectioned.

2.3.2.3 Cytospinning

Following relevant cell culture methods, cells that were to be deposited on slides in a single monolayer were re-suspended in 0.9% NaCl. Cell suspensions were cytospun onto CaF_2 slides for 1 minute at 700 rpm, through a cytofunnel and filter card (Shandon, UK). Once the cells had been deposited on CaF_2 slides, samples were placed in a petri dish and fixed using 4% PFA.

Cytospinning was an obvious choice for sample preparation for S-FTIR analysis. The technique is widely used within the clinical environment for cytology. It would be obviously beneficial if our techniques could be applied to pre-existing methods currently being used. The second value to using cytospinning as a technique is that it yields samples with flatter cell bodies. Mie scattering effects can alter the spectra gained from S-FTIR analysis if a sample is too rounded. Quite often, cell samples produce characterised shifts within the amide I region, which would then need to be corrected for. Although not excluding the Mie scattering entirely, cytospinning does appear to reduce this artefact (Pijanka, J.K. 2009).

2.3.2.4 Cryocutting

For 3D samples that are prepared as tissue slices a Clinicut 60 microtome-cryostat was used (Bright, UK) to produce 15 µm thick slices. 3D collagen gel samples were fixed in 4% PFA (see fixatives subheading) as standard. Following this, the samples were then flash frozen in liquid nitrogen for 20 seconds and then mounted in OCT (optimum cutting temperature) mounting medium. The samples were maintained as frozen within the cryostat where they were then sectioned into the slices and placed straight onto the substrate to be analysed (CaF_2). Samples were then left to defrost onto the slides momentarily, after which they were submerged in water for 1 minute to remove the OCT medium as much as possible in order to be suitable for spectroscopic analysis. Samples were then left to air dry.

A 15 µm thickness of tissue was selected as this was an optimal range to produce uninterrupted slices of tissue. Thinner slices became unmanageable due to the nature of the collagen gel.

2.3.3 Data Processing

2.3.3.1 Corrections and Software

Matlab (Matlab 7.5 Mathworks, Natick, USA) was used to apply an Extended Multiplicative Signal Correction (EMSC) in order to correct for Mie scattering effects using an algorithm created by Dr Achim Kohler (Kohler, A. 2008). Mie scattering is an effect that presents itself as a well-defined change in a cell spectrum (often as a shift in the amide I peak) due to the rounded shape of the cell body. EMSC aims to correct this artefact, which has also been reduced by the choice of cytospinning as a form of sample preparation. That is, the samples are flatter than those that would be grown straight onto the substrate.

S-FTIR Spectra were processed using The Unscrambler software (Version X, Camo, Oslo, Norway) to correct for baseline (linear-offset), normalised (Standard Normal Variate (SNV)) and smoothed (Savitzky-Golay).

Following the baseline correction and EMSC application, spectra were cropped to the area of interest for that particular analysis. For the lipid region, spectra were cropped to the region of 2700-3100 cm^{-1} and for the fingerprint area, spectra were cropped to 1000-1800 cm^{-1}. Then, the SNV normalisation was applied, which subtracts the mean spectrum and then divides by the standard deviation for each spectrum. This removes the effect of sample thickness and any baseline offset that may have occurred.

2.3.4 Data Analysis

2.3.4.1 Principle Component Analysis

Principle Component Analysis (PCA) was performed using The Unscrambler software (version X, Camo, Oslo, Norway). PCA is an unsupervised analysis that allows us to reduce large numbers of variables (our spectral wave vectors) into a few principle components (that are calculated from the covariance of the data set we are analysing). Therefore we are able to comprehend and see where differences in our data sets lay. This is repeated in a number of principal components (PC)s, the first PC is the one that contains the highest variance, PC1. Variance then reduces as the PCs continue, PC2, PC3, all decreasing in variance.

PC scores are also derived from data sets and are used to plot the variance onto a 2D axis. As the positon of the score on the axis represents the relative position of variance in relation to the other plots of variance we can visualise groups of data starting to emerge on the axis (Figure 19A shows a representative example). Loading plots are representative of how much a variable participates within each PC. It is used here to show where the high levels of variance are within a spectrum (Figure 19B shows a representative example).

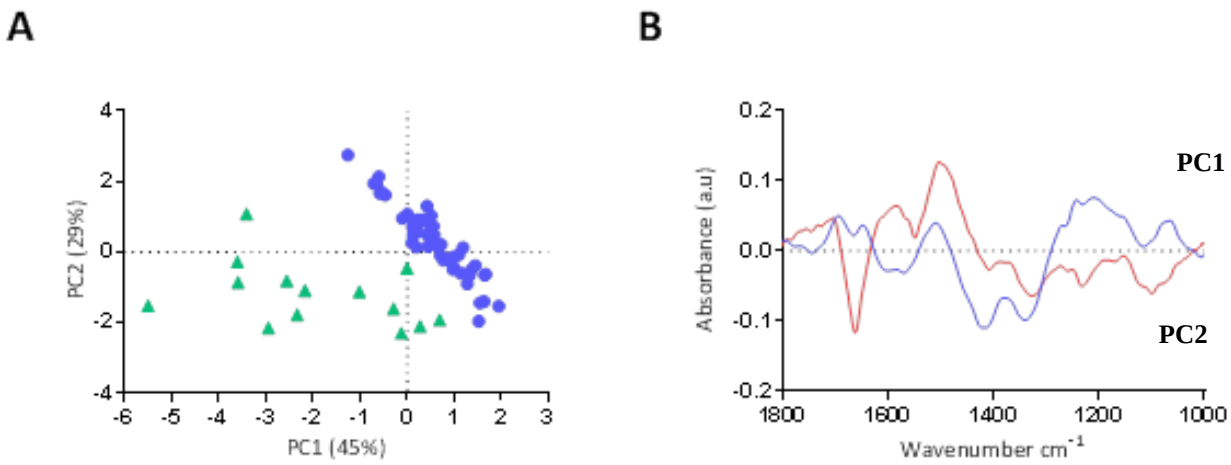

Figure 19. An example PCA, showing (A) Scores plot and (B) Loading plot.

The same software was also used to visualise the spectra, having translated the spectra from the support software used to obtain the data at Synchrotron facilities (Omnic and Opus). Descriptive statistics were also produced from The Unscrambler software. Graph Pad Prism 6 was used to create plots of the data.

Chapter 3 The Quantification, by SIFT-MS, of Acetaldehyde Released by Lung Cancer Cells in 3D Models.

3.1 Introduction

As discussed in Chapter One, lung cancer is a worldwide health issue with poor prognosis rates (typically 5-15% at 5 years) despite the introduction and constant refinement of new drugs and therapies into the management of the disease (Reck, M. 2013; Molina, J.R. 2008; Gkiozos, I. 2007) Screening for the disease using sputum cytology, chest x-rays or CT Scans may offer, in some cases, increased survival rates but it is not clear yet whether this has translated into decreased lung cancer death rates overall (Bach, P.B. 2012). The assessment of tumour response to treatment also relies heavily on these imaging processes, the pitfalls of which have been discussed in depth in chapter 1. This has lead for the need for a cheaper, real-time based, radiation free and non-invasive technique. SIFT-MS could offer these advantages to the field.

Early lung cancer diagnosis is currently a very popular topic within the breath analysis community. Gaining much attention is the hypothesis that lung cancer could be detected through the analysis of VOCs produced internally and then found within the exhaled breath of patients. If these biomarkers could be identified, they could be applied as a diagnostic tool to clinically assess ~~a~~ tumour response to treatment as well as identify those afflicted with the disease. Again, the SIFT-MS technique could be the diagnostic tool needed. The instrument is able to assess the humid, volatile breath provided by patients that have poor lung function capabilities and can perhaps only provide single exhalations, measuring in real time concentrations of volatiles that occur in few ppbv concentration. This obviates any sample

preparation needed and any invasive procedures required by other techniques (Van't-Westeinde, S.C. 2011).

Although direct breath analysis is an ideal technique to be applied in the diagnosis of lung cancer, it would also be of strong advantage to be able to diagnose the humid head space developed by *in vitro* cell cultures. This would have a number of advantages, firstly to be able to discriminate between cancerous and non-cancerous cultures but also to assess the possible markers given off during the tumour response to a treatment, for example the assessment of sensitivity to chemotherapy agents.

In the previous studies of lung cancer by the SIFT-MS (Filipiak, W. 2008; Smith, D. 2003) it has been shown that acetaldehyde[6] is a VOC of interest with regard to the study of both malignant and non-malignant lung cells. Unfortunately these studies have produced conflicting results about acetaldehyde and its release. Given that this work was conducted within a 2D matrix, it is reasonable to consider that the study of lung cancer should be completed within 3D matrices that would provide a more physiological environment. Tumour growth within the physiological state is more than just a monolayer of a single type of cells, but rather a complex tissue of varying cell types and conditions built within a 3D structure. The work in this chapter is conducted using collagen 3D models that provide an improved platform to study lung cells, creating a 3D scaffold in which the lung cells will be able to grow and proliferate into the further dimension that they would naturally be able to

[6] Acetaldehyde is known for being an intermediate in the metabolism of ethanol in humans. It is formed from the oxidation of ethanol by alcohol dehydrogenase. Outside of the human body, it is a widespread, naturally occurring liquid. It is found in plants, fruits, vegetables, cigarette smoke, petrol and diesel exhaust. It is reasonably anticipated as a human carcinogen (National Cancer Institute, 2015).

access. The chapter shall also explore the growth of different types of lung cell, including cancerous and non-cancerous cells, and to analyse if there are any notable changes between the volatiles each population would produce.

As this chapter explores not only cell type but also how the cell culture environment contributes to the VOCs produced or consumed by populations during cell metabolism it makes sense to examine not only a more physiological (3D) environment but also the media in which cells are grown. Commonly, studies have applied the suggested growth medium to cell cultures indicated by cell line providers. These media have differing components that could influence the metabolical processes undergone by cells and therefore the VOCs processed as a result. Although not commonly discussed across the previous studies, this chapter hopes to shed some light on the impact of specific growth conditions on the release of acetaldehyde.

This chapter discusses the published work on the quantification of acetaldehyde by lung cancer cells (CALU-1) compared to the acetaldehyde released by non-cancerous cells (NL20), both within a 3D model. This chapter also discusses the consequences of media choice in cell culture. The study broadens to look at 4 lung cell types and 2 different kinds of media used to prepare the cell samples, also grown within a 3D model.

3.2 Aims

1. To widen the examination of the release of acetaldehyde from differing lung cell types.

2. To improve the physiological environment that these cells are maintained in through the incorporation of a collagen 3D matrix.

3. To investigate the impact of differing media on the metabolism of VOCs by lung cell lines.

3.3 Materials and Methods

3.3.1 Cell Culture – Acetaldehyde comparison between CALU-1 and NL20

In order to compare between a cancerous and non-cancerous population the non-small cell lung cancer cell line CALU-1 (European Collection of Cell Cultures, Salisbury, UK) and the non-malignant lung epithelial cell line NL20 (ATTCC,UK) were used in this study. CALU-1 cells were cultured in Dulbecco's Modified Eagle Medium (DMEM) with 10% Foetal Bovine Serum (FBS) and glucose (4.5 g/L) within both the T75 Flask and the 3D collagen matrix. For NL20, Ham's F12 medium supplemented with FBS (4%), glucose (2.7 g/L) and growth factors (according to the provider's instructions) were used to culture the cells within the T75 flasks and the 3D collagen matrix. The tissue culture flasks (Starstedt, UK) were seeded with the relevant cell line and stored in a 37 °C, 5% CO_2 incubator. Culture medium was changed every 3-4 days (See Table I, Culture Conditions 1). Cells were first passaged and seeded at a density of 5 x 10^5/T75 and held in 2D culture for 1 week, in order to build-up the desired population. After this time the cells were dissociated (see Table I, culture conditions 1) and counted.

The desired number of cells was then seeded into a 20 mL 3D collagen matrix, rat tail collagen type I (BD Life Sciences, UK) at a collagen concentration of 1.5 mg/mL. Please see chapter 2, materials and methods for a detailed account on the production of collagen matrices). The suspended cell concentrations (10^6 cells per gel) were transferred into a 150 mL glass SIFT-MS bottle, fitted with a cap and septa. Bottles were placed within the incubator for 1 hour to solidify (caps partially open to allow for air flow). After this incubation time, the now solid scaffolds containing the cells were topped with 20 mL of freshly prepared liquid media (please see Table 1, culture conditions 1). A control gel without cells was also formulated at the same time point to be measured with the SIFT-MS to form a baseline measurement of the culture conditions. After the addition of fresh media to the cellular and control scaffolds, the gels were then left within the incubator, caps loose, for a further 24 hours. This was to ensure the cells had access to a suitably pH balanced and oxygenated air supply. The bottles were then air purged with dry bottled cylinder air (BOC, UK) and the caps closed tightly. A further 16 hour incubation time followed before a SIFT-MS measurement was taken, in order for a headspace to develop with VOCs from the cell population.

3.3.2 Cell Culture – Acetaldehyde comparison between 2 media and 4 cell types.

In order to make a comparison between 2 media and broaden the study of the effect of media on VOCs produced by cells, 4 cell lung cell lines were studied. A549, a lung adenocarcinoma cell line; CALU-1, a squamous lung cancer cell line; 35FL121, lung cell fibroblasts and NL20, a normal lung epithelial cell were included in this study. Further details of which are in chapter 2 Materials and Methods.

In order to assess the role of media within the VOCs given off by lung cells, each 1 of 4 cell lines were cultured in 1 of 4 ways. That is; firstly cultured in 2D with DMEM and moved into a DMEM gel. Secondly, cultured in 2D with DMEM and moved into a Ham's F12 gel. Thirdly, cultured in 2D in Ham's F12 and moved to a Ham's F12 gel. Finally, cultured in 2D in a Hams F12 gel and moved to a 3D DMEM gel. Please see Table 1, culture conditions 2 for the detailed components of each medium).

The culture conditions for the first part of the cell culture method here is the same as in culture conditions 1 (Table I). There only difference here being that NL20 media was changed slightly to incorporate the same concentration of glucose. This is because previous work has shown that the interaction with FBS and glucose and the metabolic influence of glucose on cells will produce an effect on the VOCs given off by cell lines (Sulé-Suso, J. 2009).

3.3.3 Survival Assays

In order to assess survival, the gels were scaled down into 200 µL gels containing 5 x 10^4, 10^5 or 2 x 10^5 populations of cells to broadly cover the cell numbers used in this study for SIFT-MS analysis. The samples were created within a 48 well plate, in triplicate, and left for an hour to set. Following this time, they were then topped with 1 mL of fresh media and cultured for 24 hours. Following a dry air purge the well plates were then sealed using parafilm before incubating within a 37 °C, 5% CO_2 incubator for 16 hours, mimicking the conditions used to create SIFT-MS samples. A standard live/dead cell double staining

kit (Sigma Aldrich) was used to stain the samples as per provider's instructions (For a more detailed instruction, please see chapter 2, Materials and Methods).

In order to assess cell survival using tyrpan blue, gels were downscaled by a factor of 10. The process above was repeated, this time scaling the gels down to 1 mL gels and seeding 10^5 cells per gel. Following the incubation times as above, the gels were then exposed to 200 µL of collagenase, placed on a rocker within the incubator and allowed to dissolve. A standard trypan blue exclusion method was then followed to count the live/dead cells.

A live/dead double staining cell kit (Fluka, 04511) was used to identify live and dead cells within the 3D models and imaged using a confocal microscope (Olympus, Japan). The 3D models used were 20 mL collagen gels, with a range of $10 – 40 \times 10^6$ cells seeded into each model. The models were those used in the SIFT-MS analysis and so underwent the same growth and preparation conditions for SIFT-MS experiments, but were then dissected and stained (as per the staining kit instructions) in order to be able to access the samples confocally.

Figure 20 is an example of (A) 1 mL scaled down gels, within a small SIFT-MS sampling bottle. (B) 200 µL gel scaled down, within a 24 well plate. (C) A dissected 10 mL collagen gel used for live/dead imaging of the cells and (D) the dissected and stained samples of the 3D model.

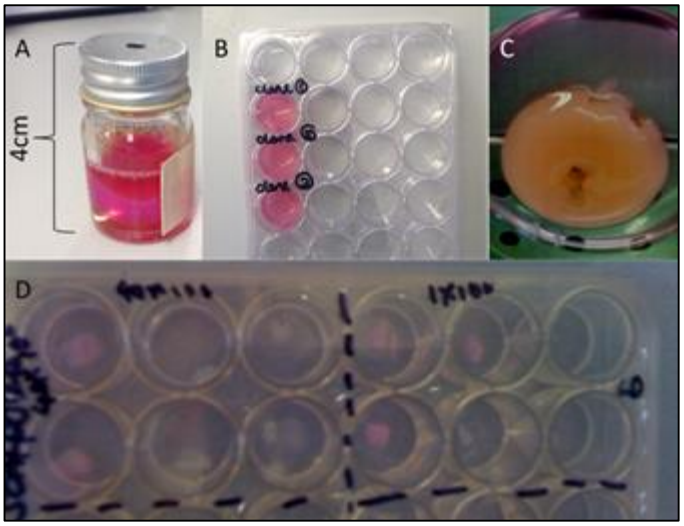

Figure 20. 3D collagen models in different formats. (A) A scaled down bottle sample. (B) 200 µL gel, (C) a dissected 10 mL gel and (D) dissected and stained samples.

3.3.4 SIFT-MS Spectra

Spectrometry measurements for both Part 1 and 2 were taken using the *Profile 3* SIFT-MS instrument (Trans Spectra Limited, UK, described in detail within chapter 2). The reagent ions selected for analysis were H_3O^+ and NO^+ given their suitability to react with the organic volatiles that could be given off by the cell cultures, known from previous studies.

A standard list of selected compounds were scanned in the "MUI" mode software, each headspace being sampled for approximately 1 minute. Compounds were chosen based on previous work completed using the SIFT-MS (Sulé Suso, J. 2009; Smith, D. 2003; Smith, D. 2011). The on-board kinetics library was able to ascertain the reaction rate and therefore quantity of the specified compounds (Smith, D. 2011) A "full scan" range was also collected for each sample, a mass range of 10 – 180 m/z was collected from 3 repetitions of 20 seconds each; 1 minute scanning in total for both reagent ions. For all samples, the

septa contained within the cap of each 150 mL bottle was punctured by the heated sampling needle of the SIFT-MS.

3.3.5 Processing

Once the profile of each headspace has been ascertained using the "MUI" software, the data is extrapolated into excel. Although the library has corrected the data for interactions and overlaps between some of the product ions (for example acetaldehyde and CO_2 having an overlap at m/z 63 in the presence of H_3O^+), it does not account for a slight variation in the humidity within the samples or in the laboratory environment. Humidity is what the quantification of product ions is based on and so here we "correct" the samples by bringing all values of products ions to what they would be if all were collected within an environment based on the humidity found within the breath of a patient (6% H_2O). This allows us to better mimic the conditions of the breath of a patient as opposed to the fluctuations seen within the bottle and laboratory environments.

3.3.6 Analysis

The analysis of the data was performed within excel (Microsoft) and GraphPad (Prism 6), to plot relevant tables and graphs.

3.4 Results

3.4.1 Survival within Collagen 3D models

The trypan blue exclusion method provided evidence that cells were alive and proliferating within the 3D models that they were seeded into. The average survival was always above 76 % for all four cell lines grown under both DMEM and Ham's F12 media.

Table II Average survival rates of 4 different cell lines grown in 2 different kinds of cell culture medium (mean of 3 independent samples).

	Average % Survival											
Media	**DMEM**						**Ham's F12**					
Cell No.	**5 x 10^4**		**10 x 10^4**		**20 x 10^4**		**5 x 10^4**		**10 x 10^4**		**20 x 10^4**	
	%	**SD**	**%**	**SD**	**%**	**SD**	**%**	**SD**	**%**	**SD**	**%**	**SD**
A549	81.39	7.50	83.08	8.14	81.77	3.97	79.37	11.00	88.33	7.26	91.32	4.85
CALU-1	79.37	8.84	81.21	9.15	79.42	1.00	91.07	7.78	89.95	9.08	95.08	5.00
35FL121	85.00	13.23	88.33	12.58	76.77	8.75	84.72	16.84	93.45	6.27	91.82	5.29
NL20	84.87	4.50	83.02	2.87	87.67	7.14	82.65	2.38	89.68	9.01	92.72	4.68

As seen in Figure 21 the survival rates within the gels kept under SIFT-MS conditions were good. The figure provides two examples of (A) CALU-1 at 10 x 10^6 cells and (B) NL20 at 10 x 10^6 cells taken using a 10x objective. The green colour (live cells) is appearing at a far higher level than the red (dead cells) and is also highlighting a healthy cell morphology. That is, that the cells are making use of their new 3D environment and appear to be spreading along the collagen fibres as opposed to the limited 2D morphology they are restricted to in

flasks. We can also observe the larger size of the CALU-1 (A) compared to the smaller NL20 (B) and the characteristic clustering that CALU-1 are known for in culture.

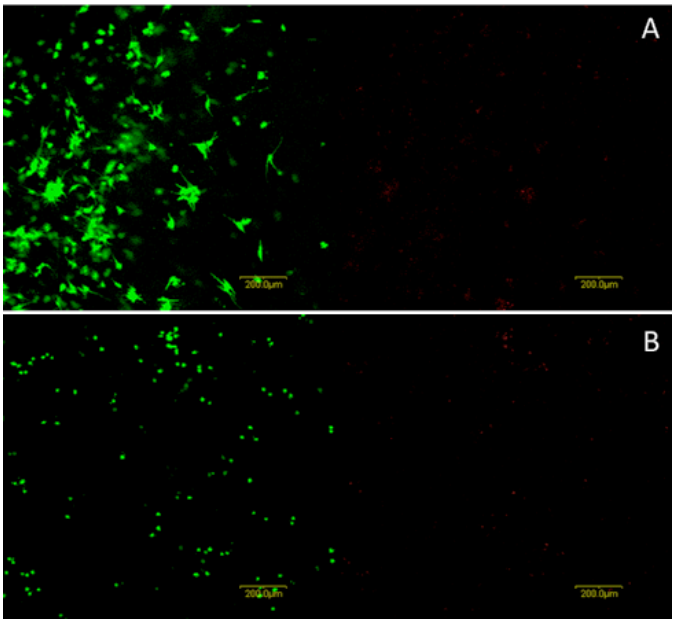

Figure 21. Live/Dead images of (A) CALU-1 and (B) NL20. Live cells are shown in green and dead cells are shown in red.

3.4.2 Acetaldehyde Release

The first observation to be made is perhaps a comparison to the earlier 2D studies performed on CALU-1 lung cancer cells that were grown directly in the SIFT-MS sampling bottles (Sulé-Suso, J. 2009). The earliest of these studies showed that AC release was directly proportional to cell population. acetaldehyde levels being produced at 10^6 molecules/minute of incubation time per cell. 40 x 10^6 cells that were cultured in 50 mL of fresh media produced acetaldehyde at a level 300 ppbv greater than the media alone was producing. In 2009, Sulé-Suso *et al.* found similar results within the headspace, acetaldehyde being at a concentration of 400 ppbv per 50 x 10^6 CALU-1 cells and increasing to 500 ppbv for 80 x 10^6. The level of acetaldehyde above the DMEM medium controls being 250 ppbv (Sulé-Suso, J. 2009). Interestingly, the NL20 cells used within this study (NL20 being a

normal lung cell line) produced lower levels of acetaldehyde, 50 $x10^6$ cells producing 300 ppbv and their media, Ham's F12 baseline extruding 100 ppbv.

The 2D results mentioned above also show an obvious trend, that with decreasing cell number the levels of acetaldehyde steadily decrease (however not for NL20). This is not the same trend that we see with the CALU-1 3D samples (Figure 22). Starting with the cell number most similar to those used within the 2D studies we can see that at cell populations of 20-40 $x10^6$ produce dramatically higher levels of acetaldehyde within their 3D environment than the 2D, by a factor of 2.

Following the observation of these differences further experiments were conducted to examine lower cell numbers. Figure 22 is a representation of the data in Table III, clearly illustrating the trend of acetaldehyde release for cells grown in 3D models. 3D Calu-1 cell populations of 10^6 are still producing double the ppbv of acetaldehyde than 40 x 10^6 cell populations grown within a 2D environment. 10^6 cells cultured within the 3D environment in fact produce the largest amount of acetaldehyde out of all cell populations, at a mean of 1973 ppbv (SD 122). This level then dramatically tails off to a mean value of 1304 ppbv (SD 219) at 10^5 and as illustrated in Figure 22. It continues to do so until reaching the baseline levels measured in the headspace of medium and 3D a-cellular scaffolds. Maximum to minimum concentrations of acetaldehyde levels obtained from 2D and 3D counterparts were calculated to range from a factor of 1.15 and 2.16, this being far greater than the inherent variability of the SIFT-MS instrument itself, which is less than 5%.

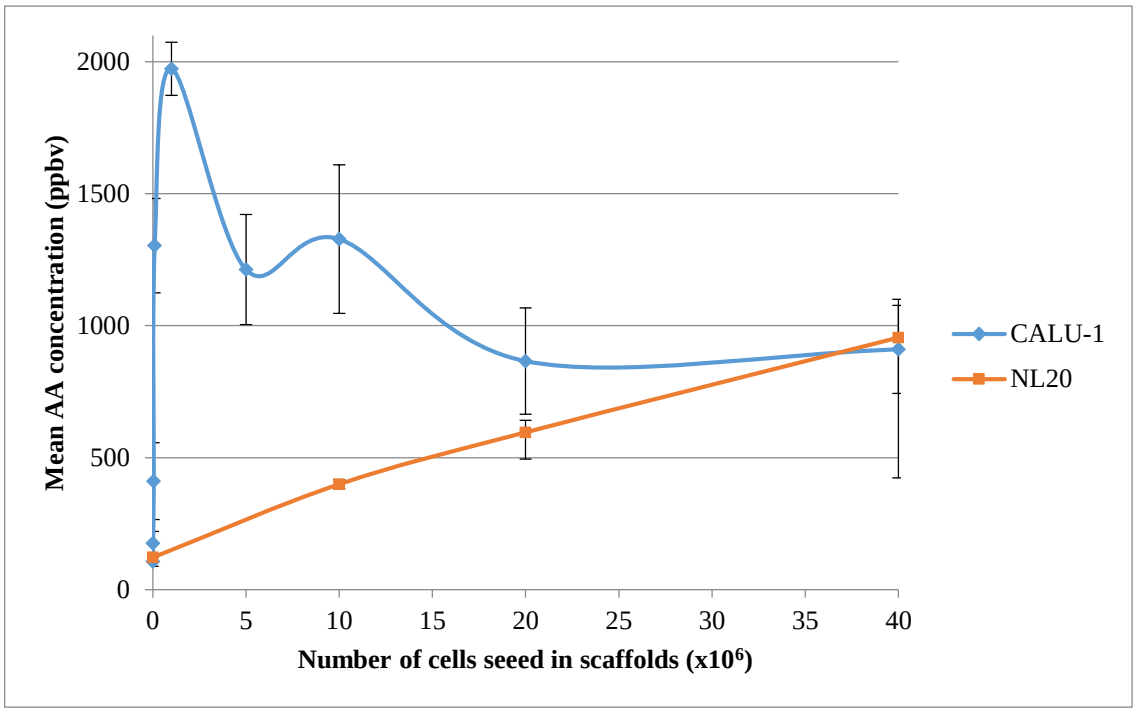

Figure 22. Average acetaldehyde release (ppbv) of 2 different cells lines, CALU-1 and NL20 grown in a 20 mL 3D collagen model.

Table III Acetaldehyde release (ppbv) by CALU-1 and NL20 cell lines grown in a 20 mL 3D collagen model.

Cell type	Number of cells seeded ($\times 10^6$)	AA concentrations (ppbv)	Mean (ppbv)
CALU-1	0	81, 99, 103, 114, 135	106
	0.01	113, 196, 218	176
	0.05	307, 310, 617	411
	0.1	1122, 1242, 1547	1304
	1	1862, 1909, 1946, 1996, 2154	1973
	5	1042, 1089, 1151, 1568	1213
	10	1060, 1157, 1170, 1411, 1842	1328
	20	550, 855, 869, 869, 1187	866
	40	687, 787, 931, 974, 1174	911
NL20	0	98, 113, 130, 133, 136	122
	10	383, 385, 394, 402, 432	399
	20	456, 530, 595, 643, 755	596
	40	505, 698, 745, 830, 1995	955

Regarding NL20, and conforming to the trend previously seen in the 2D studies discussed here; that acetaldehyde production steadily increases with the cell population. We still see dramatically elevated levels of acetaldehyde within the 3D cultured cells, compared to the 2D, acetaldehyde being produced by around a factor of 2.

2.3.2.1 Average acetaldehyde release (ppbv) comparison between 2 medias and 4 cell types.

Figure 23 illustrates the average acetaldehyde release in 10 mL collagen gel scaffolds, by 10^6 cells. The first, m\ost obvious, observation to make is that there is a dramatic increase of AC given out by those cells grown in DMEM media and then seeded into DMEM based gels (DMEM – DMEM). This is most pronounced in the cell line A549, where a 165 times increase is seen above those cells that are cultured in DMEM and transferred into a Ham's F12 based gel (DMEM – Hams). There is a 7 times increase above those grown in Ham's F12 and put into a DMEM gel (Hams – DMEM) and an 18 times increase seen above those that are cultured and transferred in Ham's F12 (Hams – Hams).

The trend seen within CALU-1 is that in DMEM media DMEM gel cultured cells, there is an 18 times increase of acetaldehyde production compared to those DMEM – Hams cultured cells. Only a 4 times increase over that of the Hams –DMEM cultured cells and a 22 times increase above the Hams- Hams model.

The normal lung fibroblasts, 35FL121, mimic a similar trend to that seen within the CALU-1. A 31 times increase in DMEM – DMEM grown cells is seen above those cells

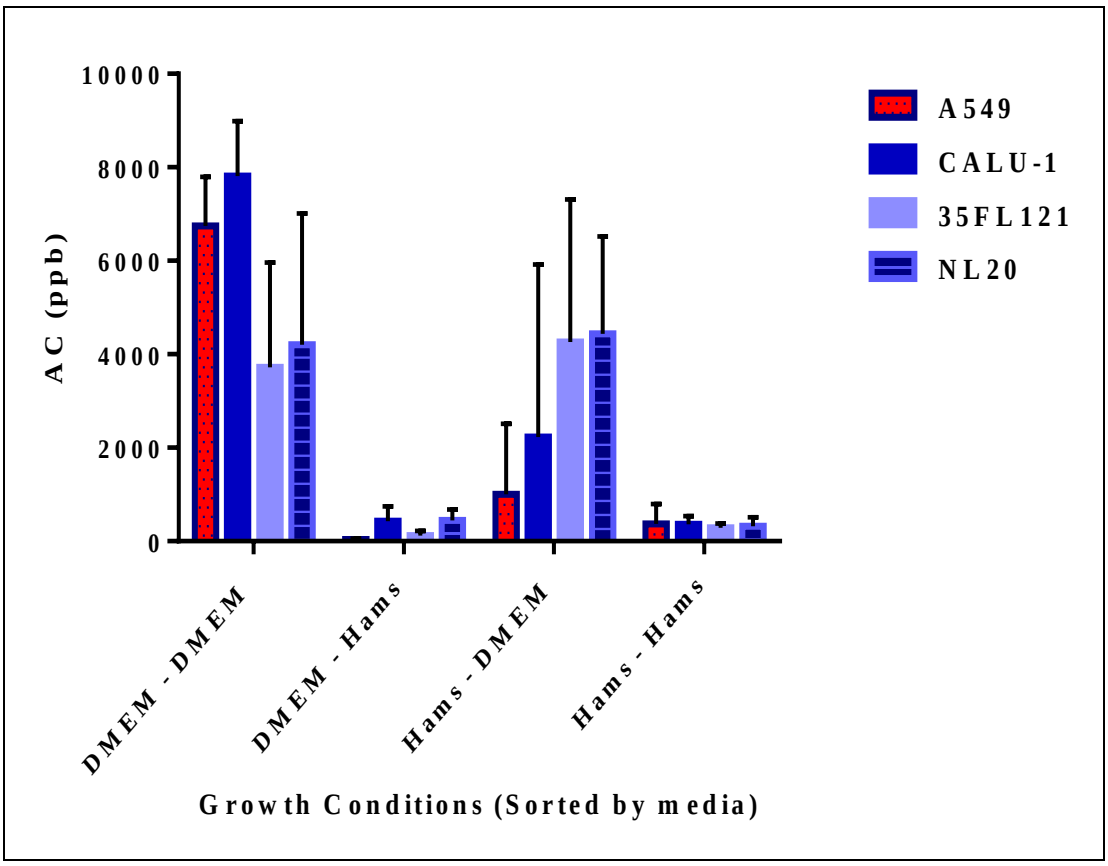

Figure 23. Acetaldehyde release in 4 cell types, A549, CALU-1, 35FL121 and NL20, grown in 10 mL 3D collagen models.

grown in DMEM – Hams conditions. Cells cultured in Hams – DMEM conditions produce a similar abundance of acetaldehyde as DMEM – DMEM grown cells. A 12 times increase is seen from those grown in a Hams – Hams model.

The NL20 cell line, again also elicits the same behaviour, DMEM – DMEM cells producing a 9 fold higher acetaldehyde level that those grown in DMEM – Hams. Hams – DMEM grown cells produce a similar amount of acetaldehyde as DMEM – DMEM grown cells. A

13 fold higher acetaldehyde level is produced in DMEM – DMEM than those grown in Hams – Hams models.

3.5 Discussion

The study of 3D CALU-1 and NL20 cells, within a 20 mL 3D collagen gel has raised many questions about the production of acetaldehyde from cells.

It is widely known that acetaldehyde is formed from ethanol metabolism via the alcohol dehydrogenase (ADH) enzyme present within the cells themselves (Figure 24). During this metabolic process acetaldehyde is also lost during metabolism, resulting in acetic acid (largely occurring as acetate ions in neutral solutions). Co-enzymes nicotinamide adenine dinucleotide (NAD^+) also participate in this process (Kalapos, M.P. 2003; Riveros-Rosas, H. 1997).

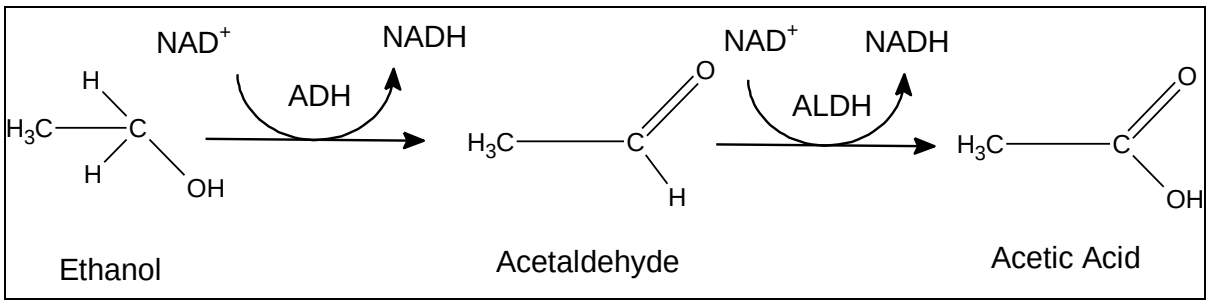

Figure 24. Ethanol metabolism by ADH, acetaldehyde being produced as an intermediate of acetic acid production by ALDH.

Saturated hydrocarbons (eg. ethane, pentane) and aldehydes are also products created during the lipid peroxidation process, undertaken within the cell membrane (Mazzone, P. J. 2008). During the SIFT-MS measurements, several compounds aside from acetaldehyde were also

measured during the analysis. Ethanol was also found to be rather prevalent within the headspace of the 3D cultures, at a level of around 2000 ppbv. Previous studies have indicated that it originates for the most part from FBS that is added to the medium as it is prepared (Sulé-Suso, J. 2009). Therefore, ethanol which could play a role within the production of acetaldehyde within the headspace, is already intrinsic to the cell culture environment. Acetaldehyde can also be measured in the headspace of DMEM of the media itself, being present at a level of 100 ppbv on average.

A major question surfacing from the results is also the cause of the dramatic increase in acetaldehyde production within 3D environments when compared to 2D. The remit behind using the 3D system is of course to mimic more readily the *in vivo* environment in which the cells would naturally reside without having to include the disadvantages direct *in vivo* study of organ systems could bring (Petersen, M.C. 2007). Figure 21 demonstrates the aptitude for the CALU-1 cells to survive within the collagen 3D models, however it has not been possible at this stage to identify whether cells are proliferating within this system. However, earlier work has also shown that CALU-1 cells will also readily invade a collagen based hydrogel and proliferate within the same type of system (Yang, Y. 2005).

It is not yet clear as to why there is a decrease in the acetaldehyde production of cell number beyond 10^6 but we could hypothesise that with increasing cell populations being put into the same environment, the proliferation rate of the cells would decrease, or perhaps slow down the metabolic processes involved in the release of acetaldehyde due to the consumption of nutrients from the media provided to the population. Further work would be needed to clarify

whether cell death, proliferation changes or changes to metabolism could be behind the change in acetaldehyde production.

Through standard deviations within the results we can also observe the variation of acetaldehyde release within the samples, when in previous work variation was fairly limited (Smith, D. 2003; Sulé-Suso, J. 2009). The culture methods behind the studies differ slightly. In this study, cells were left within the 3D environment for an extra 24 hours, this was to allow cell populations to acclimatise to the new gels, having being transferred from a 2D flask system. This extra culture time could perhaps explain the variation seen in acetaldehyde levels.

The study has produced two notable points based on the data presented here. Firstly that the VOCs produced by lung cancer samples are dependant heavily on the cell culture conditions and the experimental parameters under which the samples are produced (namely the 2D vs 3D growth conditions). Secondly, the difference in the levels of acetaldehyde produced between lung cancer and normal lung cells is so high, by a factor of 3, that further work will be required to extend the analysis of acetaldehyde to more lung cell types.

The study of 4 different lung cells lines grown in one of 4 growth conditions, within a 10 mL 3D model, has suggested that the role media has to play on the VOCs released by cells is great. The difference in acetaldehyde release of those cells grown in DMEM media and DMEM gel compared to those under the influence of Ham's F12 media is marginally larger, across all four cell lines, suggesting that a component of the media is influencing the cell's metabolism of acetaldehyde in some way.

Importantly the first observations here are that a cancerous cell line, CALU-1, may produce greater levels of AC than the normal counterpart, NL20, is fortunately extended to A549 (an adenocarcinoma) within those cells grown in DMEM media and transferred to a DMEM gel. Unfortunately this is not a pattern seen across the other 3 culture conditions. This could have implications for using acetaldehyde as a diagnostic marker for cancer, as there could be a component of the media required to see this difference. It is therefore increasingly necessary to try and identify this mechanism.

As discussed previously, the presence of acetaldehyde in mammals is as an intermediate in the metabolical pathway of ethanol (Riveros-Rosas, H. 1997). But acetaldehyde can also be found elsewhere. Threonine aldolase (TA) catalyses a pyridoxal-dependant, reversible reaction between threonine and acetaldehyde plus glycine (Ogawa, H. 2000) and is a common metabolical pathway studied in microbial subjects (Figure 25). Literature suggests that the role of TA within animal tissues is relatively unexplored, especially when compared to a second enzyme, serine hydroxymethyltransferase (SHMT) which has been found to be responsible for a majority of threonine degradation in animal tissues. Interestingly, both pyridoxal and threonine are components within the cell culture media within this study (Please see Appendix for a full list of media components) and could be serving to trigger a metabolic process involving TA.

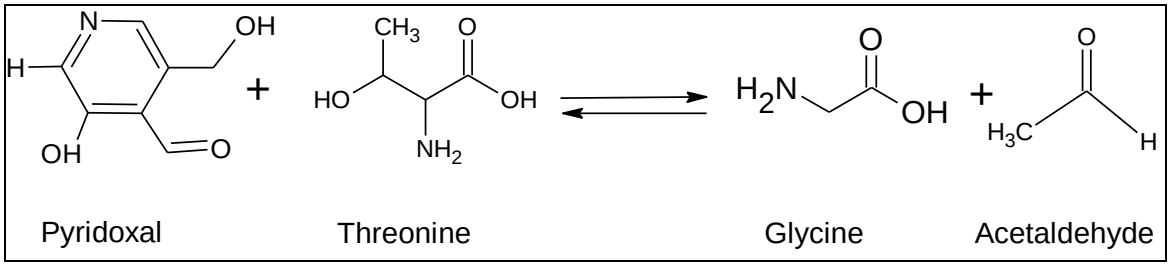

Figure 25. The reversible reaction of threonine with pyridoxal to produce glycine and acetaldehyde.

Table IV illustrates the levels of both pyridoxal and threonine found within the media and 3D model used within this study. The "10x MEM powder" and the "10x Hams F12 powder" being the base medium used to create the 3D model gel used here.

Table IV Levels of pyridoxal and L-threonine found within 2 different cell culture medium types (mg/L).

	Concentration mg/L	
	L-Threonine	**Pyridoxal Hydrochloride**
DMEM	95	4
Ham's F12	11.9	-
10x MEM Powder	48	1
10x Ham's F12 Powder	11.9	0.06

If the metabolical pathway being triggered here is TA dependant, the table goes some way to explaining the results that have been found with the differing culture methods. The cells have the most contact with 3D model as they are embedded into it, although there is an exchange flow with the medium in this model. The table shows clearly that DMEM has

higher levels of both threonine and pyridoxal, compared to the Ham's F12 media, this correlates with the levels of acetaldehyde production found within the cell containing samples. Interestingly, the cells grown in DMEM – Hams models did not yield much acetaldehyde and cells cultured within Hams – DMEM models produced around half the amount of acetaldehyde as those cultured in DMEM – DMEM models. This could be due to the higher prevalence of threonine and pyridoxal in DMEM – DMEM models and also due to the direct contact cells have with higher levels within the Ham – DMEM model over that of the DMEM – Hams model. Further work is needed to explore these finding and investigate the TA pathways that may be being triggered here.

Each media was also assessed for components that may inhibit ADH or ALDH action. Appendix 5 is comprised of both activator and inhibitors of ALDH and ADH enzymes for reference. None of the media contain any inhibitors of either enzyme, except for L-tryptophan. Ham's F12 was found to contain 2 mg/L, 10 mg/L in 10x MEM and 16 mg/L in DMEM. Previous studies in mammalian tissues have already identified L-tryptophan as an inhibitor of ALDH2 specifically (Badawy, A.A. 2011; Badawy, A.A.B. 2007). ALDH2 is one of the 19 isozymes of ALDH, with the highest affinity for acetaldehyde oxidation than other isozymes from the same family (ALDH1A1 and ALDH1B1) that have also been known to contribute to acetaldehyde `metabolism (Koppaka,V. 2012; Badawy, A. A. B. 2007; Wang, M. 2009). Badawy, A.A. *et al* (2011) found that an acute exposure of L-tryptophan (and its metabolites) in rat livers at doses between 1-10 mg/kg were effective after as little time as half an hour. It is therefore reasonable to assume that the L-tryptophan present in the media used here could have an effect on the ALDH2 activity in the cells. Further work is needed to examine the quantity of ALDH2 enzymes present within the 3D models used in this thesis, to establish the significance of the level of L-tryptophan dosage

being applied here. Although non-specific to ALDH2, the ALDEFLUOR^{TM} Kit (Stemcell Technologies) which utilises flow cytometry techniques to identify ALDH activity, would be a practical starting point to help quantify this level in the cell lines used.

The results presented here are of significance not only to a cell culture community but also to the oncology community. ALDH levels have been found to be elevated in cancer stem cell populations (Tanei, T. 2009) and have been examined as functional marker/markers of tumour initiator cells for various cancers such as bone (Wang, L. 2011), breast (Croker, A. K, 2009), colorectal (Dalerba, P. 2007), thyroid (Todaro, M. 2010) liver (Ma, S. 2008), prostate (van den Hoogen, C. 2010), pancreatic (Kim, M. P. 2011), head and neck (Clay, M.R. 2010) and lung cancers (Ucar, D. 2009; Moreb, J.S. 2008) to name a few. Several studies have related ALDH activity to the resistance of cancer to chemotherapy agents, alluding to a cause for relapse in cancer patients (Kim, M. P. 2011; Honoki, K. 2010). Many of these studies have not examined the role of ALDH2 specifically, often opting to look at the ALDH family (non-specially) or the more commonly expressed ALDH enzymes seen mammalian tissues (ALDH1A1 and ALDH1B1). This study has the potential to provide a new technique that could identify ALDH activity through the acetaldehyde produced by the cell cultures here and detected with SIFT-MS. It has also raised important questions about the effect of the cell culture conditions used in the previous studies listed here that have utilised cell lines in their methodologies.

3.6 Conclusive Remarks

The role that acetaldehyde could play as a biomarker within the clinical setting to help identify cancerous populations is justifiable. Acetaldehyde is a known carcinogenic and

mutagenic agent; that is, it is disruptive to the synthesis of DNA (Jelski, W. 2008), binding to proteins causing both structural and functional alterations (Guo, R. 2010) of the enzymatic processes involved in DNA repair (Seitz, H.K. 2007). All these being factors that could contribute to the development of a tumour.

ADH activity is also significantly higher within some cancerous tissues than within healthy ones, for example in the liver, stomach, oesophagus and colorectal (Jelski, W. 2008), which could suggest that cancer cells here would have a greater ability to undergo ethanol oxidation, producing higher levels of acetaldehyde. The same cancer cells are also noted to have decreased activity levels of ALDH when compared to ADH and so are less efficient at removing the acetaldehyde that they have created (Jelski, W. 2008). The data presented here conforms to the findings from the Jelski *et al.* (2008) group, that acetaldehyde is released in far higher levels than that found within the normal lung samples.

This work should be continued, acetaldehyde production clearly being dependant on some aspect of the cell culture conditions used in the study. This has implications not only for acetaldehyde's use as a practical way to identify lung cancer but also as a methodological consideration for cell culture experiments. The data from all of the SIFT-MS studies within this chapter is promising, but further work would be required to assess if such a large differential in acetaldehyde is identifiable within the breath of patients and control cases without lung cancer.

Chapter 4 The Application of Labelled Compounds for use with VOC Analysis using SIFT-MS

4.1 Introduction

SIFT-MS (*Profile 3)* is a highly sensitive technique that is able to assess changes in VOCs in real time (Smith, D. 2011; Smith, D. 2011; Španěl, P. 1996). This increased sensitivity is able to pick-up subtle differences in the change of VOCs given out by cells that could be due to a change in their metabolic processes. Already we have seen, as discussed earlier, that literature has reported two differences in the metabolism of acetaldehyde in the cancerous cell line CALU-1 (Mazzone, P. J. 2008; Sulé-Suso, J. 2009; Rutter, A.V. 2013). It has also been reported that the interaction between the components in the culture medium can also generate a VOC signature that will contribute to the headspace of cell cultures (Please see chapter 3). Both ethanol and acetone baseline levels seen in a-cellular samples (containing only DMEM media and supplements) have been attributed to the FBS (10%) content (Sulé-Suso, J. 2009). In fact baseline levels of acetaldehyde, ethanol and acetone were present in these controls. Further investigation in this study concluded that these compounds originate from the FBS over than of the glucose within the medium, through the sampling of headspace from neat FBS serum alone. This is an unsurprising conclusion as these compounds are already known as being produced endogenously within mammals. Acetaldehyde was also reported in the CALU-1 cell line containing samples, by a markedly higher level, indicating that the cells themselves are in fact responsible for this production.

Studies like this highlight the importance of the contribution made by the components of the medium to our VOC profiles. Chapter 3 has already identified some of the issues associated with using different medium in cell culture for the same cell lines. In this chapter the 3D

model will again be utilised to increase the physiological aspect of the lung cell culture, with a focus on the glucose metabolism seen within these models.

Further to these studies, the role of glucose metabolism in cancer is a hot topic and has been for some time. The Warburg effect being one of the oldest and hotly debated cancer phenomenon (Warburg, O. 1956; Warburg, O. 1924).

The Warburg effect hypothesises that cancer metabolism differs from normal tissue by rate of glucose metabolism. In fact metabolising glucose up to 10 times faster and undergoing a rate of glycolysis over 200 times higher in cancerous tissues, producing lactic acid under aerobic conditions (Kim, J.W. 2006; Koppenol, W. H. 2011). The study of this key metabolic change in tissue behaviour is mainly characterised through inferred gene/protein expression, and whilst useful does not provide a complete story of the metabolic changes that occur within a malignant phenotype, and also the lack of a real-time *in situ* practise (Fisher A.B. 1984; Fan, T.W. 2009) for the diagnosis or disease monitoring that lung cancer so desperately needs.

One such avenue to study glucose metabolism is to utilise ^{13}C labelled compounds, as diagnostic tests for human metabolic studies. The use of a diagnostic probe in the form of the stable isotope[7] ^{13}C can be applied to identify changes in metabolism in the presence of a disease or the activity change of a specific enzyme. This can be identified through the observation of $^{13}CO_2$ after the application of a labelled ^{13}C compound. This is a relatively

[7] Isotopes are elements that have the same number of protons in each atom, but differ in neutron number.

old practise, the ^{13}C labelled compounds first being used by Lacroix in 1973, who utilised ^{13}C labelled glucose to study oral glucose tolerance tests and the isotopic ratio of expired CO_2. The ingestion of a labelled compound (glucose) produced a markedly increased ratio of the isotope $^{13}CO_2$ to $^{12}CO_2$ in the expired breath of their participants (Lacroix, M. 1973). ^{13}C studies are hugely attractive to the clinical world, being non-invasive, non-radioactive, simple, safe, fast and economic (Amann, A. 2013).

Lung cancer specifically has also been studied through the ingestion of ^{13}C labelled glucose. Metabolic changes were investigated in lung cancer patients through the infusion of ^{13}C labelled glucose into lung tissues, following which, nuclear magnetic resonance (NMR) and GC-MS techniques were used to investigate extracts from tissues and blood plasma (Fan, T.W. 2009). The study found many metabolites to be considerably upregulated within the lung cancer tissues and notably showed the upregulation ^{13}C-2,3 Glu isotopomer – leading to the conclusion that pyruvate carboxylation (PC) was activated in the cancerous tissues. It is thought that this upregulation occurs to fulfil a high anabolic demand of a rapidly proliferating tumour tissue (Fan, T.W. 2009). This work provides a platform in which to apply SIFT-MS to see if these metabolic changes found using previous techniques could be seen in the VOCs in human breath or indeed from the cancerous cells *in vitro* and compared to their normal counterparts. SIFT-MS would also provide perhaps a more suitable clinical technique than those used in the study above, as no tissue processing is needed and the results could be analysed immediately with little expertise.

Encouragingly, 3 ^{13}C labelled breath tests are already FDA approved and clinically used in the United States, the first being ^{13}C labelled urea for the detection of *H.Pylori* infection

(Graham, D. Y. 1987), the second a test for asthma (Silkoff, C. 2004) and thirdly, an alkanes breath test for heart transplant rejection (Phillips, M. 2004). The SIFT-MS therefore should be seen as a suitable and exciting clinical candidate.

4.2 Aims

To improve the overall experimental setup of measuring lung models with SIFT-MS in two ways;

1. Firstly, to improve the lung model, moving to a 3D construct and establish the appropriate medium to grow cells in, required for SIFT-MS analysis.
2. Secondly, to examine a methodology leading to identifying labelled VOCs, in this case from labelled glucose, within samples that could then be used as metabolical markers.

4.3 Materials and Methods

4.3.1 Cell Culture Conditions

Four lung cell lines were investigated in this chapter. A549 is an adenocarcinoma of the lung, CALU-1 a squamous carcinoma of the lung, 35FL121 a lung cell fibroblast and NL20 which is a normal lung epithelial cell line. Further details are given in chapter 2, Materials and Methods.

Prior to SIFT-MS experimental setup, all cell lines were maintained under culture conditions 1 (Please see Table I in chapter 2), media changes completed every 2 days and passage, as listed, weekly.

3.4.2 Generation of 3D Collagen Models

10 mL of 3D model was created from rat tail collagen (10.59 mg/ mL, BD Life Sciences), details of which can be found in chapter 2. 10x PBS was used as the base medium for the creation of the matrix. Gels were produced to have a final concentration of collagen of 1.5 mg/mL. Where appropriate, 10^6 cell populations were incorporated into the solution before being set.

Final 3D models were then topped with 10 mL PBS supplemented with 10% FBS and either glucose or glucose^{13} at a concentration of 4.5 g/L.

3.4.3 Survival Assay

1 mL gels were created to mimic the samples in this study. Gels were created according to the same protocol within chapter 2, Materials and Methods. Gels were created in 48 well plates, air purged and sealed with parafilm (to mimic the sealing process that the bottles undergo) and placed within a 37 °C, 5% CO_2 incubator for 24 hours. Following this cells were removed from the scaffold (again, please see chapter 2). Cells were then counted with trypan blue to determine the percentage viability of the sample.

3.4.4 Preparation of Cultures in SIFT-MS Bottles

The gelation of the 3D models was completed in SIFT-MS experimental bottles, 150 mL in size, fitted with a steal cap and rubber septum that allows the penetration of the SIFT-MS sampling needle. Once the liquid model was added to the bottle, the sample is then covered

with the cap and put in the incubator to set for 1 hour. Following which, 10 mL of PBS medium added to the top of the set gel. The samples are then purged for 1 minute with dry cylinder air. The sample bottles were then sealed with the cap and parafilm and placed back into the 37 °C, 5% CO_2 for 23 hours.

3.4.5 SIFT-MS Analysis

Following the total 24 hour incubation period, the headspace of the samples was measured with a *Profile 3* SIFT-MS instrument. Two precursor ions, H_3O^+ and NO^+ were both used to analyse the headspaces using both MUI and Full Scan modes of the instrument. The headspaces of each bottle were sampled for 1 minute.

3.4.6 Post Analysis Correction of SIFT-MS data

Samples were corrected to have 6% water levels within each headspace using the flow rate function built into the SIFT-MS software as accurately as possible. Microsoft excel was then used to normalise the data to 6% exactly.

3.5 Results

4.4.1 Survival Data in Unlabelled Glucose (^{12}C) and Labelled Glucose (^{13}C) 3D Models

Survival data for 24 hours in a PBS based model is greater than 70% in all cell lines (Table V).

Table V. Survival data for 4 different lung cell lines grown in a PBS based 3D collagen model with both labelled (^{13}C) and unlabelled (^{12}C) glucose supplemented culture medium (mean of 3 independent samples).

		Average (%)	SD
Unlabelled (^{12}C) Glucose	**A549**	83.70	14.29
	CALU-1	76.49	8.58
	35FL121	75.79	9.55
	NL20	78.87	8.75
Labelled (^{13}C) Glucose	**A549**	83.33	14.43
	CALU-1	88.89	19.25
	35FL121	72.70	6.76
	NL20	84.13	16.72

4.4.2 Acetaldehyde Release Seen Using H_3O^+ Precursor

Figure 26 shows the acetaldehyde released from all cell types under both unlabelled (indicated with a ^{12}C) and labelled (indicated with a ^{13}C) glucose conditions. The data are taken from MUI sampling profiles using the H_3O^+ precursor.

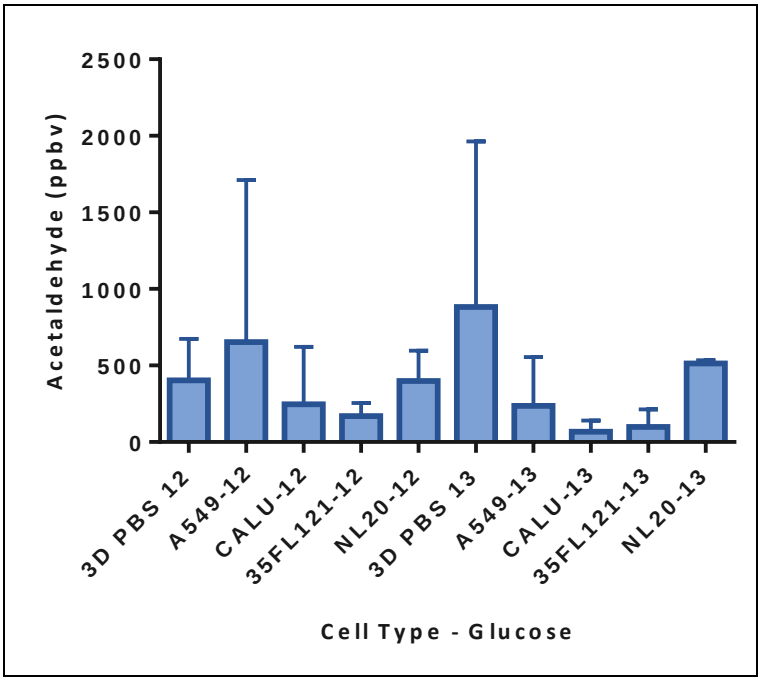

Figure 26. Acetaldehyde release from 4 different lung cell types, grown in PBS based 3D collagen models, supplemented with labelled (^{13}C) and unlabelled (^{12}C) culture media using H_3O^+ precursor (N=3).

4.4.3 FSM profiles using H_3O^+ precursor

Figure 27 displays the average (N=3) plot of FSM profiles taken using the H_3O^+ precursor ion for the range m/z 10-180. The heat map displays the highest abundance of the compound m/z 19, seen as an obvious red line and denotes the H_3O+ compound used as the precursor ion. The other prominent bands seen clearly in the heat map are at m/z 37, 55 and 73 which are hydrates of the precursor ion formed on the association with water vapour in the sample.

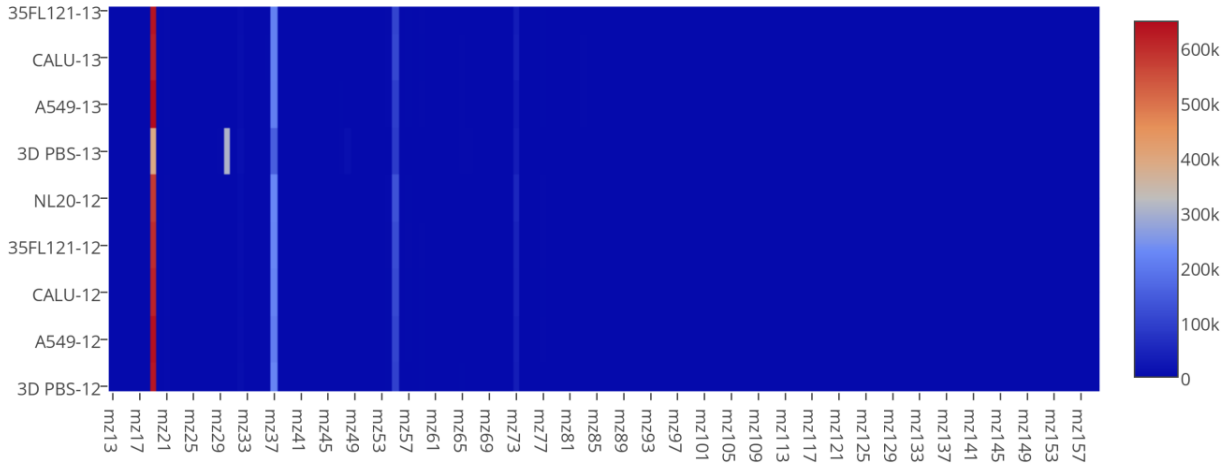

Figure 27. Heat map displaying the full scan profiles of 4 lung cell lines, grown in a PBS based 3D model analysed with H_3O^+ precursor ion. The colour denotes the abundance of the compounds (red being 6 x 10^5 counts/sec - blue being 0 counts/sec).

4.4.4 FSM profiles using NO^+ precursor

Figure 28 displays the average (N=3) plot of FSM profiles taken using the NO^+ precursor ion for the range m/z 10-180. The heat map displays the highest abundance of the compound m/z 30, seen as an obvious red line and denotes the NO+ compound used as the precursor ion. Other bands here are not clearly seen and demonstrate the difficulty in interpreting full scan data.

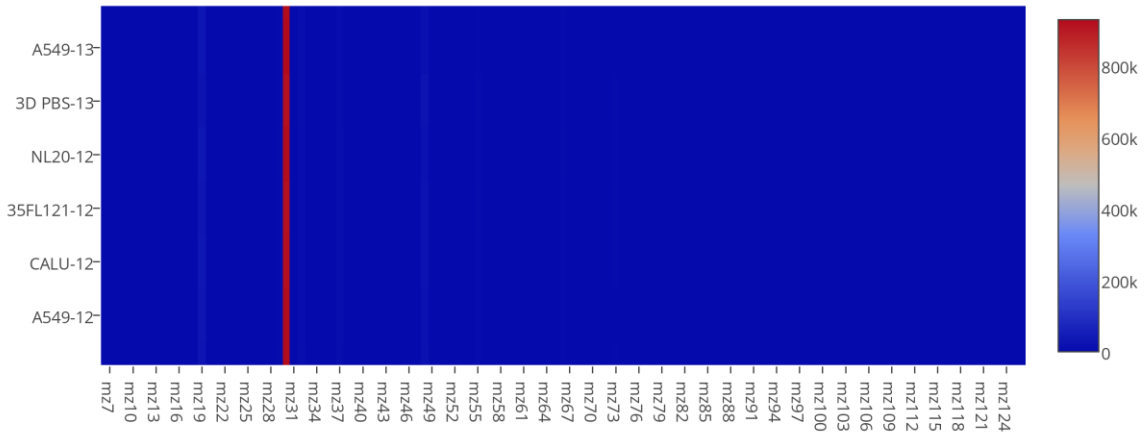

Figure 28. Heat map displaying the full scan profiles of 4 lung cell lines, grown in a PBS based 3D model, analysed with NO^+ precursor ion. The colour denotes the abundance of the compounds (red being 8 x 10^5 counts/sec - blue being 0 counts/sec).

4.4.5 Principal Component Analysis of FSM using H_3O^+ precursor

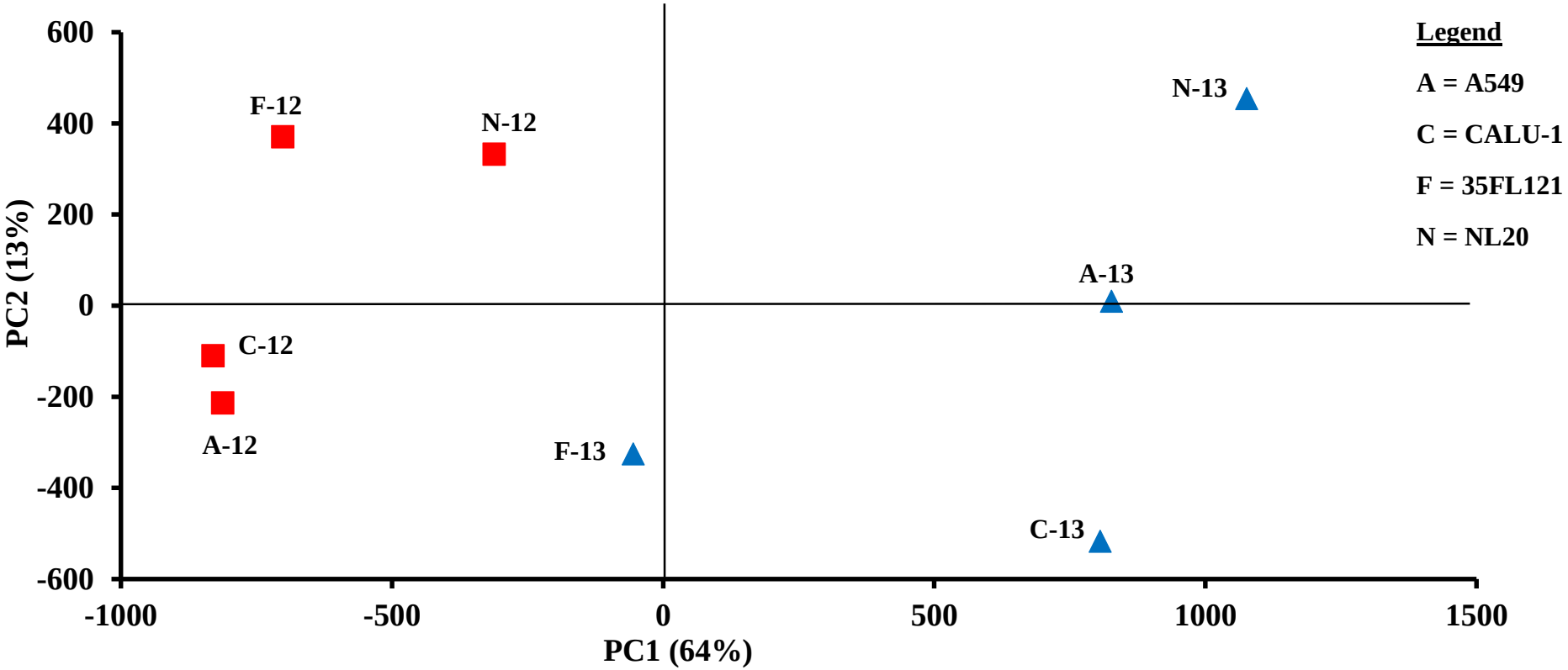

Figure 29 PCA scores plot of labelled (13) and unlabelled (12) headspaces taken from 4 cell lines, analysed with H_3O^+ precursor ion.

Figure 29 is a PCA of both unlabelled (12) and labelled (13) sample headspaces taken from all cell lines using the H_3O^+ precursor ion. The loading plot displays PC1 and PC2 loadings for the range of m/z 11 – m/z 180.

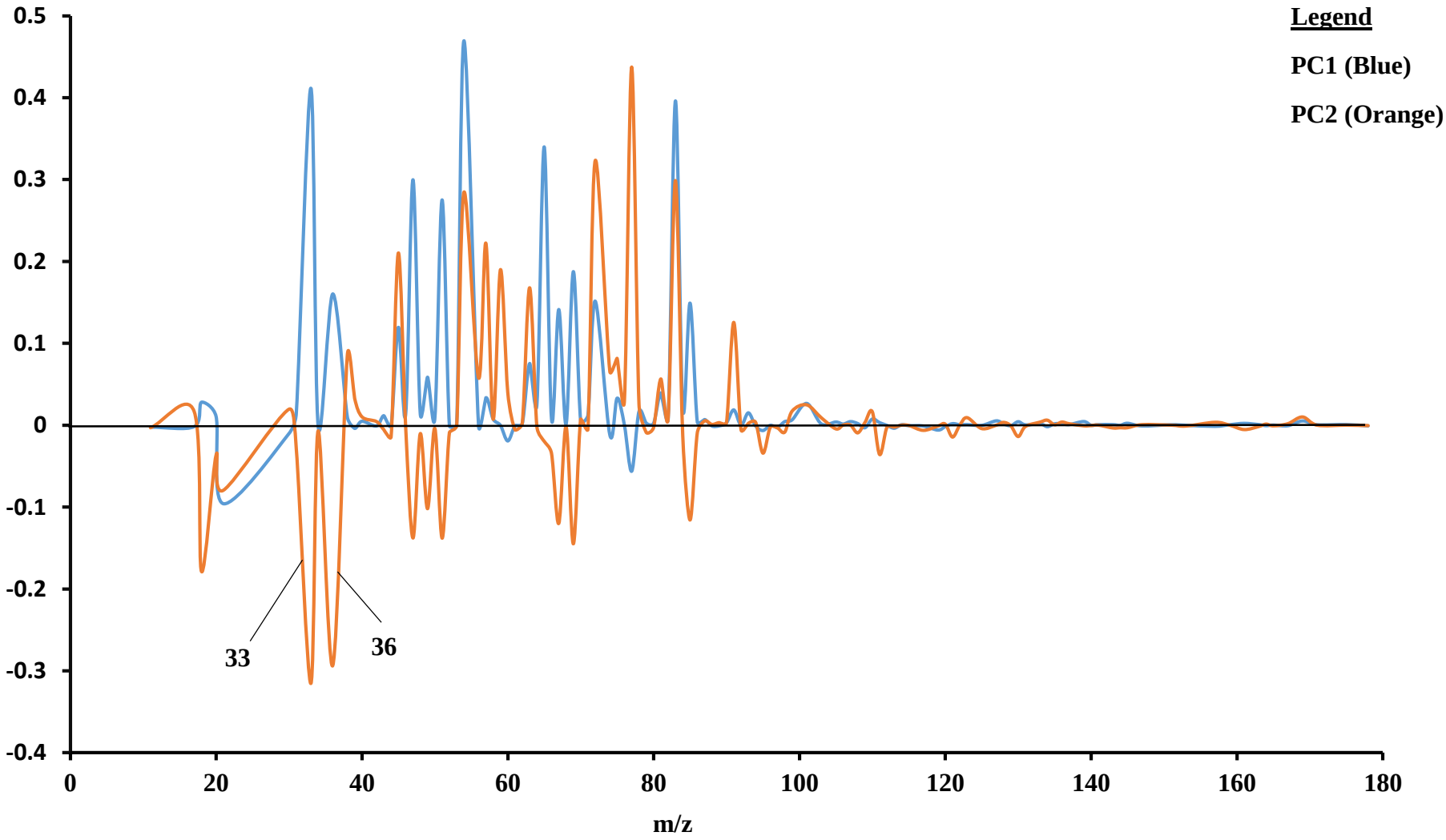

Figure 30. PCA loading plot of labelled (13) and unlabelled (12) headspaces taken from 4 cell lines, analysed with H_3O^+ precursor ion.

4.4.6 Principal Component Analysis of FSM using NO^+ precursor

Figure 31 is a PCA of both unlabelled (12) and labelled (13) sample headspaces taken from all cell lines using the NO+ precursor ion. The loading plot displays PC1 loadings for the range of m/z 18 – m/z 180.

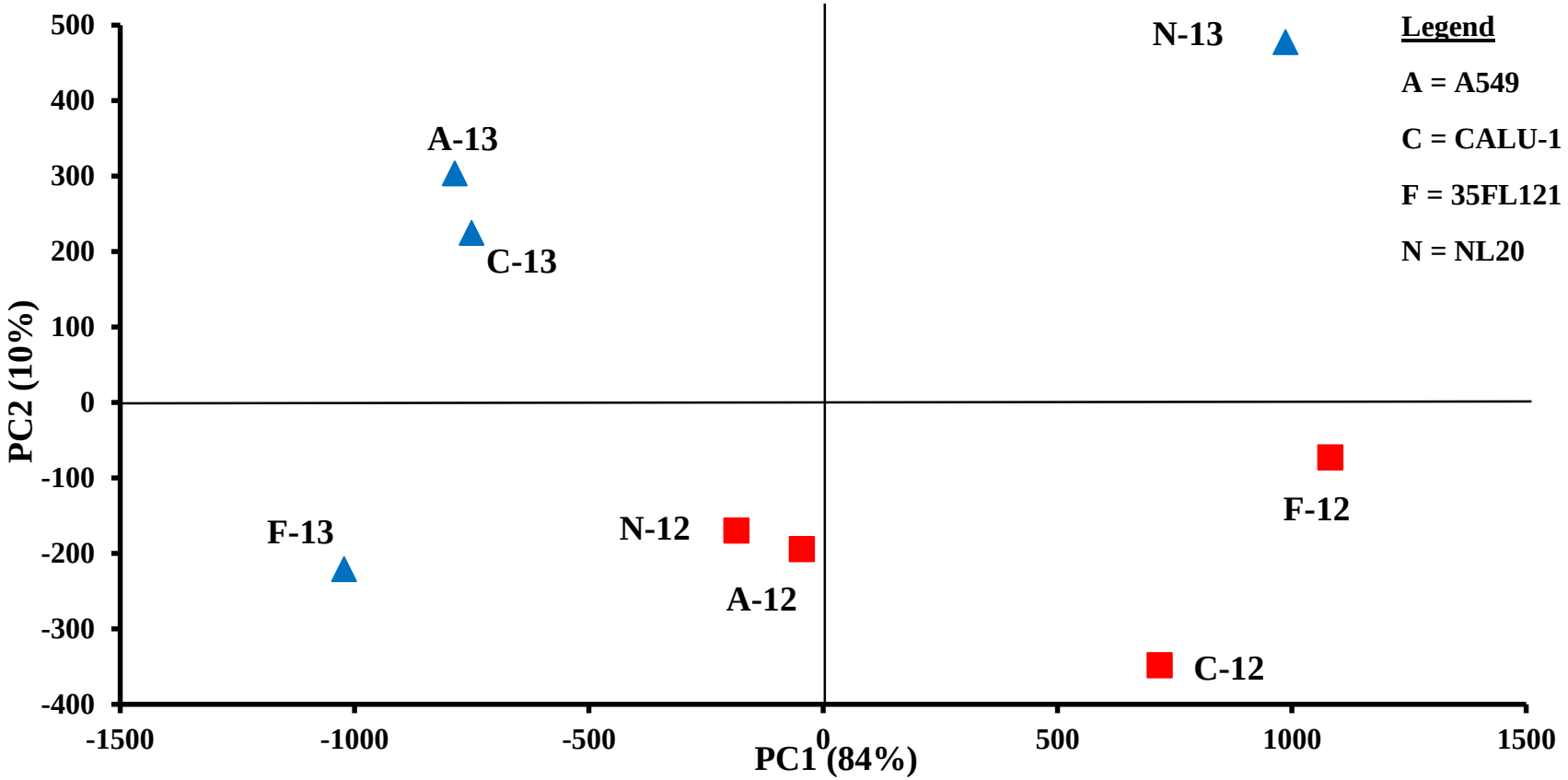

Figure 31 PCA scores plot of labelled (13) and unlabelled (12) headspaces taken from 4 cell lines, analysed with NO^+ precursor ion.

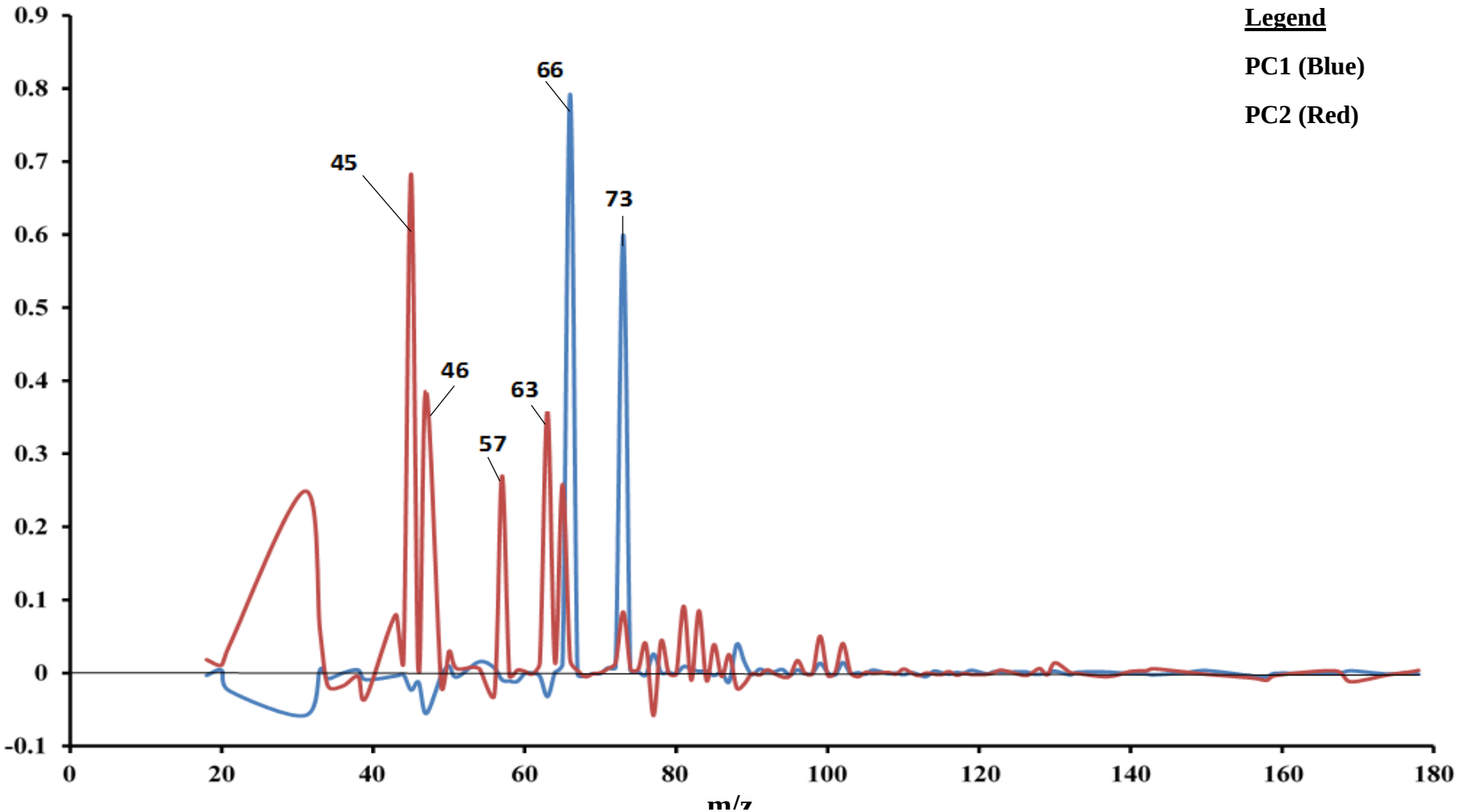

Figure 32 PCA loading plot of labelled (13) and unlabelled (12) headspaces taken from 4 cell lines, analysed with NO+ precursor ion.

4.5 Discussion

The first aim of this chapter was to address a suitable 3D model that is improved upon from the media based 3D models used previously. This could be, as discussed in chapter 3, because media can have a heavy influence on a cell's metabolism and it is not yet known which components of the media could cause, and to what extent, changes in the VOCs profile.

It was therefore hypothesised that the use of PBS and the minimum components of media used to sustain a healthy cell culture would reduce the influence of the medium on the VOCs profile. Figure 30 demonstrates that despite the reduction in components in a PBS based cell culture medium, the resulting profile given out by cells is still a complex one, with numerous compounds for analysis.

The suitability of the PBS gel as a cell culture substrate was confirmed as apt; Table V shows a good standard of viability for these simpler 3D constructs, compared to those in chapter 3, for all 4 cell lines used. This 3D model could then be used for further studies to examine the metabolism of cells in an increased physiological manner when compared to the previously used 2D models (Sulé-Suso, J. 2009). The PBS model does however limit cells to a shorter culture time as prolonged exposure to a cell culture medium lacking in vital components could limit the cell populations ability to proliferate and even survive in the long term (3 days plus). Other essential media components could be used to prolong culture time in a PBS based medium with components added after the assessment of headspace using SIFT-MS has been explored. Overall the impact of exploring PBS based hydrogels for use in cell cultures when studying headspaces with mass spectroscopy is important. This study

highlights the impact of cell culture medium on the headspace produced by cells and is a cautionary message; well thought out cell culture methods should be considered. This method should make comparisons across studies more practical, allowing for a higher level of reproducibility and cross-study conclusions to be made.

The second aim of this chapter was far more challenging; attempting to see if the use of labelled compounds for the study of metabolical markers using the SIFT-MS was possible. The labelled compound was the non-radioactive, non-toxic glucose with carbon -13 (^{13}C). Each cell line was cultured in a 3D PBS model, supplemented with 10% FBS and 4.5 g/L of either ^{12}C glucose or ^{13}C glucose. The viability for each cell line in culture with ^{13}C glucose was similar to cells cultured with ^{12}C glucose (Table V).

As suggested by our previous knowledge of acetaldehyde metabolism, and the previous studies that have shown this VOC to be of interest (Sulé-Suso, J. 2009), the first examination of the SIFT-MS data was to look at the acetaldehyde released by the cell cultures. Figure 26 shows the acetaldehyde release studied using the precursors H_3O^+. There is no discernible trend in the metabolism of acetaldehyde seen in ^{12}C or ^{13}C glucose across all cell types. All cellular samples have acetaldehyde levels below their a-cellular PBS control, except for A549 grown in ^{12}C glucose (unlabelled), implying the metabolism of acetaldehyde is underway in a majority of cell samples.

The PCA of the full scan data showed a clear separation between cells cultured in ^{12}C glucose and ^{13}C glucose when using either H_3O^+ or NO^+ precursors. In the case of H_3O^+, the loading

plot showed differences at m/z 33 and 36. m/z 33 is associated with methanol while m/z 36 has not yet been assigned. In the case of NO^+ precursor, the main differences reside in m/z 45, 46, 57, 63, 66 and 73. m/z 45 is associated with ethanol, m/z 57 is associated with 2-methyl propane and m/z 73 is associated mostly with 2-butanol and (di)ethyl ether. m/z 46 has not been assigned yet.

Changes in the levels of CO_2 were also measured for. However, m/z 63 contains CO_2 and acetaldehyde. It was not possible to identify any possible changes in CO_2 levels following the incubation with either ^{12}C glucose or ^{13}C glucose. Further work is needed to better clarify this issue.

The overall impact of the use of labelled components to the mass spectrometry community is perhaps smaller. The use of labelled glucose already being explored in the literature. This study serves to refresh the concept of using labelled products to explore metabolic pathways within cell cultures and with SIFT-MS.

To summarise; these data not only indicates that it is possible to measure VOCs from lung cells incubated in 3D gels made up of PBS. This work now sets up the basis to study metabolical pathways of VOCs in different cell lines, using labelled compounds for a basis of identification of specific metabolic pathways.

Chapter 5 Breath of Patients

5.1 Introduction

As discussed previously in the introduction of this thesis, the power of an ideal breath test for lung cancer would have multiple advantages over the currently used diagnostic techniques, such as x-ray, CT scan etc., namely; non-invasive, real-time, radiation free, economical and able to identify the cancer within its early stages. SIFT-MS is a candidate technique to offer this wealth of advantages as a tool to analyse people's breath and ultimately identify lung cancer.

Most quantitative research has had a focus on identifying those trace compounds found in the healthy population, which is vital if we are to be able to establish a deviation from healthy, ie. cancerous breath profiles. With a focus on SIFT-MS specifically, as is the focus of this thesis, we can see these studies have examined ammonia, acetone, propanol (Turner, C. 2006) and isoprene (Španěl, P. 1999; Turner, C. 2006; Španěl, P. 1999) in healthy volunteers across different age ranges (Španěl, P. 2007; Enderby, B 2009; Smith, D. 2010) and during exercise (Senthilmohan, S. T. 2000).

As a result disease state profiling has now become the target of the growing body of scientists that use the SIFT-MS. The technique has been used to study bacteremia in blood cultures (Scotter, J.M. 2006; Allardyce, R. A 2006), lung cancer (Sulé-Suso, J. 2009; 35 Smith, D. 2003; Rutter, A. V. 2013) bladder and prostate cancers (Španěl, P. 1999), pseudomonas associated with cystic fibrosis (Enderby, B. 2009; Carroll, W. 2005), urinary tract infection (Smith, D. 1999; Storer, M. K 2011) and diabetes (Turner, C. 2009).

As mentioned previously, lung cancer is particularly problematic due to the late stages in which it is currently being diagnosed or perhaps that symptoms do not occur until the later stages of the disease. This is primarily because patients present late to clinics with symptoms. Therefore in order to improve diagnosis the disease needs to be recognised at the very early stages of tumour growth, preferably before the tumour causes symptoms. Ideally, if early stage tumours release VOCs into the breath of the patient, the SIFT-MS could be used to identify the disease.

Exhaled breath as a profiler for lung cancer has also been reviewed previously (and discussed in some detail in the introduction) (Mazzone, P. J. 2012; Amann, A. 2011; Phillips, M. 1999) but no clinical tool has yet been used as standard in clinical practice. As discussed in these reviews, different sampling techniques can be used to sample the breath of patients with suspected lung cancer, such as direct breath sampling and bag sampling. The first being advantageous as it avoids the potential loss of useful VOCs. Direct breath sampling also allows for the real-time observation of a single compound to be monitored, from oral exhalation to the end-tidal part of a person's exhalation (Smith, D. 2014). However, direct breath sampling also has its limitations. The sampling mode itself is limited by the exhalation time being provided by the patient. In patients with disease, this exhalation time maybe relatively small and therefore the sensitivity of the instrument to detect and quantify VOCs that are present in low concentrations may not be possible. Direct sampling may also be limited by the patient's capacity to move to the machine itself. This could have serious implications for the use of direct sampling methods as a clinical tool unless small portable instruments are developed.

Bag sampling however offers an alternative to direct breath sampling and in some ways overcomes some of the pitfalls listed above. For example, allowing the storage of a sample; particularly relevant in a busy clinical setting. The bag sampling method also allows for a longer sampling time, not being limited to the exhalation time provided by a patient. This will also increase the sensitivity of the instrument for VOCs trace compounds. Bag sampling is however not without its disadvantages, for example the potential loss of valuable VOCs due to diffusion from the sampling vessel and/or surface absorption and adsorption (Smith, D. 2015). A previous study has already assessed the suitability of bag sampling for a study specific to the identification of cystic fibrosis in children (Gilchrist, F. J. 2012), with a focus on hydrogen cyanide and acetone. The study highlights that bag sampling needs to be considered on a single VOC basis, some being suitable for analysis with this method, such as hydrogen cyanide and acetone, which maintain concentrations up to a 24 hour period. Some compounds could however be more problematic. Water vapour itself fell within the bags quickly, within 24 hours becoming the equivalent to the lab air. This highlights the need to perhaps examine the suitability of bag sampling on a case by case basis.

SIFT-MS studies are needed to continue this work, expanding the technique to assess if a viable profile of lung cancer can be generated above a "normal" counterpart. This chapter will explore the suitability of bag sampling and also bottling sampling for the breath of healthy volunteers but with a focus on those compounds that have already been identified as VOCs of interest by the cell line work with lung cancer cells (ie. acetaldehyde) (Sulé-Suso, J. 2009; Rutter, A.V. 2013).

Following this, using SIFT-MS, the VOCs profile from patients with lung cancer and patients with basal cell carcinoma (BCC) or squamous cell carcinoma (SCC) of the skin were studied in order to characterise any differences between the groups. Healthy volunteers are also recruited in order to serve as a further control of breath profiling.

5.2 Aims of the Study

1. To establish a methodology suitable for the acquisition of breath samples from patients with lung cancer.
2. To be able to profile lung cancer patients and differentiate them from those without lung cancer with use of SIFT-MS analysis.

.

5.3 Materials and Methods

5.3.1 Patients

This study has received ethical approval form the Local Ethics Committee. Patients with lung cancer and patients with BCC or SCC of the skin but without lung cancer attending the Oncology Department at the Royal Stoke University Hospital were recruited. All patients were given an information sheet explaining what the study entailed and were given time to ask questions. They were then given 24 hours before signing a consent form. Patients with lung cancer had their disease previously diagnosed both radiologically and histologically.

Control cases (patients with BCC or SCC of the skin) were asked to have a Chest X-Ray in order to rule out the presence of a lung tumour. Patients with previous history of other malignant tumours were not included in the study. This was a pilot study including 50 cases with lung cancer and 50 control cases. This is still an ongoing study. The data presented here is preliminary data from 15 lung cancer patients and 12 control cases.

5.3.2 Sampling Methods for Control Healthy Participants

Healthy participants were asked not to consume anything but water following their evening meal the night before, except for medications where needed. Participants were also asked not to brush their teeth or use cleaning products before the sampling was taken. Each sample was taken at 9 am. Table VI shows the sampling methods taken for healthy participants; that is direct, bag and bottle sampling at different time points and in triplicate.

Table VI Participant type and details of sampling modes and methods.

Participant Type	Precursors	Sampling Method	Time Points (hours)
Healthy Participants	H_3O^+, NO^+	Direct	0 (in triplicate)
		Bag	0 (in triplicate), 1, 3, 6, 24
		Bottle	0 (in triplicate), 1, 3, 6, 24
Lung Cancer Patients	H_3O^+, NO^+	Bag	0 (within 30 minutes)
Patients with BCC or SCC of the skin	H_3O^+, NO^+	Bag	0 (within 30 minutes)

5.3.3 Bottle Sampling from Control Healthy Participants

Control participants were asked to fill 150 mL sterile glass bottles using a straw that was 10 cm in length, protruding into the bottles around 8 cm. Participants were asked to fill the bottles with deep breaths. The bottles where then sealed tightly with caps containing a septum, suitable for puncture by the SIFT-MS sampling needle. Bottles were then sealed with parafilm until sampled from. Unless sampled from immediately, bottles were kept at room temperature, under ambient conditions. Preliminary work was done to assess the number of breaths. One exhalation did not provide higher levels of VOCs when compared to ambient air. On the other hand, 5 exhalations did not provide VOCs in higher concentration when compared to 3 exhalations.

Figure 33 SIFT-MS sampling bottle, with steel screw cap and penetrable rubber septum.

5.3.4 Bag Sampling from Control Healthy Participants

SIFT-MS bags were produced as detailed in chapter 2 (Chapter 2, SIFT-MS) and participants were asked to fill each bag with three direct breaths. Each bag was then sealed with a lure lock syringe and wrapped in parafilm. Bags were stored at room temperature, under ambient conditions until sampling time.

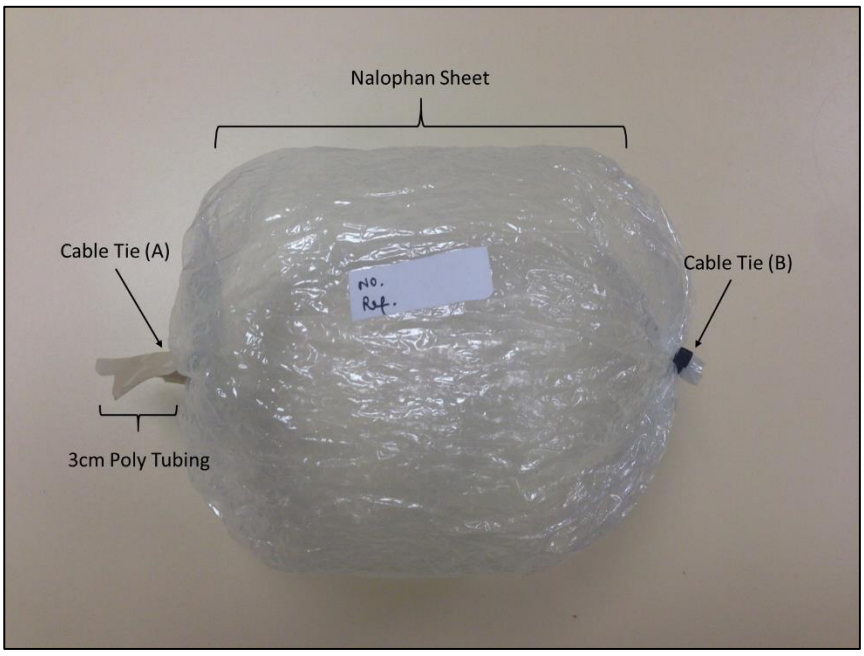

Figure 34 SIFT-MS bag sampling method, comprised of a nalophan sheet, cable ties and poly tubing sampling orifice.

5.3.5 Direct Breath Sampling from Control Healthy Participants

Direct breath samples were obtained through a sterile sampling tube attached to the sampling arm of the SIFT-MS, in replacement of the sampling needle. Participants were asked to give one long, continuous breath, directly into the sampling line of the SIFT-MS tube. Healthy participants were asked to breathe out for as long as possible, in order to maximise the sample for analysis. Samples were obtained between 5 and 20 seconds. Participants gave these breaths in triplicate, and for each precursor ion (H_3O^+ and NO^+).

5.3.6 Profiling Lung Cancer and "Control" Patients

For both lung cancer patients and control cases alike, bag sampling was used to collect a sample of the participant's breath. Each participant was given two bags to breathe into and asked to provide full bags using 3 separate breaths. All participants managed to supply this.

Each participant would arrive at 8 am for sampling, having not eaten or drank anything other than water since the night before. Participants also refrained from brushing their teeth. Prior to breathing into the bag, a cup of water was provided to rinse the mouth with. From the sampling room, 2 bags were also filled with room air using a 50 mL syringe, in order to provide an air control. The bags were then sealed with a lure lock syringe inserted into the sampling pipe and parafilmed. Bags were then taken directly to the laboratory where the SIFT-MS is located (approximately 5 minutes away).

5.3.7 Spectrometry – SIFT-MS Sampling

SIFT-MS (*Profile 3*)

A *Profile 3* SIFT-MS was used to analyse the breath samples provided by participants. Two precursors, H_3O^+ and NO^+ were used in the analysis. Both MUI and FSM were utilised for both healthy participant breath and patient breath analysis. For bottle sampled breath, the bottle environment pressure was equilibrated by using a bag of dry purged air attached to a puncturing needle, placed through the septum of the sampling vessel. Please refer to chapter 2 for a detailed method using the SIFT-MS.

5.3.8 Processing

As previously described in chapter 2, all data ascertained using the MUI method was corrected to 6% water by flow rate adjustment in the SIFT-MS software, followed by a final adjustment to precisely 6% in excel.

5.3.9 Analysis

Data was further examined using PCA to detect any differences between sampling groups. PCA was performed using The Unscrambler Software (Camo, Norway) and plotted in 3D using the same software package. 2D plots were created using Graph Pad Prism 6.

3.4 Results

5.4.1 Identification of Optimum Sampling Vessel Using Control Samples

Table VII gives an approximation of the relative humidity (RH) taken directly from the different sampling vessels (bags or bottles) and direct measurements from healthy controls without a water correction applied (mean of 5 independent experiments). The table illustrates that the RH in bags has decreased rapidly after one hour of storage at room temperature but the bottles are maintaining a relatively stable level of RH inside them.

Table VII. Average relative humidity before 6% correction is applied. Data procured using H_3O^+ precursor ion.

	Average Relative Humidity with H_3O^+ Before Correction (%)					
Time (Hours)	**Direct**	**SD**	**Bottle**	**SD**	**Bag**	**SD**
0	5.74	0.22	4.65	0.22	4.72	0.05
1	N/A	N/A	4.59	0.62	2.55	0.71
3	N/A	N/A	4.84	0.23	2.00	0.61
6	N/A	N/A	5.84	0.74	1.87	0.81
24	N/A	N/A	5.68	2.29	2.27	0.88

5.4.2 The variation of Acetaldehyde between controls at 0 hours

Figure 35 shows control data taken in triplicate at 0 hours for direct, bag and bottle sampling techniques. It demonstrates the real time fluctuation of acetaldehyde across samples taken by the SIFT-MS *Profile 3*.

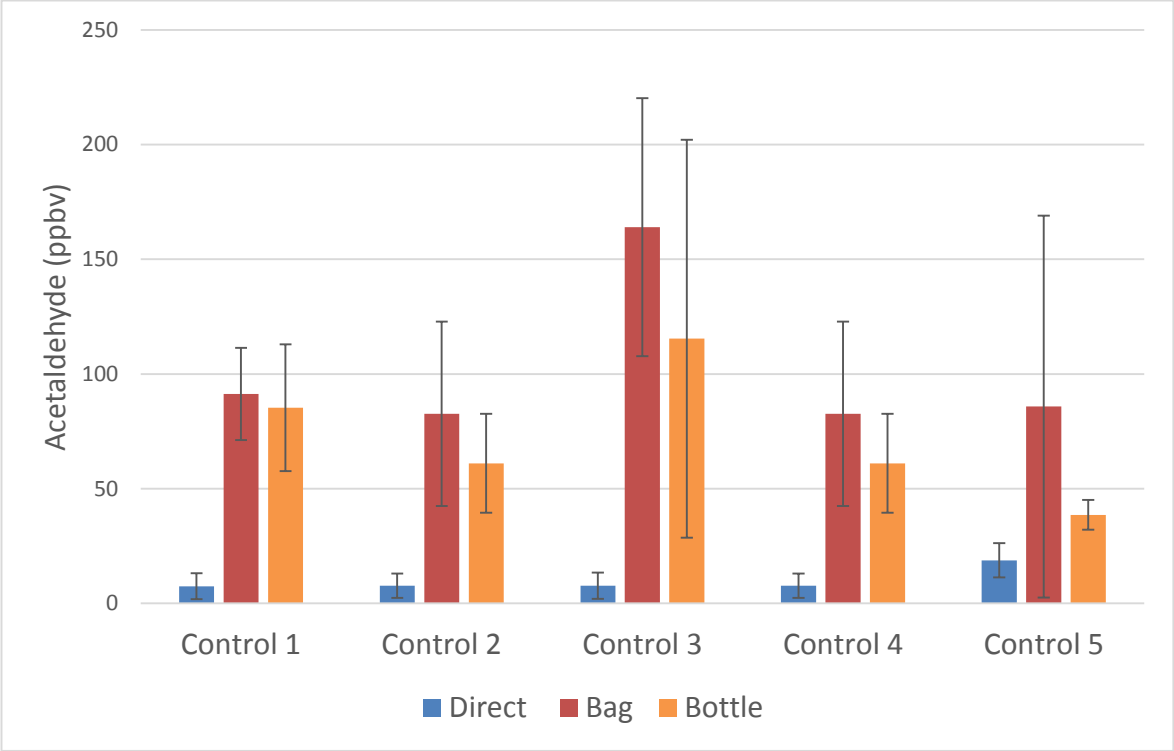

Figure 35 Control participant data for acetaldehyde release (ppbv) analysed using H3O+ precursor ion for 3 different sampling methods; direct, bag and bottle N=1.

5.4.3 The variation of acetaldehyde over time in bottles and bags.

Figure 34 shows the levels of acetaldehyde at different time points for 3 individual cases. All the graphs in this figure demonstrate a fluctuation from 0 hours to 24 hours and a divergence between bag and bottle sampling. Table VIII shows the percentage difference between each condition. The first column indicating the difference between samples taken at 0 and 24 hours from a bottle, the second column 0 and 24 hours taken from a bag, the third column the difference between a bag and bottle sample taken at 0 hours and the final, fourth column show the differences between the bag and bottle samples taken at 24 hours. Those shaded cells with a bold border indicate those changes that are within the 10% instrumental error margin of the SIFT-MS, *Profile 3.*

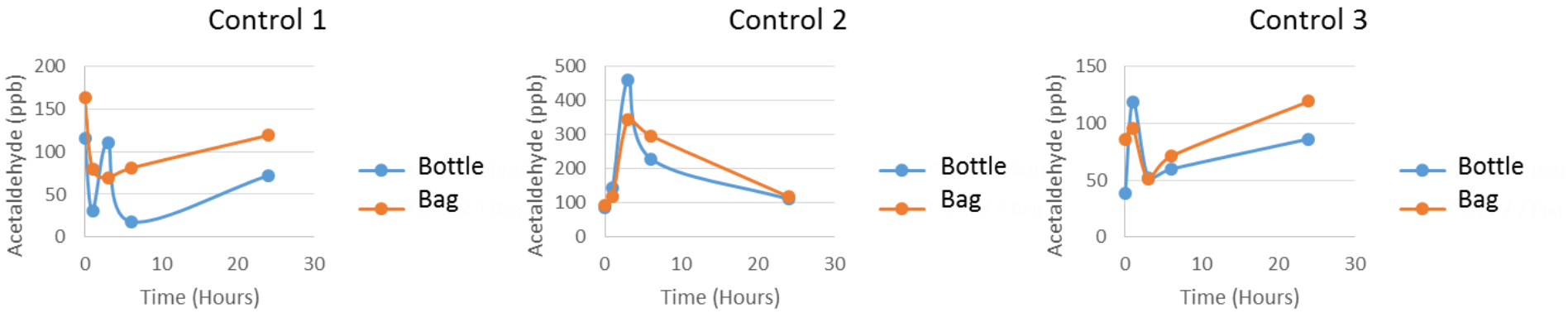

Figure 36 Acetaldehyde release in control participants 1, 2, and 3 for both bottle (blue) and bag (orange) sampling methods across time (hours).

Table VIII. The % difference of acetaldehyde release (ppbv) seen at different time points for 3 control participants (Boxed section indicates those samples within SIFT-MS error margin).

	% Differences			
	0-24 Hours Bottle	**0-24 Hours Bag**	**Bag - Bottle 0 Hours**	**Bag - Bottle 24 Hours**
Control 1	-37.56	-27.33	29.65	39.55
Control 2	23.26	22.78	6.64	6.06
Control 3	55.28	28.04	55.02	27.63

5.4.4 VOCs released by lung cancer patients and control cases

Using the MUI system, no differences between the levels of acetaldehyde released in the breath of lung cancer patients (mean of 128 ppbv, SD 99) and control cases (mean of 120 ppbv, SD 90) were seen. On the other hand, acetone was present in higher concentration in the breath of control cases (mean of 1002 ppbv, SD 608) when compared to patients with lung cancer (mean of 540 ppbv, SD 240). Also, propanol was present in higher concentration in the breath of control cases (mean of 482 ppbv, SD 64) when compared to the breath of lung cancer patients (mean of 209 ppbv, SD 174). Regarding full scan using H_3O^+, Figure 35 shows the ratio of VOCs present on the breath of patients with lung cancer over VOCs present on the breath of control cases.

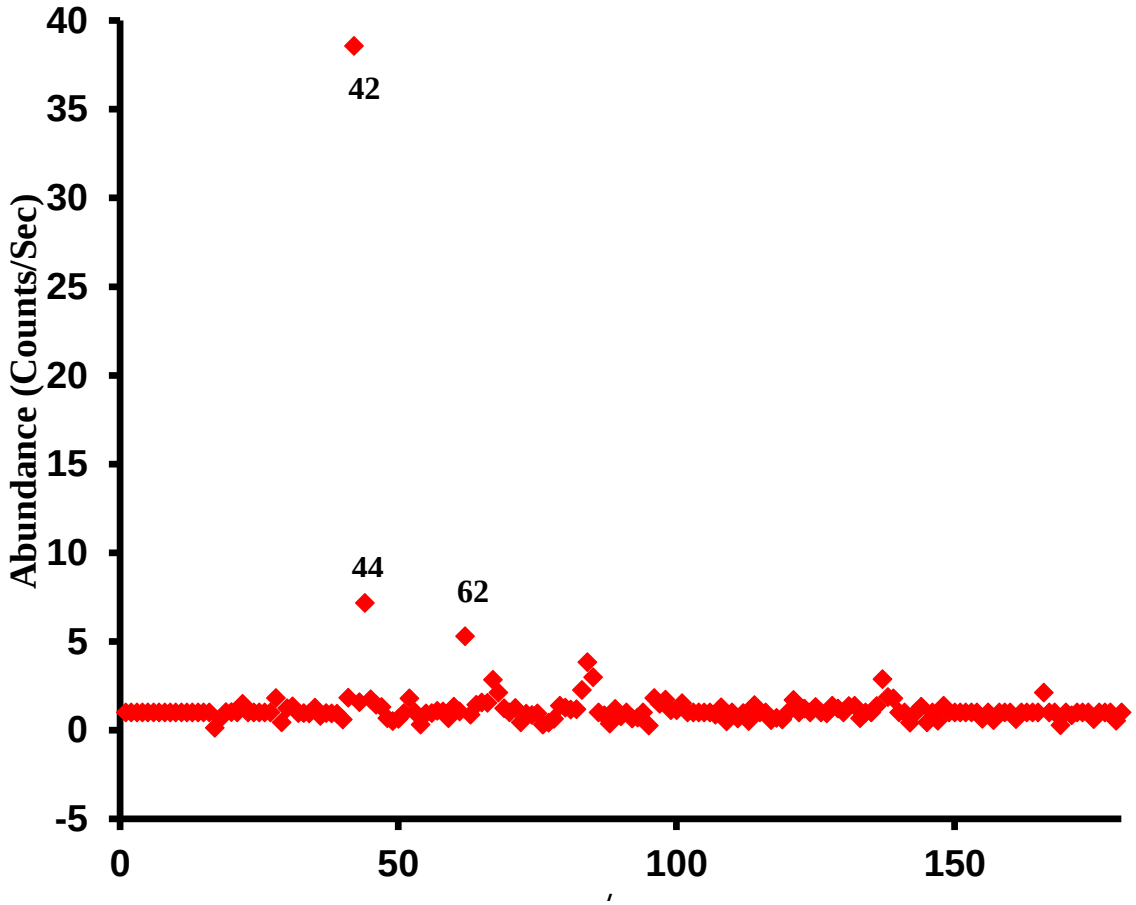

Figure 37 Ratio of VOCs present in the breath of patients with lung cancer over the breath of control participants.

Only 3 m/z seem to be present in higher concentration in the breath of patients with lung cancer when compared to control cases. While m/z 44 has not been assigned yet, m/z 62 corresponds to nitromethane. Interestingly, m/z 42 was present at much higher concentration in the breath of patients with lung cancer when compared to other analytes. m/z 42 corresponds to acetonitrile, a component of tobacco (Abbott, S.M. 2003).

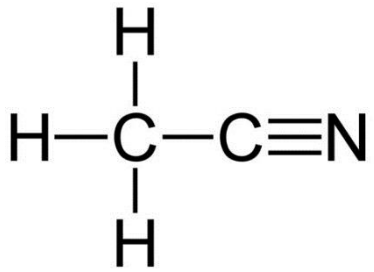

Figure 38 The biochemical structure of acetonitrile.

Therefore, the next step was to plot acetonitrile against the smoking status of the participants used in this study (Figure 38). Levels of the compound were higher in smokers and decreased with the level of time the participant had quit smoking.

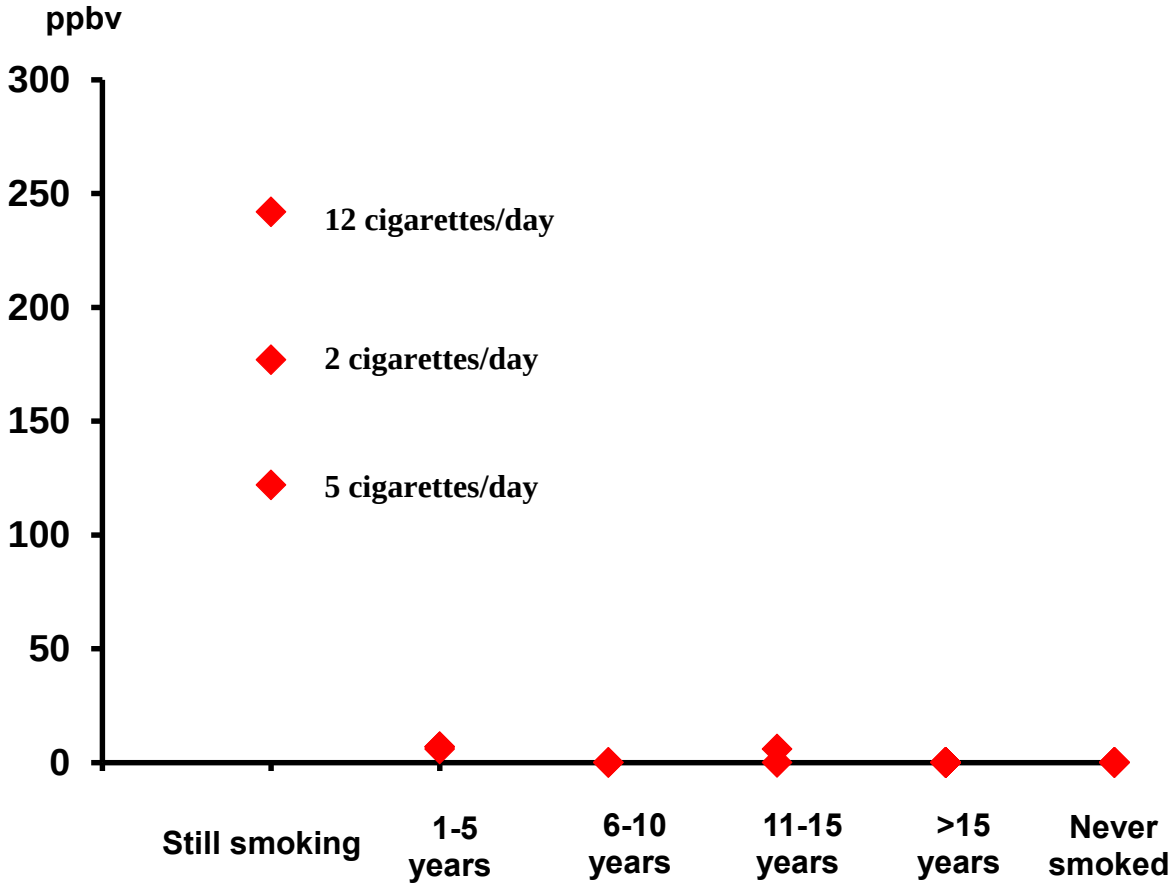

Figure 39 A graph of levels of acetonitrile (ppbv) in the breath of patients plotted with smoking status.

5.5 Discussion

Using breath diagnosis to try and improve the outcome of those suffering from lung cancer presents itself with many challenges, both experimentally and clinically. This study has faced several facets of these challenges, starting from the sampling methods that could be used to gather viable samples for analysis and also meeting some of the clinical challenges provided by a clinical cohort of participants.

5.5.1 Establishing a suitable method of sampling breath

Following previous studies that discuss the optimum methods for breath sampling, including those communications that discuss the main pitfalls of the use of breath analysis itself (Smith, D. 2015) as well as those that are more specific to the disease/clinical need (Gilchrist, F.J. 2012), this study started with the aim of identifying the most suitable and available technique to gather breath samples. Control, healthy participants' breath was analysed using a variety of sampling methods through direct sampling (blowing directly into the machine), bottle and bag sampling.

Table VII examines the RH loss from direct, bottle and bag samples and also compares the sampling efficiency to a direct breath measurement that would give a level of 6% (when the SIFT-MS is running under optimum conditions). Samples were also analysed at different time points to assess the suitability of the methods to be used in the long term, such as in a clinical setting where immediate analysis may not be practical. The first time point at zero hours shows that the RH seen within both bags and bottles is similar (4.65-4.72 %). The direct breath measurement giving the appropriate value of 5.74%. This illustrates the stability of the SIFT-MS *profile 3* and suitability for the instrument to be used across different clinical times. The disparity between RH across sampling methods therefore is mostly likely the sampling methods itself, such as the materials used and the methods for making the samples air tight. This could be improved upon in several ways in future work; firstly the bottle sampling method is filled by an open straw which could eventually become an enclosed unit. The septum and lid itself could become a single structure allowing for a more tight fit seal. This would allow easier storage and transport when compared to bags. Bags are currently sealed with a syringe, a process that could allow a small exchange of the sample with the atmosphere, decreasing the relative humidity. Despite both methods being

sealed with parafilm it is clear there is a slight loss in the RH within the samples. Both bags and bottles provide the same standard of sampling collection as at 0 hours the sampling methods are similar with little deviation.

The story is less clear for 1, 3, 6 and 24 hour time points[8]. Bottle sampling vessels seem to maintain the RH levels although the standard deviation of measurements here starts to become larger with time. In bag sampling, the RH decreases quickly, losing nearly half the RH after one hour. Bag sampling maintains a 2% RH level for the 24 hour experimental duration.

Figure 35 shows the effect this loss has on the measurement of acetaldehyde, as the compound of interest. Direct sampling shows acetaldehyde present between 7-18 ppbv. This is far from bag samples that deviate between 82 ppbv and 164 ppb and bottle samples at 38 ppbv to 115 ppbv of acetaldehyde. This difference in compounds could be owed to a variety of factors influencing each sampling method differently. There is a difference in the nature of the breath collected between direct sampling and both bottle and bag sampling. Direct sampling is measuring in real time a full exhalation of a person breath and is considered advantageous for a number of reasons. Firstly, a direct sample avoids the problematic loss of trace compounds that could occur during depositing the sample. Direct sampling also allows the analysis of the end-tidal portion of a person's exhalation by itself (Španěl, P. 2011). Direct breath sampling is not without its limitations, unfortunately the quality of the analysis is affected by the exhalation time of the sample. Compounds that are

[8] Direct samples are not relevant here as they cannot be stored.

present at low concentrations within the breath could be overlooked. Particularly with lung cancer patients, exhalation times could be very limited.

As mentioned, bag sampling allows the storage of samples which is highly desirable in a clinical setting. By extension the sampling method also offers longer analysis time and therefore increased sensitivity in identifying compounds that could be at low concentrations within the breath of patients. The limitation of bag sampling being the loss of useful trace compounds during the sample deposit into the balloon and also the loss that could occur due to the surface adsorption/diffusion through the materials that compromise the bag (Gilchrist, F.J. 2012).

Bottle sampling methods offer the same limitations and advantages as bag sampling, however the inflexibility of the sampling vessel does offer challenges for prolonged measurements or repeats, as the sample pressure inside the bottle needs to be equilibrated. In this study, dry purged air was used to re-establish equilibrium, diluting the sample slightly.

5.5.2 The variation of acetaldehyde over time in bottles and bags.

Both table VIII and Figure 35 demonstrate large differences in the acetaldehyde levels between 0 hours and 24 hours sampling time. In the bottles a range of acetaldehyde loss and gain is seen. Acetaldehyde is seen to increase up to 55% in bottles, but is also seen to be sampled at a loss of 38% after 24 hours in 1 case. Bag sampling also tells a similar story, losses of 27% and acetaldehyde increases of 28%.

When bag and bottle sampling is compared at 0 hours, acetaldehyde levels were found to differ in measurement by as much as 55%. Only 1 sample, control 2, differed within a range under the 10% error allowance of the SIFT-MS *Profile 3*. A similar story is also seen for a comparison of the sampling vessels at 24 hours.

These results demonstrate a problematic variance that is occurring in the sampling of acetaldehyde. As the previous figures have shown, RH decreases at different rates within both sampling vessel types as time progresses. Acetaldehyde levels are also dependent on this. Despite the 6% H_2O^+ water vapour correction applied to the data it is clear that further work to establish the effects a wait time on analysis has on the acetaldehyde levels caused by the presence of other compounds (and therefore have the potential to interact with) as well as the sampling materials. Previous work has discussed (Smith, D. 2011) and explored the interactions of acetaldehyde with metabolites present in the breath and atmosphere (Španěl. P. 2008). The study concludes acetaldehyde has considerable interactions with CO_2 present in the exhaled breath, which must be accounted for when quantify acetaldehyde. This work studies these reactions in real-time analysis but perhaps there are also consequences to storing acetaldehyde with CO_2 for longer durations of time, such as the 24 hours in this study.

5.5.3 Variation between Control Patients and Lung Cancer Patients

The comparison between the VOCs present in the breath of patients with lung cancer and control cases has shown that the main difference lies on the levels of acetonitrile. Furthermore, these levels clearly separated smokers from non-smokers. And the levels

decreased the longer patients had quitted smoking. Acetonitrile has already been found in the breath of smokers using PTR-MS (Hansel, A. 1995) and SIFT-MS previously (Abbott, S.M. 2003; Španěl, P. 1996). Previous studies found acetonitrile being produced within a range of 17 ppb – 124 ppb (with a mean of 69 ppb) and also dependent on the number of cigarettes smoked per day, which is similar to the range seen here. These findings show the suitability of the bag sampling method to assess the current smoking status of a patient when needed, for example during treatment advice and also assessment of the suitability of lung transplant.

This has important implications in clinical practice, especially in lung transplant. In potential cases where lung transplant is required, it is prudent that patients should have stopped smoking for at least 6 months, ideally, but 12 months have been recommended (Todd, J.L. 2010). Smoking status is presently assessed by measuring the levels of cotinine, the main breakdown product of nicotine, in blood and urine. SIFT-MS could become a non-invasive tool to assess smoking patterns in patients requiring lung transplant.

5.5.4 Conclusions

The SIFT-MS technique has demonstrated a degree of suitability for the profiling of patients' breath, that is, bag and bottle sampling has provided a suitable method for which breath samples can be taken with ease and implemented directly into a clinical setting.

An established methodology still needs further work before an ideal sampling method is chosen due to the difficulties faced with wait time and the chosen metabolites of interest (in

this case acetaldehyde). This can be addressed through re-visiting the sealing methods for the sample vessels, materials, storage temperatures and times.

As of yet, very preliminary data does not show clear differences in the profiling of the breath of participants has allowed us to identify lung cancer patients from control counterparts. This too can be revisited, perhaps with the refinement of the nature of the profile taken, to include FSM of each participant.

The overall impact of this chapter on the field of breath analysis serves to identify the difficulties and practicalities encountered during a clinical study. Having identified the sampling vessel as the main limitation, imposing both time and analytical restraints over the field of breath analysis. The literature analysis and the methods used within this chapter show the lack of clear sampling methods identified by the field as a whole. As of yet the field of breath diagnosis is still yet to identify the gold standard substrate.

Chapter 6 FTIR Methodologies; 2D v 3D, Collagenase and DAPI

6.1 Introduction

Having already established the value of studying lung cancer with spectrometry and spectroscopic techniques, it is important to discuss the practical implications of the microspectroscopy of these cells. Previous studies have already addressed the practicalities of preparing biological substrates for study with FTIR microspectroscopy (Movasaghi, Z. 2008; Krafft, C. 2008; Miller, L.M. 2005) and also the implications of different fixatives used on biological samples (Ó Faoláin, E. 2005). Further to this, it is vital that we establish the best preparation of the biological sample itself. That is, how can we create viable biological samples that best mimic an *in vivo* environment or that best serve to answer our research question?

A starting point is to look at what sample formats have been used so far. FTIR microspectroscopy can be applied to a broad range of sample types, each with positives and negatives (this has been discussed in some details in the introduction of this thesis). Briefly, single cells can be prepared by cytospinning cells onto the substrate or a population of cells can be grown directly onto the sample substrate. A choice of fixative then follows, or cells can be measured live. Tissue maybe applied to a substrate, following sectioning into a specific thickness (typically mimicking the thickness a histologist would use within the clinical setting, between 5-10 μm). Biofluids can also be sampled using FTIR microspectroscopy.

S-FTIR based work is highly suited to the single cell analysis of samples, given the small aperture size and improved signal/noise ratio over that of current benchtop instruments available. The main focus of this work was on the single-cell analysis of lung cells, collecting spectra from the nuclei of the cell. Previous studies have shown that the nucleus provides a source of spectral information that enables us to characterise lung cancer cells efficiently (Pijanka, J.K. 2009).

As this thesis has a focus on lung cell lines grown within a tissue culture lab and transported to a synchrotron, the focus will also be on those cells that are fixed and either cytospun onto the substrate or part of a sectioned tissue model containing the cells. The aim of this chapter is to identify the most appropriate sample format to prepare for S-FTIR analysis using lung cells.

In order to create the most physiological environment possible for cell lines, cells are grown in a 3D model comprised of the natural polymer collagen. As the main component of mammalian derived extracellular matrices, it is no surprise that it is the most widely used natural polymer. The 3D models created for this purpose are typically 100 µL in size, around 5 mm in thickness and too large to be used for S-FTIR analysis. These samples as a whole would also be far from any clinical samples used for diagnosis. Therefore models are either sectioned to mimic clinical histological samples or cells are removed from the model and cytospun to mimic that of a cytological sample. In order to remove cells in a viable state from the 3D model, collagenase can be used. Collagenase is an enzyme that is able to digest collagen without affecting cell proliferation and/or survival as it will be shown later.

6.2 Aims

1. To establish a methodology to increase homogeneity in our cellular populations.

2. To identify if passage in our 3D models will cause spectral differences.

3. To establish a method to confirm the identification of cells in the 3D models using FTIR microspectroscopy.

4. To establish a method to analyse 3D grown cells using S-FTIR microspectroscopy and assess how the presence of the collagen scaffold modifies the S-FTIR spectra.

1.2 Materials and Methods

6.3.1. Cell Culture

CALU-1, a non-small cell lung cancer cell line (ECACC, Salisbury, UK) was used in this study. The cell line belongs to the squamous epithelial group of cells and was grown under the 2D Cell Culture Conditions 1, listed in Table I of this thesis.

6.3.2 Improving Homogeneity - Experimental Setup of Clonal Populations of CALU-1

Clonal populations of CALU-1 were produced as described in the previous section, chapter 2, of this thesis. Following the establishment of a clonal population the cells were then transferred into 2D, or 3D cultures for the next stage of the experiment.

Once the clonal population has been established each population is then split into four. The first subdivision is kept for 2D samples, used to prepare samples taken at different passages

of this population (passages 1, 3 and 5). The second sub-division is used for 3D samples that will have an end point at 24 hours. The third sub-division is used for 3D samples that will have an end point at 48 hours. The fourth sub-division is used for 3D samples that will have an end point of 72 hours.

Please see the Figure 40 below as an explanation of this process.

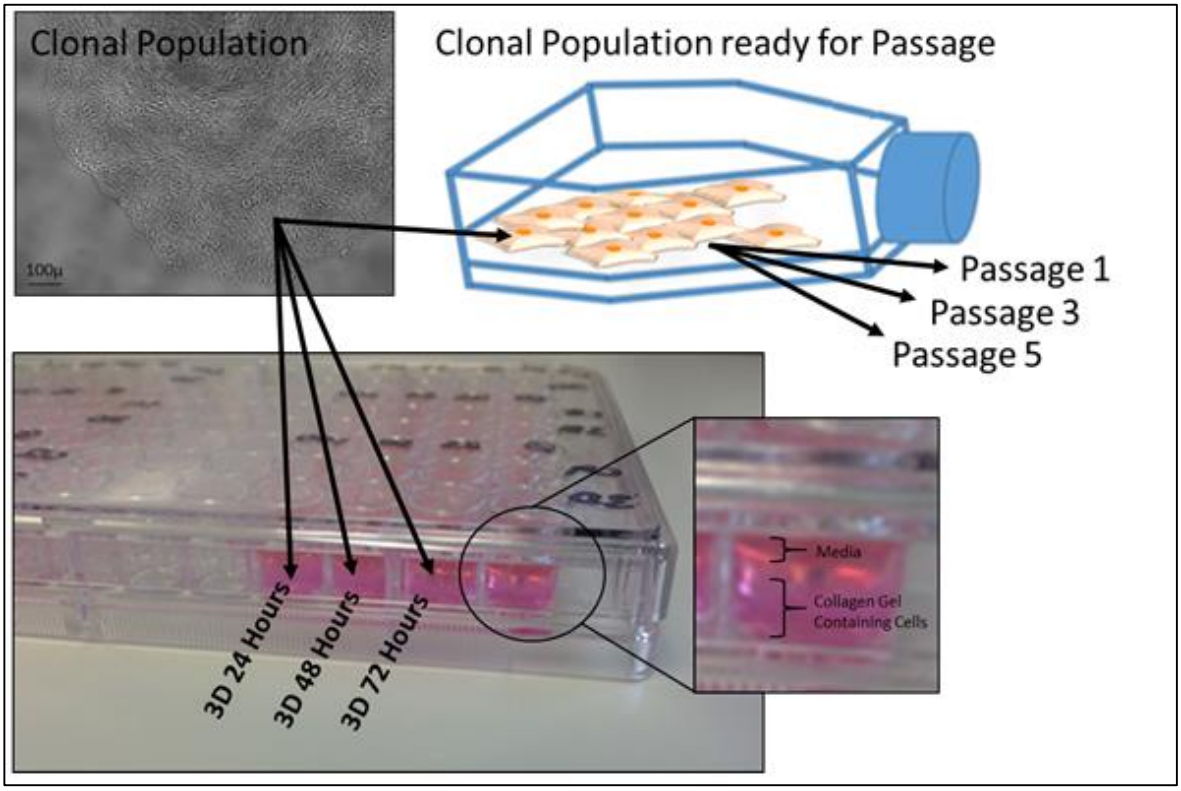

Figure 40 The subdivision of a clonal population of CALU-1 into 6 different samples.

3D Samples were prepared in 100 µL of collagen as previously described in chapter 2. Cells were not counted in this process to avoid losing part of an already small population, instead each quarter of the population was simply transferred to a new well.

6.3.3 Improving Cell Signal – Preparation of NaCl 2D and 3D Samples

In order to try and improve the IR signal obtained from cells, NaCl was used to grow the cell populations. This is because the media contains proteins and other biological molecules that may contribute to the IR spectral information (see Appendix 4 for a full list of the components of media).

Cell samples were prepared in both 2D and 3D formats. 2D samples were prepared as usual standard cell culture conditions but replacing the DMEM medium base with NaCl, the added extra components were the same as listed in Table I, chapter 2, 2D Culture Conditions 3. This was also applied to 3D samples, the conditions being the same as those listed in Table I, chapter 2, 3D Culture Conditions 3. For the preparation of the 3D gel scaffold 10x NaCl was used and the pH adjusted to 7 (adjustment with NaOH, 1M).

Following survival assay of cells grown in NaCl, it was determined that cells would be kept in NaCl culture for 24 hours before being fixed, and prepared onto the substrate.

6.3.4 Preparation of Cell Populations onto the Substrates

When assessing the difference between parental and clonal populations, cells were cytospun onto 0.5 mm CaF_2 slides as described in chapter 2 and then fixed as also listed previously (Chapter 2). Samples were prepared in duplicate.

Where tissue sections are used, 3D samples were physically removed from their well and flash frozen in liquid nitrogen (-150°C). Following this, the samples were mounted in Cryo-OCT Compound mounting medium (Tissue-Tek) and sectioned into 15 µm sections straight onto the CaF_2 slides. The samples were then fixed with 4% PFA and washed as per listing in chapter 2. Each sample was created in duplicate.

For those cells that were grown in 3D but were to be removed from the matrix enzymatically, 200 µL of collagenase was added to each gel for 1 hour (described in detail in chapter 2). The whole suspension was then centrifuged and the cells resuspended in 200 µL of NaCl before being cytospun onto CaF_2 slides, in duplicate, 100 µL of suspension being used per spin.

6.3.5 Identification of Cells within 3D, Cryocut Samples

FTIR spectra produced from collagen and cells are hard to distinguish without the aid of multivariate statistical techniques. Cells that are embedded into the collagen are also difficult to identify by microscopy alone. In order to overcome this, cells were stained with DAPI stain (as described in chapter 2), Figure 41 is a typical example of a stained 3D cryocut sample.

2D Samples were also DAPI stained as a control, to determine whether any spectral artefacts may occur as a result.

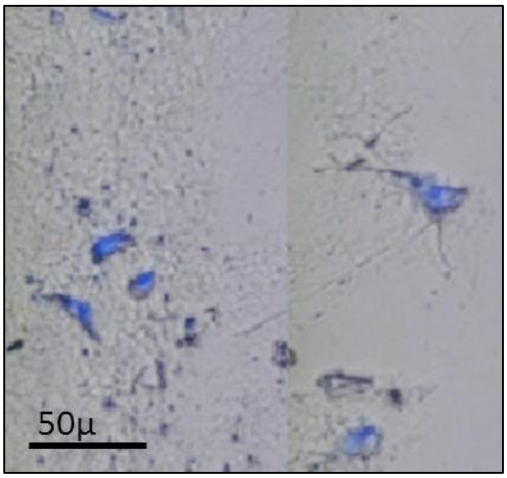

Figure 41 A cyrocut sample of a 3D collagen model containing CALU-1 cells stained with DAPI stain.

In order to see the DAPI stain, the Nicolet microscope was coupled with an Olympus fluorescence accessory (Olympus, U-LH100HGAPC), fitted with an Ushio USH102D mercury lamp, and a U-MWU cube corner filter (excitation 330-385 nm, dichroic 400nm, barrier filter 420 nm). An image was captured before switching to MidInfrared acquisition mode.

6.3.6 S-FTIR Microspectroscopy

Spectra for all experiments in this chapter were obtained at both Soleil (France) and Diamond Light Source (Oxford) synchrotrons. Further details of which are listed in chapter 2. Detection settings were duplicated. That is; 256 scans per samples, 4 cm^{-1} resolution and a 15 x 15 µm aperture were used.

6.3.7 Data Processing

EMSC was used to correct for the Mie Scattering artefact created by Dr Achim Kohler (Kohler, 2008), this was performed in Matlab Software (Mathworks, Natick, USA). The spectra were then processed within Unscrambler software for baseline (linear-offset), normalised (SNV) and smoothed (Savitsky-Golay). Data was then cropped to the areas of interest (See chapter 2) at the fingerprint and lipids regions.

6.3.8 Data Analysis

Analysis of the spectra was completed in The Unscrambler Software (Version X, Camo, Oslo, Norway). PCA was used to visualise the differences between the spectra and where those differences lay (loading plots).

6.4 Results

6.4.1 Increasing the Homogeneity of Cell Samples

Figure 41 shows an example of 2 cell populations, 1 parental and 1 clonal, after passage 3 and kept in 3D culture conditions for 1 day.

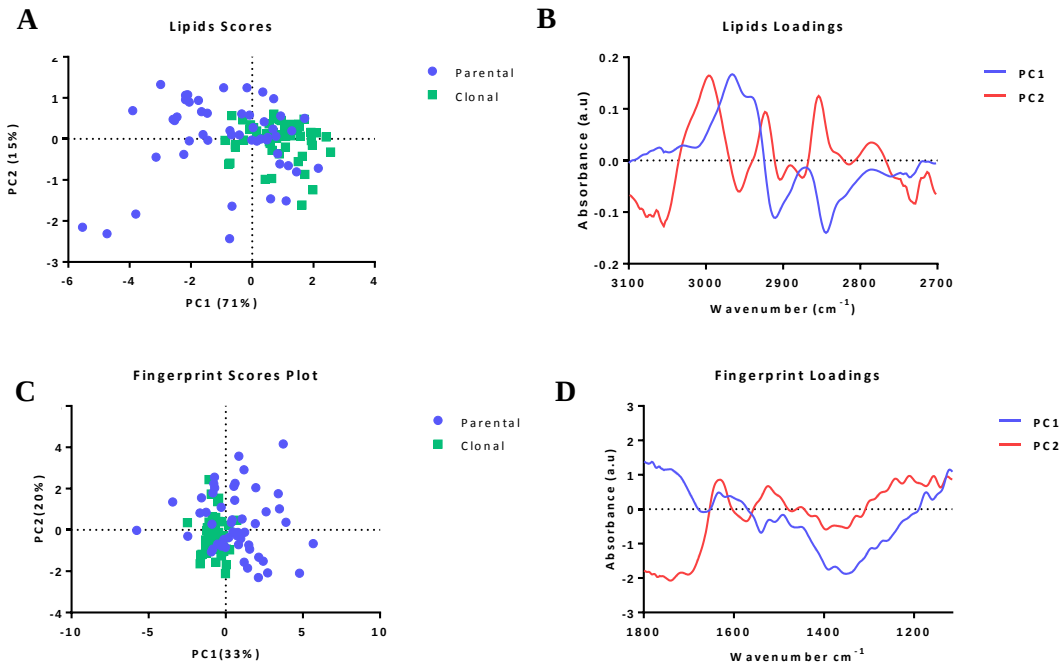

Figure 42 A PCA showing parental and clonal populations of CALU-1 cells (A) scores of the lipid region (B) loading of the lipid region, (C) scores of the fingerprint region and (D) loading of the fingerprint region (N=70).

The plots demonstrate that the populations are similar, there is some degree of overlap between the two and this is expected as they are originally the same cell line. The main message is seen within the spread of the scores plots. The scores plots for the parental population are far wider spread in both lipid and fingerprint regions when compared to the tighter scores plots of the clonal population. This points toward a clonal cell population that is of higher homogeneity than its parental counterpart, even after 3 passages.

6.4.2 Does Passage make a Difference?

Figure 42 shows the scores plots of 1 clone at different passages. It can be seen that the early passages of clonal populations still maintain a degree of homogeneity. The spread of data in

the scores plots for each example of a passage number start off close together and spread out ass passage number increases, passage 5 showing the widest spread of points.

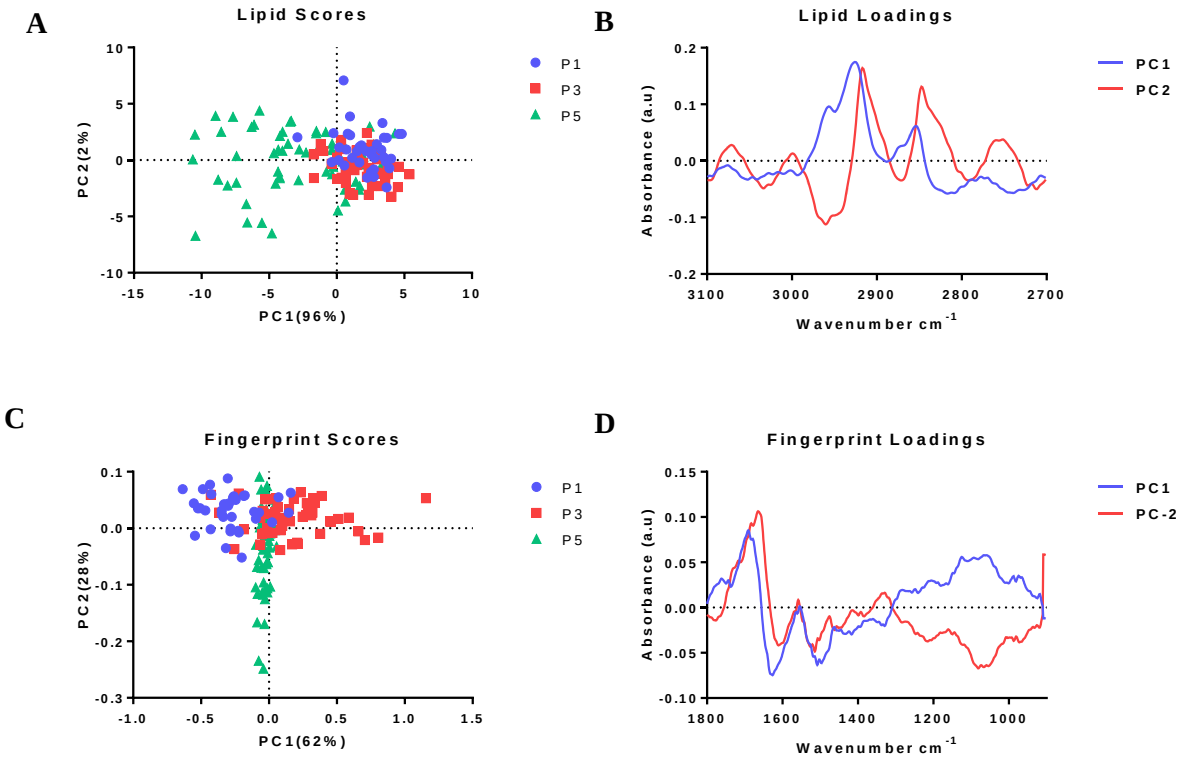

Figure 43 PCA depicting 3 different passage numbers of clonal populations of CALU-1 (A) the scores plot of the lipid region, (B) the loading plot of the lipid region, (C) the scores plot of the fingerprint region and (D) the loading plot of the fingerprint region.

6.4.3 Identification of Cells within 3D, Cryocut, Samples

Figure 44A shows unstained CALU-1 cells while Figure 44B shows DAPI stained CALU-1 cells. Figure 44 shows CALU-1 cells within a 3D following staining with DAPI. While cells can easily be identified in cytospun models as seen in Figure in 44A, this might become more difficult with smaller cells in 3D collagen gel models. However, the use of the DAPI stain allows the clear identification of cells within the 3D samples Figure 44.

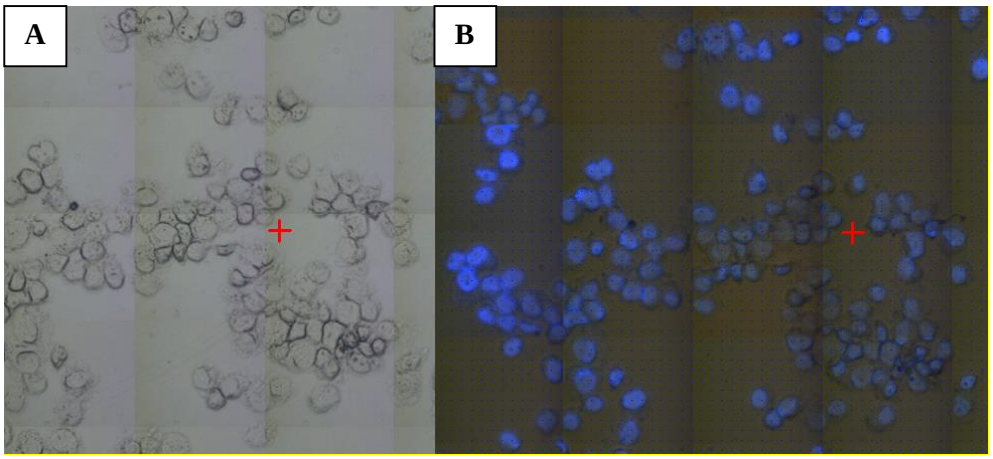

Figure 44 Light microscopy image of 2D, cytospun CALU-1 cells unstained (A), and ultraviolet (UV) image of DAPI stained cells (B).

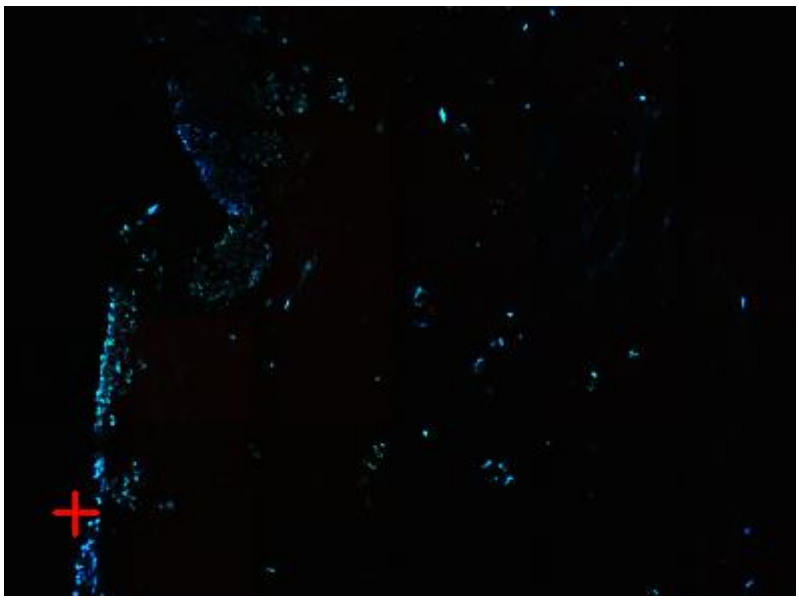

Figure 45 The UV image of a DAPI stained 3D collagen model containing CALU 1 cells.

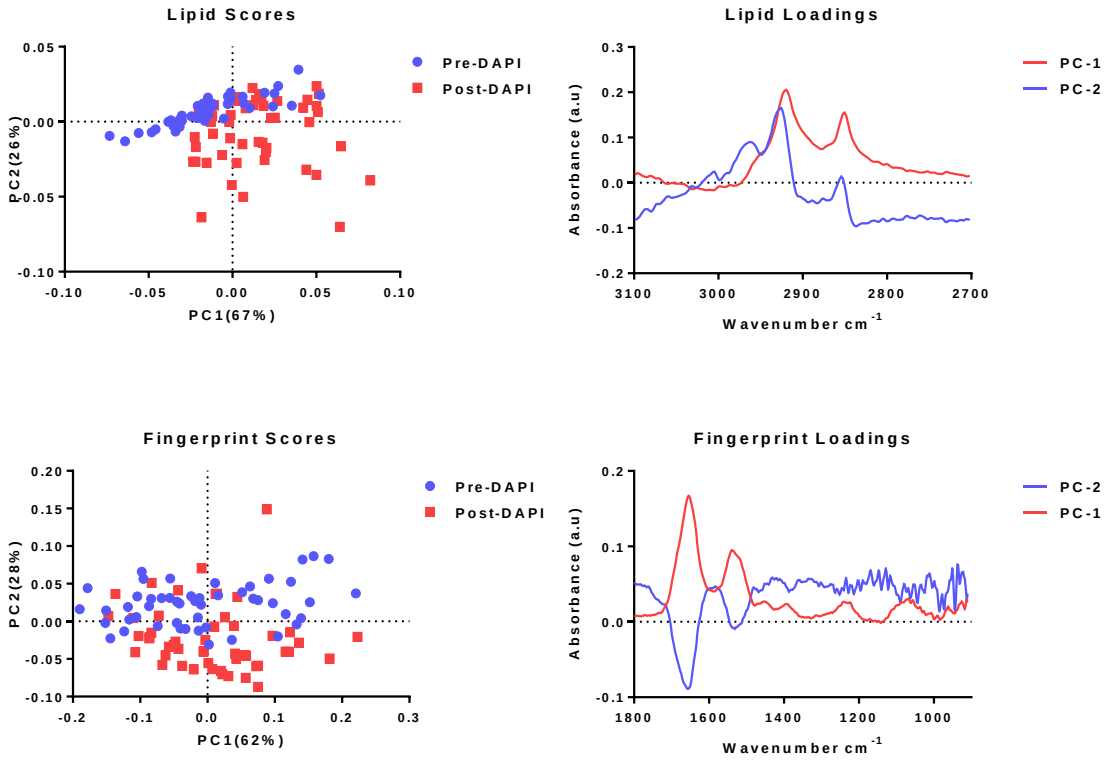

Figure 46 PCA of pre and post DAPI stained, 2D grown CALU-1 cells. (A) The scores plot of the lipid region, (B) the loading plot of the lipid region, (C) the scores plot of the fingerprint region and (D) the loading plot of the fingerprint region.

The scores and loadings plots taken from these spectra demonstrate that the DAPI stain has a slight contribution to the spectra taken from the cells post exposure. It could be argued that if the spectral changes caused by DAPI stain could be well characterised, then this methodology could help to better identify cells within a 3D matrix prior to obtaining their FTIR spectra.

6.5 Discussion

The first aim of this chapter was to produce cell populations with increased homogeneity. This was established through producing clonal populations of the lung cancer cell line CALU-1. The PCA plots for these results were compelling, Figure 42 showing clearly that

parental populations of CALU-1 were more spread across scores plots in both lipid and fingerprint regions. The loadings plots show that there is a degree of difference between the two populations, not large enough to highlight a different cell type but enough to suggest differences in the populations. The lipid region loadings show a difference at 3000cm^{-1} which is indicative of CH_2 and CH_3 stretching and also at ~2850cm^{-1} which also indicates a change in symmetrical C-H stretch of CH_2 in fatty acid chains (Barth, A. 2009). The loadings displayed as the fingerprint region display similar spectra for PC1 and PC2, with the main differences occurring around 1550cm^{-1} suggesting changes within amide II and separation around ~1240 – 1310cm^{-1} that suggest amide III band components of proteins (Barth, A. 2009). This indicates that parental populations of cells are less similar to each other. The clustering of the clonal populations of cells is far tighter within both lipid and fingerprint scores plots, indicating a more homogenous population. The overlap of both types of samples, that is, clonal and parental is a positive result. It has shown that the cloning process of the CALU-1 cell line has not affected the phenotype of the cell and that the PCA itself cannot clearly distinguish between clonal and parental populations.

In order to produce large enough cellular populations for S-FTIR and statistically viable samples, clonal populations have to be passaged in cell culture. This chapter addresses the extent to which passage has an effect on these cells. The scores of the PCA plot of a single clone can be seen in Figure 43, displaying the clone at 3 different passage numbers. There is little difference seen between passages 1 and 3. Passage 5 is when the differentiation of cells begins to occur. The loading plots indicate that the change is occurring within the lipid region at ~2950 cm^{-1}, which is due to the C-H stretching vibrations of the CH_3 and CH_2 groups of acyl chains (Lewis, R.N.A.H. 2006). The fingerprint region suggests the main differences here are between 1200-900cm^{-1} which are the wavenumbers assigned to C-O,

C-C stretching, C-O-H, C-O-C deformation of carbohydrates (Barth, A. 2009). The main separation seen within the scores plots of this PCA analysis are seen within the fingerprint region, which suggests this is where the SFTIR is first able to detect changes, perhaps mutations, that are seen as the clonal population begins to lose clonality.

In the introduction to this chapter, the question was asked, "How can we create viable biological samples that best mimic an *in vivo* environment or that best serve to answer our research question?" This chapter utilised 3D collagen models to mimic the *in vivo* environment that has already been identified in the introduction of this thesis as a suitable matrix in which to grow cells (Lee, K.Y. 2001). This is a compromise when producing biological samples that best enable us to answer our research question. 3D collagen models as kept in culture are not suitable to direct analysis with S-FTIR due to their large size. Therefore in order to produce samples that, "best answer our research question", the samples needed to be cryocut into thin slices that are eligible for analysis with S-FTIR.

Cryocutting of samples in 3D collagen models brings with it the challenge of identifying cells in the sample effectively. As mentioned earlier in this chapter some cells are small and less obvious in these sectioned pieces. This chapter overcame these challenges by utilising a DAPI stain to successfully identify cells within these difficult samples. The use of the DAPI stain did show some slight differences on the PCA plots in Figure 45 although this could attributable to noise on the spectrum. This is particularly obvious within the fingerprint loadings of the PCA plots where PC1 is seen as noisy. The lipid loadings suggest that there is a slight baseline shift in the data obtained, which could be attributed to the DAPI stain or the quality of the spectra obtained itself. Cryosectioned collagen gels have provided a

challenging substrate in which to cryo-section, the samples are highly susceptible in changes to temperature, warmth meaning the gel contracts behind the OCT cutting medium and lower temperatures meaning that the gel becomes too fragile for sufficient preparation. A change in baseline shift could also suggest that the sample surface is not entirely homogenous when prepared in this way. Besides a baseline shift and the presence of noise within the spectra there are changes in the loadings plots at ~2850cm^{-1} which wavenumber has been assigned to the C-H symmetrical stretching of CH_2 of fatty acids. The loadings plots on the fingerprint region show clear changes at bands 1650cm^{-1} and 1550cm^{-1}, these wavebands are assigned to amide I of α-helical structures and amide II. Further work will be needed to clarify the nature of these differences if the DAPI stain is to be utilised in further work.

6.6 Conclusions

Clonal populations do provide a cellular population with increased homogeneity that can be maintained for an early number of passages.

DAPI stained can be used to identify cells within 3D collagen models, but further work is needed to identify the true effects the stain has on the cells' spectra.

Chapter 7 A Study of Gemcitabine Sensitive/Resistant Lung Cancer Cells by Cell Cloning and FTIR Microspectroscopy

7.1 Introduction

The application of chemotherapy drugs in medicine is based on multicentre studies that have identified the most appropriate anticancer drugs (or combination of) for individual types of cancer. Unfortunately, not all cells exhibit the same sensitivity to anticancer drugs within tumours and therefore success rates can differ among patients. The development of new drugs is also thwarted by the lack of a clear method to establish tumour cell sensitivity that has a direct clinical application that can improve the outcome of patients with cancer (Schrag, D. 2004; Samson, D. J. 2004). Current assays include those such as gene expression profiling, *in vitro* clonogenic and proliferation assays, cell metabolic activity, molecular assays, *in vivo* tumour growth and survival assays to name a few (Chang, J.C. 2003; Robert, J. 2004; Blumenthal, R. D 2007; Cree, I .A. 2009). Positively, they are applied across a wide spectrum of cancer types. However, as they are proving difficult to apply within a clinical setting, they are currently holding back the delivery of a tailored treatment for each individual patient.

This is perhaps where spectroscopy could step up to the treatment challenge. Already several tentative studies have shown detectable differences between cells prior to, and after the application of anticancer drugs, using benchtop FTIR techniques (Gasparri, F. 2003; Sulé-Suso, J. 2005; Gasper, R. 2009; Derenne, A. 2012; Derenne, A.2012; Machana, S. 2012) and synchrotron based FTIR microspectroscopy (Draux, F. 2009; Bellisola, G. 2010). Both techniques have been previously discussed in depth in chapter One

and Two. Therefore, in brief, we can consider here the advantages of synchrotron facilities for treatment development.

S-FTIR microspectroscopy can offer us the opportunity to examine a cancer cell's interaction with a drug on a subcellular level, helping to characterise spectral biomarkers of sensitivity. S-FTIR microspectroscopy can also characterise differing cellular morphology through the spectral deformations caused by Mie scattering and dispersive artefacts caused, amongst others, by the domed shape of the cell nucleus (Marcsisin, E.J.S. 2012; Mohlenhoff, B. 2005; Romeo, M. 2005; Pijanka, J.K. 2009). While this may prove useful in some scenarios, here as we are applying chemotherapy agents, changes in cell morphology are indicative to dying cells rather than those that maybe sensitive or resistant to drugs.

7.2 Aims

1. To better characterize spectral biomarkers of cell sensitivity to chemotherapy in 2D models of lung cancer, following the addition of the drug.

2. To be able to identify sensitivity/resistance of lung cancer cells to a given drug prior to the addition of the drug.

7.3 Materials and Methods

7.3.1 Cell Culture

CALU-1, a non-small cell lung cancer cell line was used in this study. The cell line belongs to the squamous epithelial group of cells and was grown under the 2D cell culture conditions 1, listed in Table I of this thesis.

7.3.2 Experimental Setup of Clonal populations of CALU-1

In order to be able to assess the sensitivity of the cells to be characterised by S-FTIR microspectroscopy and to maintain a higher level of homogeneity across a cellular population, clonal culture methods were established.

The cells were cultured in standard conditions within T75 flasks and dissociated according to the details under "2D Culture Conditions 1" (Table I, chapter Two). Following dissociation, cells were then counted using the trypan blue exclusion method and seeded in 96 well plates at a concentration of 0.5 cells/well. Each well was then topped up to a total of 200 µL with fresh medium. A total of 5 x 96 well plates were used to ascertain between 25-30 clonal populations. Once seeded, the stack of plates were foil wrapped to avoid dehydration, stored in a 37 °C, 5% CO_2 incubator and allowed to culture for two weeks. After 1 week, a single media change was performed, replacing 180 µL with fresh medium to avoid disturbing fragile clonal populations. Each well was inspected regularly to ensure that only populations formed from a single clonal cluster would be selected.

Once the 2 week culture was complete, the selected clones were dissociated from their plate using 10 µL of trypsin-EDTA for 5 minutes within the culture incubator. 190 µL of fresh medium was used to quench the trypsin. Each clonal population was then split proportionally across five wells of a new flat bottomed 96 well plate (40 µL into each well) and topped with 160 µL of medium (Figure 48). Cells were not counted here to avoid the loss of cells from an already relatively low cell number. The cells were then left to acclimatise for 24 hours before the addition of the chemotherapy drug (Figure 48).

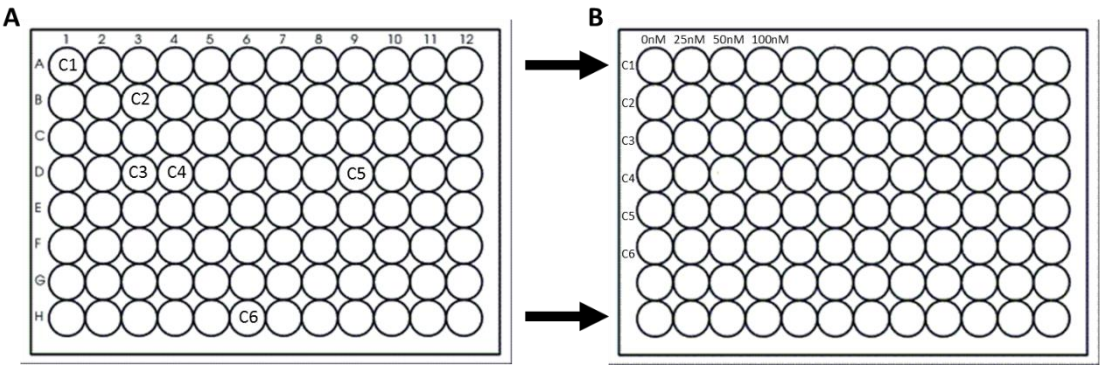

Figure 47 96 well plate layout of CALU-1 clonal population. (A) Clonal populations before passage and (B) the subdivision of passaged, clonal populations of CALU-1 exposed to 3 different doses of gemcitabine and a control case.

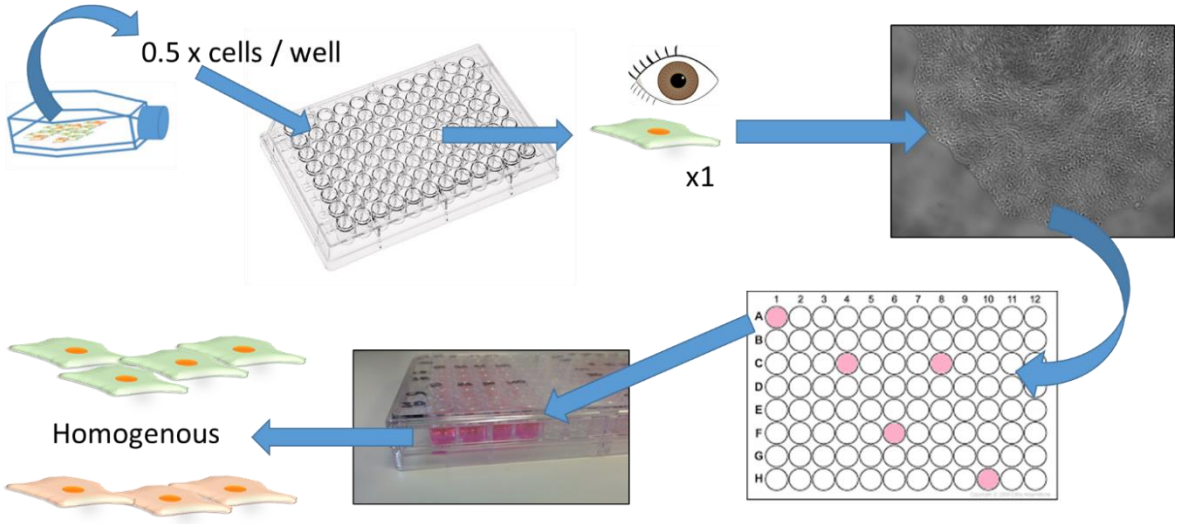

Figure 48 Illustration of the CALU-1 cloning process and the identification of viable clonal populations of cells.

7.3.3 The Application of Chemotherapy Agents to Clonal Populations

Gemcitabine was applied at doses of 25, 50 and 100 nM and a control well with 0 nM. The dose was determined by preliminary experiments that showed at 25 nM all clones were able to survive and that 1 mM was a 100 % cytotoxic dose for all cell clones. Table IX shows the list of clones produced for this study following the addition of gemcitabine at different doses.

Clones were exposed to gemcitabine for 5 days. In order to be able to measure sensitive cells with S-FTIR microspectroscopy, some cells had to be salvageable from the 100 nM wells. Five days was a compromise, allowing enough time to establish if the cell population was sensitive to the drug but also to be able to harvest a few cells for characterisation. Synchrotron beam time is limited in its allocation, this means only a few clones were selected for analysis (clones 4, 5, 6, 8, 12 and 13 were chosen, in bold in Table IX). Clones were selected based on their quality, choosing examples of obvious sensitive clone (populations that were few in number) or resistant clones (populations that were greater in number) to different doses of gemcitabine.

Table IX. CALU-1 clones produced for this study, following the addition of gemcitabine agent for 5 days.

Clone number	0 nM	50 nM	100 nM	Clone number	0 nM	50 nM	100 nM
1	++	++	+	**15**	++	++	+/-
2	++	++	++	**16**	++	++	+/-
3	++	++	+	**17**	++	++	++
4	++	++	++	**18**	+	+/-	+/-
5	++	++	+/-	**19**	+	+	+/-
6	++	++	++	**20**	++	+	+/-
7	++	+	-	**21**	++	++	++
8	++	+/-	-	**22**	++	++	++
9	++	++	+/-	**23**	++	++	++
10	++	++	+	**24**	++	++	++
11	++	++	+	**25**	++	++	++
12	++	-	-	**26**	++	-	-
13	++	-	-	**27**	+	+	+/-
14	++	++	-	**28**	++	++	++

Confluent wells were labelled with two crosses, semi-confluent wells were labelled with one cross, wells with sparse number of cells were labelled +/- and wells without cells were labelled with a minus sign. Figure 49 shows some examples.

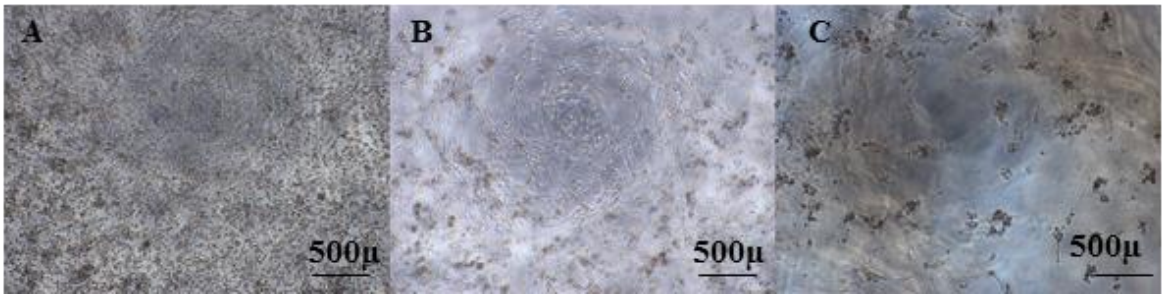

Figure 49 Example of clonal populations of CALU-1 of (A) Resistant (B) Semi-Sensitive (C) Sensitive to gemcitabine

Sensitive populations were not counted in order to maximise cells available for S-FTIR analysis. Control and resistant cell population's survival was greater than 90% on collection.

7.3.4 Sample Preparation

Collected clones were cytospun at 1000 rpm for 1 minute onto 0.5 mm thick CaF_2 slides (Crystan) and fixed with 4% paraformaldehyde in 0.9% NaCl in H_2O for 20 minutes at room temperature. Samples were then washed once with NaCl and three times with distilled water. Samples were then air dried at room temperature.

7.3.5 S-FTIR microspectroscopy

SFTIR spectra were obtained at the SMIS beamline, Soleil Synchrotron. A Nicolet Nexus 6700 FTIR Spectrometer was used, coupled to a Nicolet Continuum XL Infrared Microscope, which was fitted with a 32x infinity corrected Schwarzschild objective. A liquid nitrogen cooled 50 µm S MCT /A detector was used. The system was able to collect spectra at a resolution of 4 cm^{-1} using an aperture size of 15 x 15 µm. This aperture was based around the size of a cell's nucleus, a point of interest due to gemcitabine's mode of action being within this part of the cell and also because previous work had already determined the size

of the CALU-1 nucleus when cytospun as 10 µm in diameter (Pijanka J.K., 2009). Therefore, on this basis a 15 x 15 µm aperture was applied, centred to incorporate a whole cell's nucleus.

For each clone 50 control cells were measured. Where gemcitabine had been applied varying numbers of spectra were obtained due to varying cell numbers being harvested for sample preparation. In the latter case, as many cells were analysed as possible. Images of the cell population were obtained throughout and cells labelled so each cell was analysed only once (Figure 49).

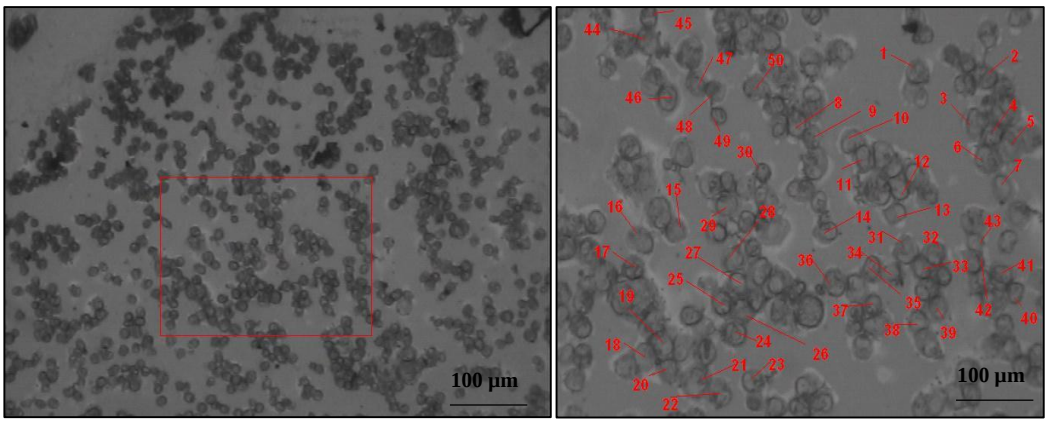

Figure 50 Image of cytospun cells, depicting the labelled cells that FTIR measurement had been taken from in order to only analyse each cell once.

Spectra were then pre-processed as follows. A nonresonant Mie correction was applied (an extended multiplicative signal correction, EMSC) developed by Dr Achim Kohler (Kohler, A. 2008). Mie scatter is a well characterised spectral component (often seen as a shift in the Amide I region) which is confounded by the rounded shape of a cell, especially the cells nucleus. Here, cytospinning of the samples helped reduce this artefact by producing flatter cellular samples and no major amide I shift in the spectra was observed. Therefore due to the quality of the raw spectra obtained we did not apply the resonant Mie scatter correction.

Following this consideration, spectra were cropped to specific regions to be analysed; 2700 -3100 cm^{-1} for lipid regions and 1000-1800 cm^{-1} for the fingerprint region. Then spectral groups were normalised (using the standard normal variate, SNV).

7.3.6 Analysis

Spectra analysis using multivariate statistics, principle component analysis in particular, was performed within Unscrambler Software (CAMO).

7.4 Results

7.4.1 FTIR Analysis of Clonal Populations Exposed to Gemcitabine

The premises of this study were, first, to identify spectral markers of tumour cell sensitivity to gemcitabine. Second, to obtain S-FTIR spectra of resistant and sensitive cells prior to the addition of the chemotherapy agent, in order to avoid measuring any morphological changes that would be caused by the apoptosis process that the cells would undergo as a result of drug exposure. Firstly, the mean spectra of each clonal population was analysed, comparing cells of the same clonal population that had been exposed to different concentrations of gemcitabine. Figures 51 A-C shows the mean spectra of the individual CALU-1 clones with different degrees of sensitivity to gemcitabine. Figures 51 A-B (chosen clones 6 and 5) are both examples of resistant clones; those cells that did not respond to the drug treatments at 50 nM and 100 nM. Figure 51 C (chosen clones 8) is an example of a clone that is semi-resistant. That is, C is representative of a clone that is mostly resistant to a 50 nM dose of

gemcitabine but still shows signs of death when exposed to the 100 nM dose; only 16 cells were recovered suitable for S-FTIR analysis following sample preparation.

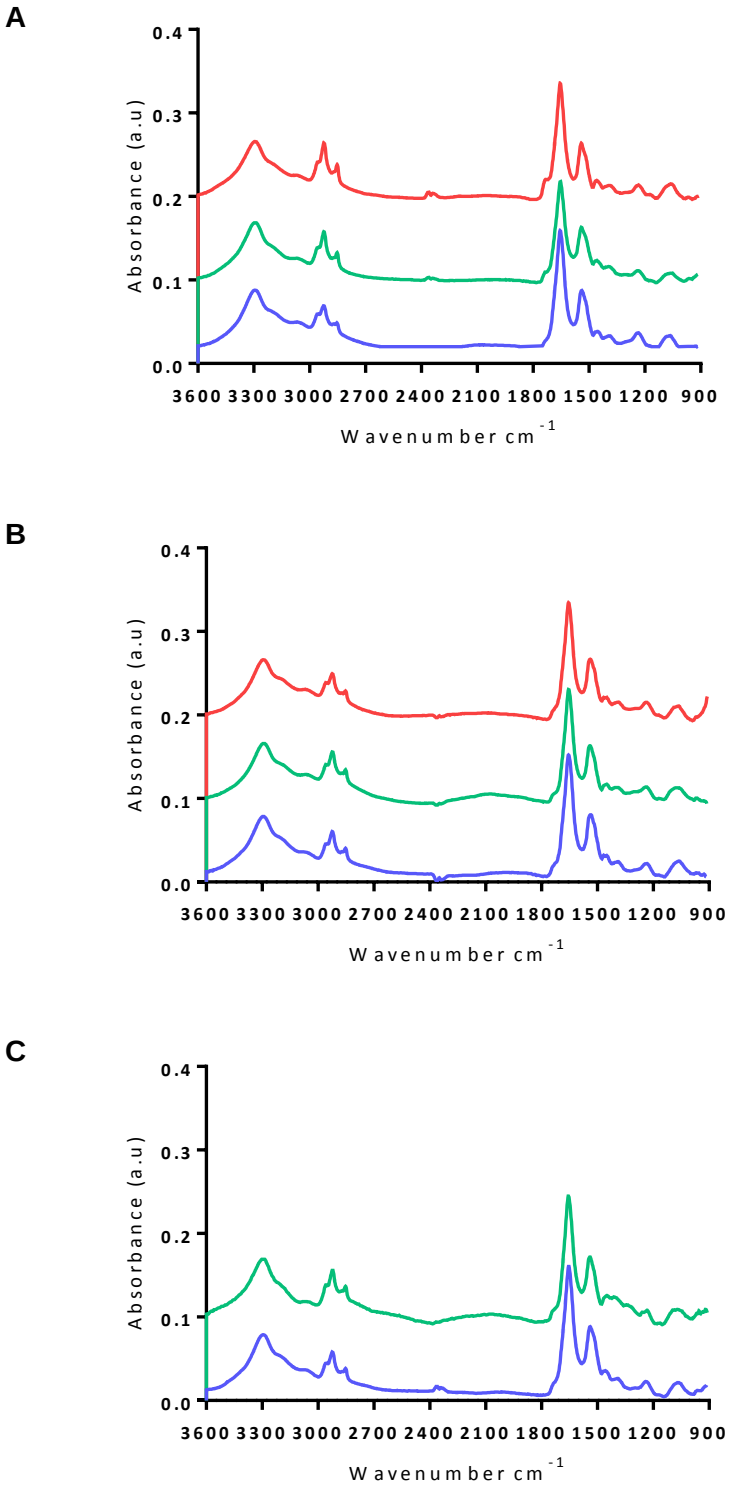

Figure 51 Mean spectra of (A) Resistant clonal population, (B) semi-resistant clonal population and (C) sensitive clonal population, exposed to 0 nM (blue), 50 nM (green) and 100 nM (red) doses of gemcitabine.

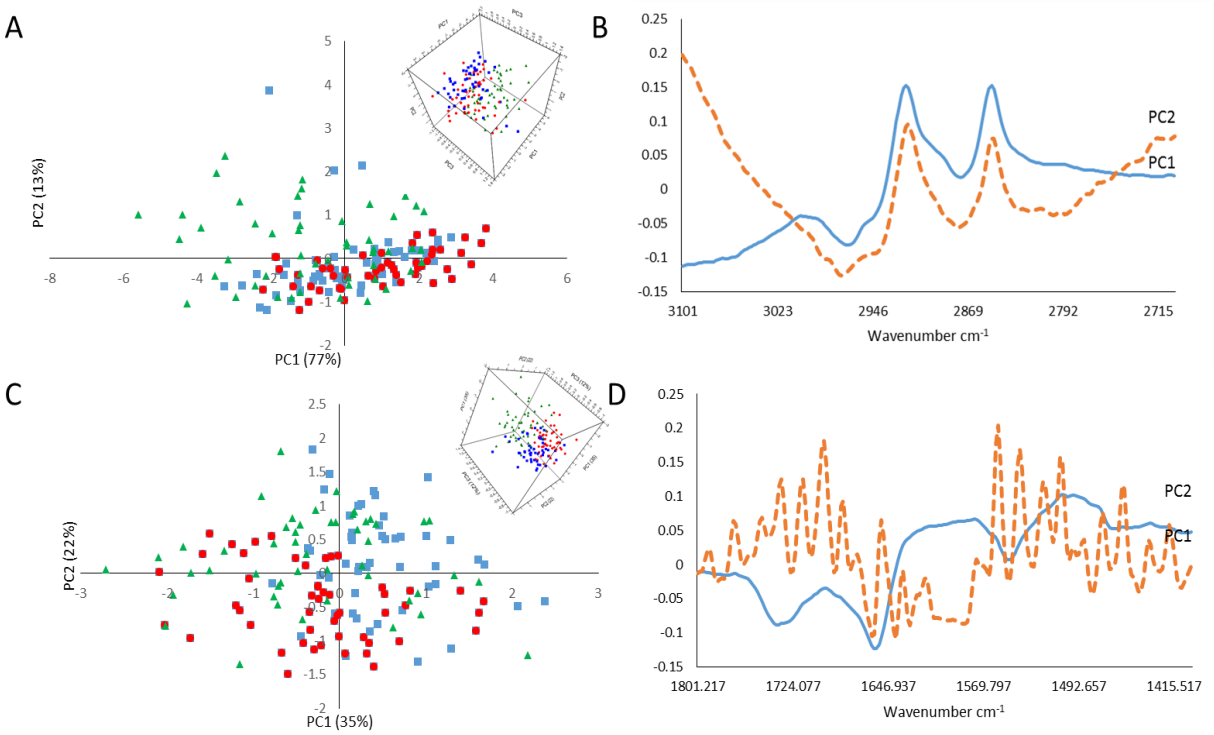

Figure 52 PCA of resistant clone 4 including (A) scores plot of lipid region, (B) loading plot of lipid region, (C) scores plot of fingerprint regions and (D) loading plot of fingerprint region. Inserts in (A) and (C) depict 3D scores plot.

The PCA for resistant clone 4 (Figure 52) does not show any major separations between the control samples (0 nM, squares) and those exposed to 50 nM of gemcitabine (circles), however if we plot the PCA scores within a 3D scatter plot (see inserts of A&C) a slight separation can be seen with the 100 nM exposed samples (triangles) in both the lipid and fingerprint regions.

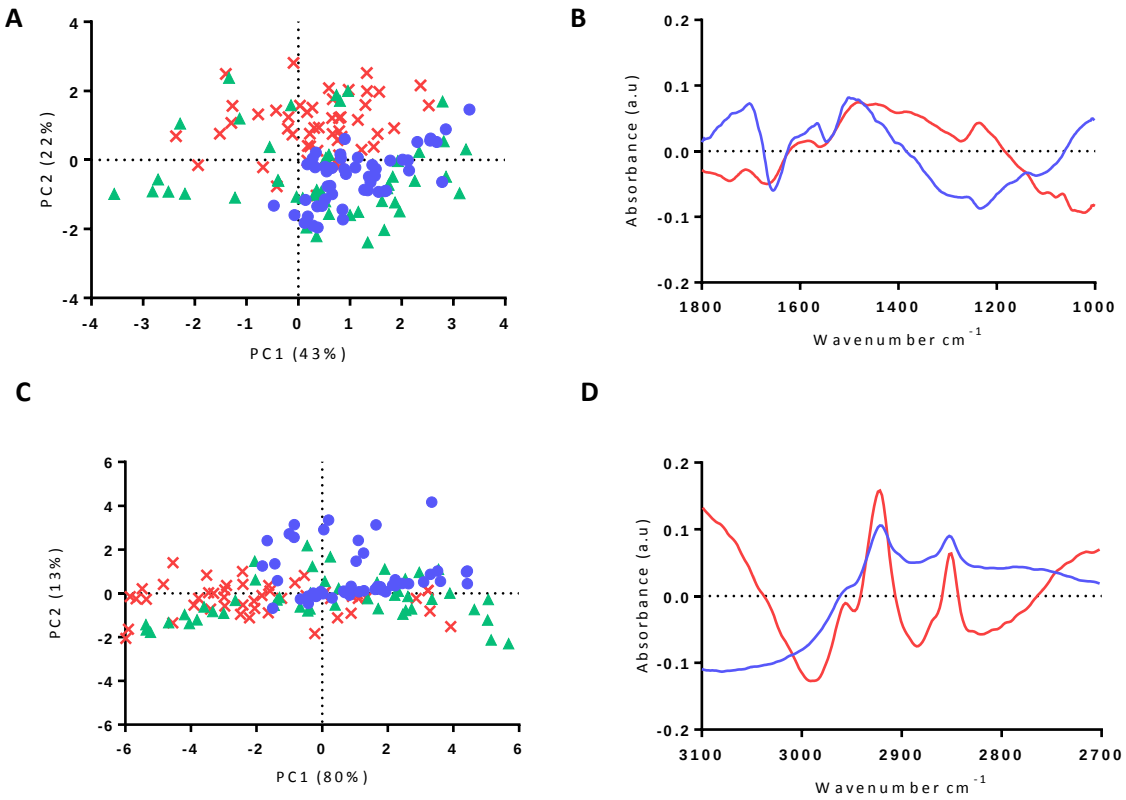

Figure 53 PCA of resistant clone 6 depicting (A) scores plot of fingerprint region, (B) loading plot of fingerprint region, (C) scores plot of lipid regions and (D) loading plot of lipid region.

PCA for resistant Clone 6 (Figure 53) did not show well defined separation within the lipid regions between any of the samples. In the fingerprint regions (A and B, above) we can see a slight separation between 100 nM dosed cells (crosses) when compared to 50 nM (dots) and 0 nM (triangles).

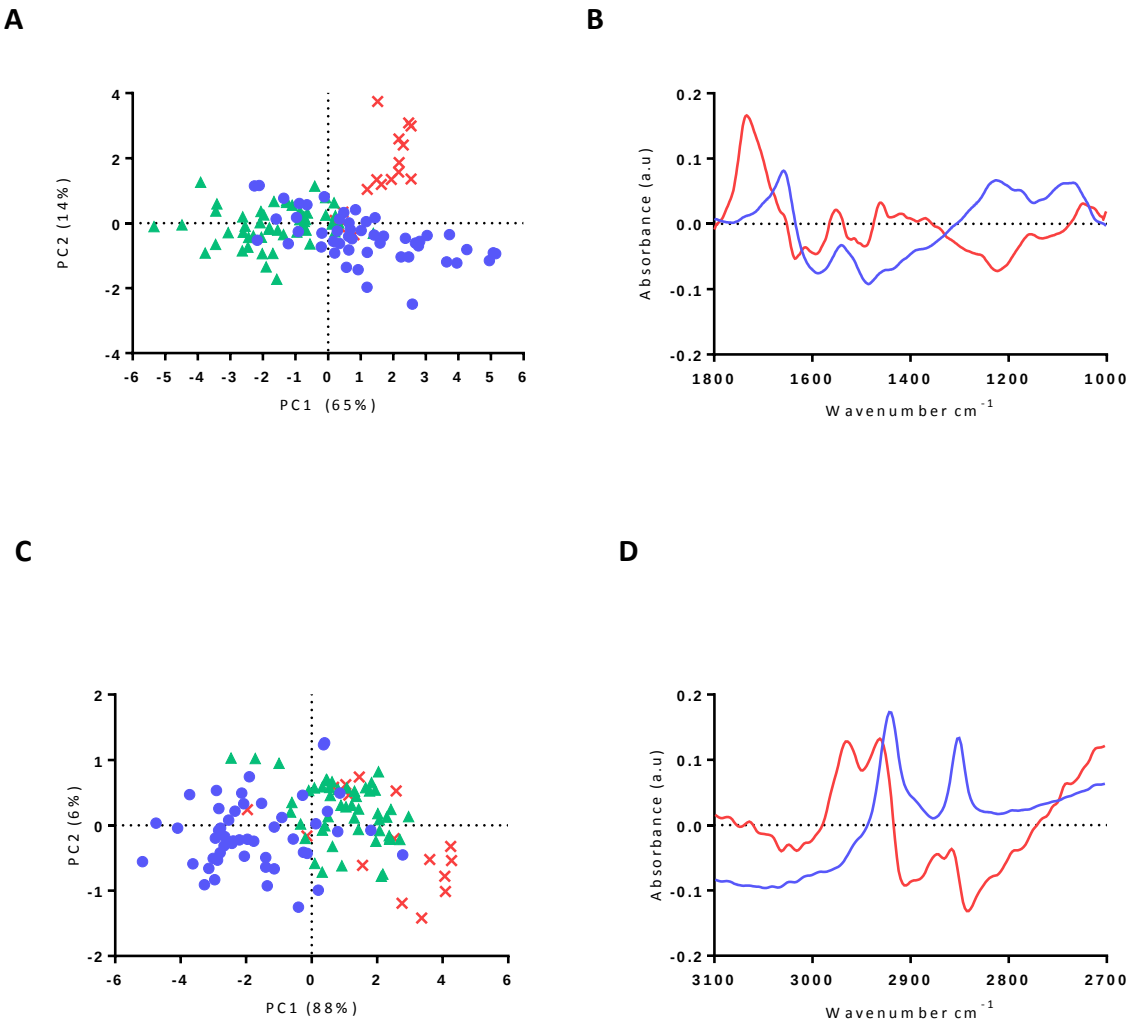

Figure 54 PCA of semi- resistant clone 5 (A) scores plot of fingerprint region, (B) loading plot of fingerprint region, (C) scores plot of lipid regions and (D) loading plot of lipid region.

The PCA for semi-resistant clone 5 (Figure 54) shows a far more well-defined separation in both the lipid and fingerprint regions for 100 nM dosed cells (crosses) when compared to 50 nM (dots) and 0 nM (triangles).

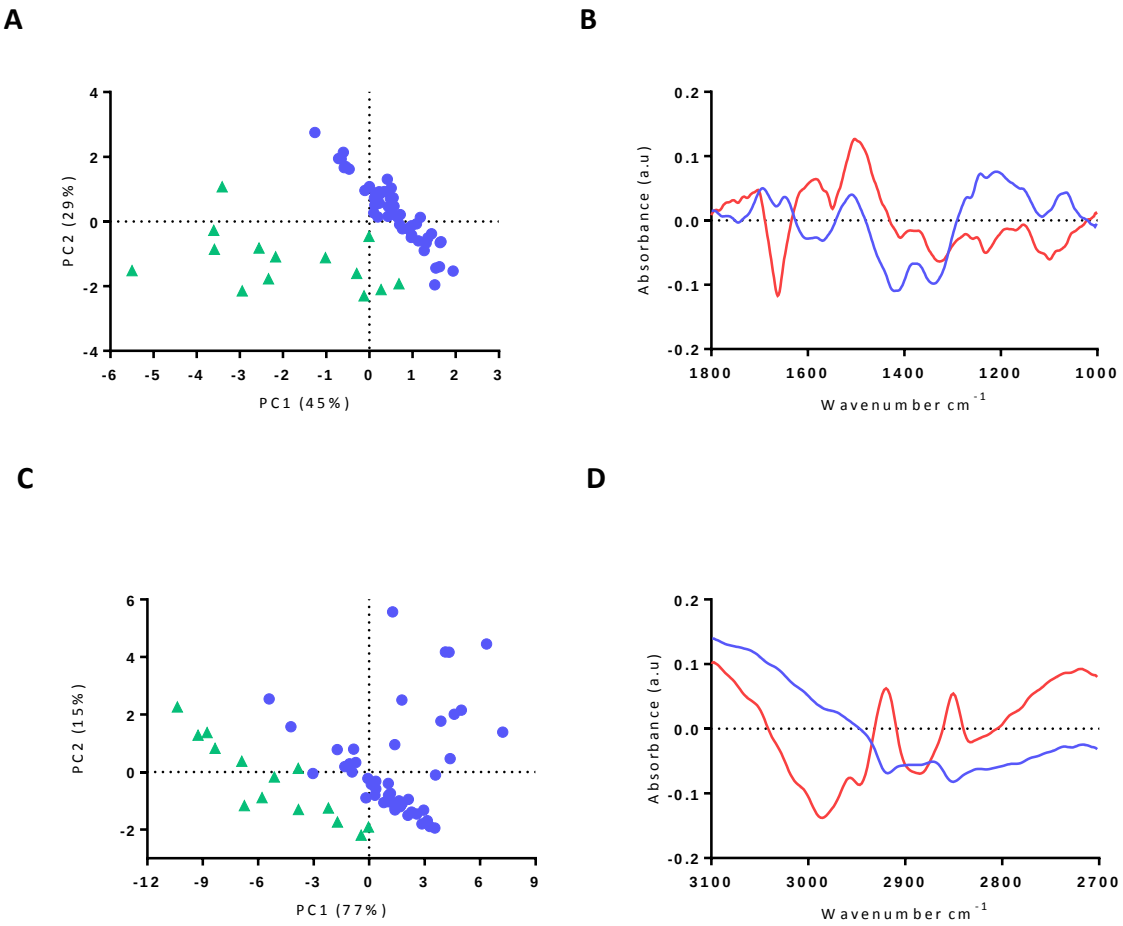

Figure 55 PCA of semi-resistant clone 8 (A) scores plot of fingerprint region, (B) loading plot of fingerprint region, (C) scores plot of lipid regions and (D) loading plot of lipid region.

The PCA for clone 8 (Figure 55) shows a strong separation between the control sample (0 nM, triangles) and the 50 nM exposed sample (dots). This can be seen clearly for both lipid and fingerprint regions in the loading plots (B and D above). Interestingly, clone 8 is the most sensitive of the semi-resistant clones analysed, no cells having survived when exposed to 100 nM compared to clone 5 above, where some cells were able to survive the 100 nM drug exposure.

Individual PCA for sensitive clones 12 and 13 were not performed as only control samples (0 nM) were obtained.

One of the aims of this study was to assess if it is possible to identify spectral differences between sensitive and resistant cells prior to the addition of gemcitabine. Therefore, the following figure is a PCA of resistant clone 6 (triangles) and sensitive clone 13 (dots) exposed to 0 nM of gemcitabine.

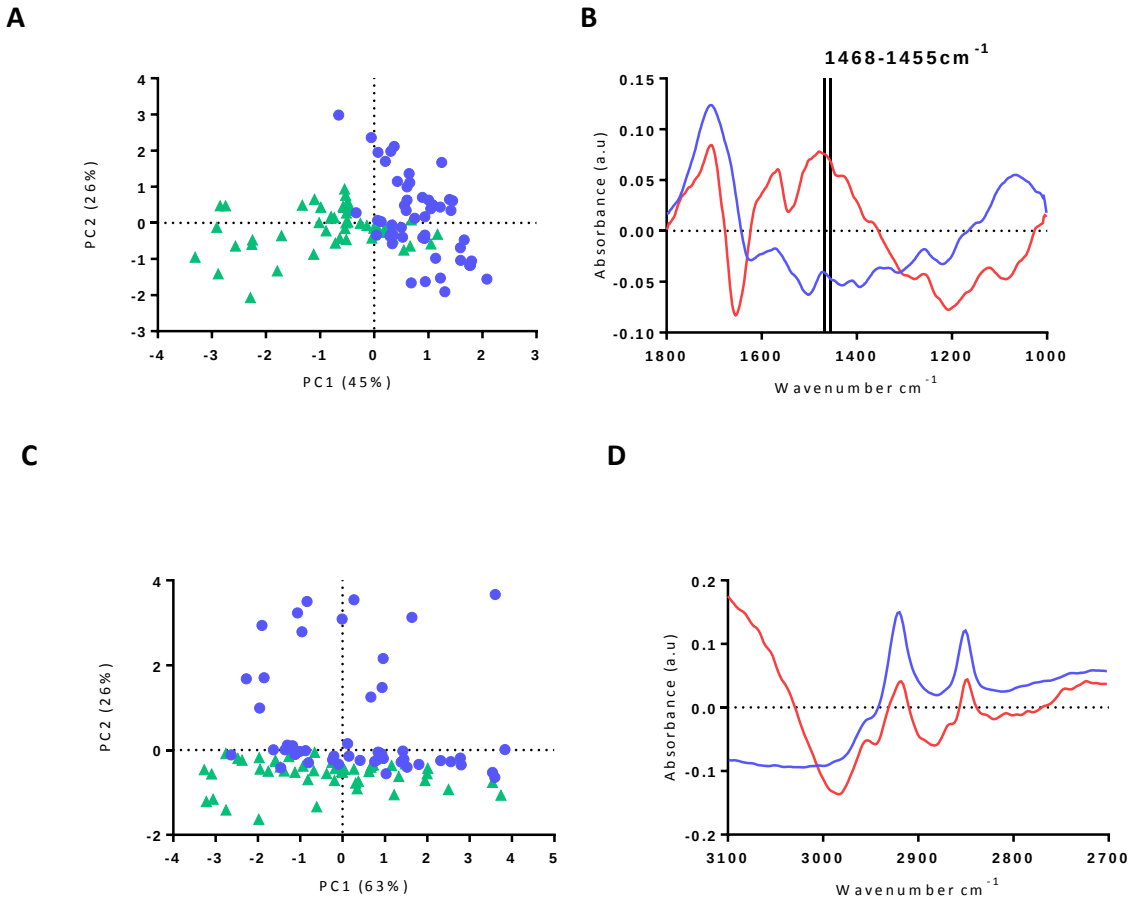

Figure 56 PCA plots for sensitive and resistant clonal populations (A) scores plot of fingerprint region, (B) loading plot of fingerprint region, (C) scores plot of lipid regions and (D) loading plot of lipid region.

There is a clear separation between sensitive and resistant clones here both in the lipid and the fingerprint regions, which can be seen clearly in the scores plots of Figure 56. The loading plots also represent this difference, the fingerprint loading plot in particular illustrating changes at 1468-1455 cm^{-1}. These band regions as mentioned earlier are indicative of CH_3 and CH_2 groups of lipids and proteins. The lipid loading plot indicates a less clear separation. This could suggest that S-FTIR microspectroscopy distinguishes sensitive and resistant clones prior to the addition of drugs, and therefore that sensitive and resistant clones have different spectral profiles. However, we have to acknowledge that some of the differences may be due to the fact that they are different clones.

Figure 56 also serves to demonstrate that the spectral differences seen between the cells is not due to biochemical changes induced by the drug. The PCA was completed using the clones from 0 nM, control conditions and still shows clear separation between both cell types.

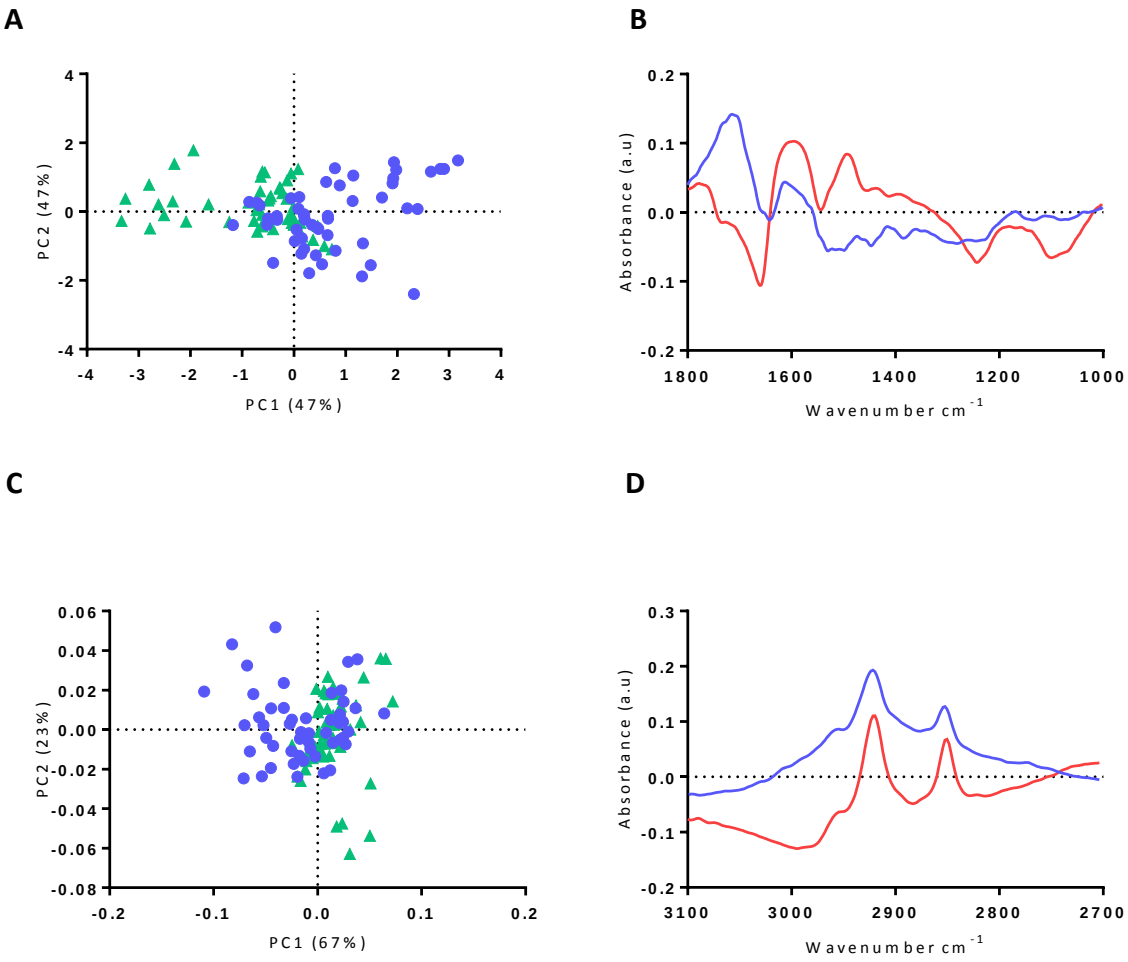

Figure 57 PCA of sensitive clones 12 and 13 at 0 nM exposure of gemcitabine (A) scores plot of fingerprint region, (B) loading plot of fingerprint region, (C) scores plot of lipid regions and (D) loading plot of lipid region.

The PCA for both sensitive clones 12 (triangles) and 13 (dots) in Figure 57 shows that there is no clear separation between the two in both lipid and fingerprint regions, the lipid region showing a well-mixed population of scores. This is markedly different from the clear separation seen between a PCA of sensitive and resistant clones (Figure 57).

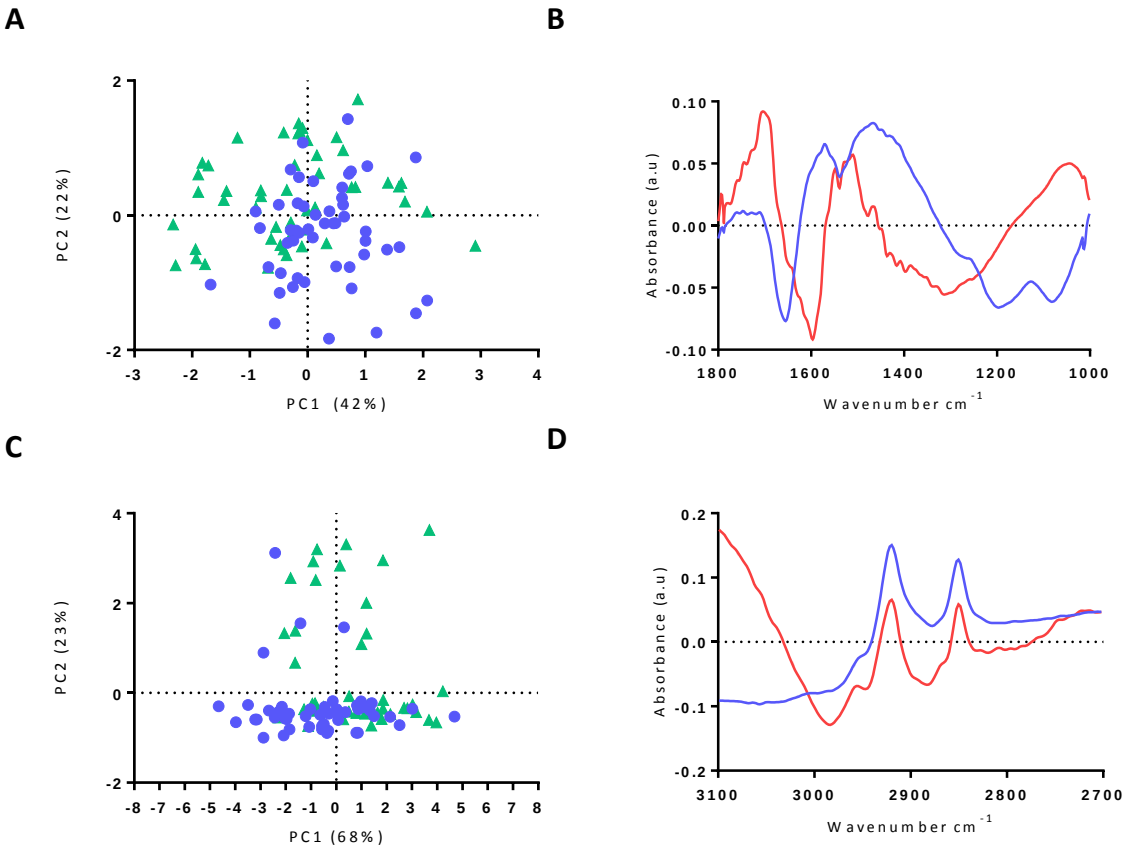

Figure 58 PCA of 2 resistant clones 4 and 6 at 0 nM gemcitabine exposure (A) scores plot of fingerprint region, (B) loading plot of fingerprint region, (C) scores plot of lipid regions and (D) loading plot of lipid region.

Figure 58 shows the PCA scores and loadings for two resistant clones (Clones 4, triangles, and 6, dots). Again, as we see with the sensitive clones, there is no particular clear separation of the two when compared to the separation we see when we compare a sensitive with a resistant clone.

Figures 57 and 58 address an important point. They would suggest that the spectral differences seen between the sensitive and resistant clones are not just due to the fact that

they are different cell populations or samples. Two control cases from sensitive clones do not show separation and neither do two control cases from resistant clones.

The data indicate that the spectral differences between sensitive and resistant control clones are possibly produced by the innate characteristics of tumour cell sensitivity to the drug. Further studies to clarify this with more cancer cell lines and drugs are required.

7.5 Discussion

As discussed, a widely known character indicative of cancer cells within a tumour is the nonhomogenous nature of cells themselves (Aktipis, C. 2013). This, of course poses the problem that some cells could be sensitive to a chemotherapy agent whilst others are resistant, with varying degrees of sensitivity between these two possibilities. This unfortunately means that we are currently unable to predict a tumour's response to the assigned treatment. Previous methods have been applied to assess the tumour cell response to treatment, although they are not currently practiced within the clinical setting yet (Cree, I.A. 2009) leaving the management of patients with lung cancer to be based on data taken from multicentre studies.

A majority of the work completed so far, using vibrational spectroscopy, to assess a variety of cancer types' response to drugs has used these mixed populations, studying the cells both prior to and after the addition of the drug itself (Draux, F. 2011; Bellisola, G. 2010; Derenne, A. 2012; Marcsisin, E.J.S. 2012; Sulé-Suso, J. 2005; Machana, S. 2012; Gasper, R. 2009; Gasparri, F. 2003). Some of the architecture of

the spectra presented in these studies could be as a result of the drug itself and/or the metabolites present after the addition of the chemical. This study perhaps avoids this confounding factor; within the data collected from the resistant 2D clones with both the addition and absence of gemcitabine we cannot see any major spectral changes. This could indicate the lack gemcitabine's contribution to the obtained spectra. Perhaps this is due to the inhibition of the transport of gemcitabine in resistant cells; that is perhaps the resistance here was due to the drug not being internalised by the cells. Or perhaps due to an inhibition of the metabolical pathway gemcitabine must undergo to become an active compound in the resistant cells (Moysan, E. 2012).

Another factor when considering a mixed population of cells is the idea that perhaps within this population are resistant cells that have suffered damage from the drug dose but are then able to recover from this damage, or perhaps sensitive cells that are damaged but still alive when collected for S-FTIR analysis. These damaged cells could perhaps elicit perceived spectral differences between those cells that have and have not been exposed to drugs, making the interpretation of any useful information difficult. This highlights a need for a system that can reduce these variables as much as possible.

Here we have aimed to control this by implementing the study of cancer cells that have originated from a single cell (Zarcone, D. 1987). This provides the study with a population of cells with far more uniform characteristics given they are analysed having only undergone few cell divisions after the clone has been identified in culture. Using the experimental setup described previously (Chapter 2), it was possible to study the spectral differences of both sensitive and resistant clones within a far more uniform population.

Earlier studies of chemotherapy drugs applied to cancerous populations of cells have shown spectral differences within the lipid regions (Liu, K.Z. 2001), amide regions (Gasparri, F. 2003; Zhou, J. 2001), nucleic acids (Sulé-Suso, J. 2005; Liu, K.Z. 2001) and the lower lipid:protein ratio within resistant cells (Gaigneaux, A. 2002). But these differences could be indicating a difference within the mixed populations of cells. The data presented in this study has shown clearly that the more sensitivity shown by cells to gemcitabine, the larger the difference between cells prior to and after the addition to the drug. Therefore within mixed populations, the spectral changes would be magnified, following the addition of a drug, if the mixed population were to contain a higher number of cells sensitive (and still alive when collected for S-FTIR analysis). However, further work is needed to clarify this hypothesis. Our sensitive populations did show an increased intensity within the peaks at 2850 and 2920 cm^{-1}, which corresponds to CH_2 stretching of methylene chains within lipid membranes, and also at the peak 1740 cm^{-1} which corresponds to the carbonyl C=O stretching of the phospholipid (Jamin, N. 1998, Holman, M. 2000).

This relative increase in the intensity of the lipid peaks has already been well documented amongst different cell lines (Zhou, J. 2001; Travo, A. 2012; Gasper, R. 2009; Liu, K. Z. 2001; Machana, S. 2012). The sensitive clones studied here also show this increased intensity, that indicates the increase of lipids with the increase of apoptosis within cells (Liu, K. Z. 2001). It has been discussed that this is a consequence of the cell membrane changes within the apoptotic state; phosphatylserine exposure, membrane blebbing and vesicle formations (Zelig, U. 2009). The changes seen here at the peak 1740 cm^{-1} have also been described as a biomarker for oxidative stress (Vileno, B. 2010), which is also associated with apoptosis (Holman, H.Y.N. 2000).

Before we can consider the change in lipid intensity as a form of marker for tumour sensitivity to gemcitabine, we must take into account the changes that could be caused by the fixation methods used in this study. The use of paraformaldehyde as a fixative induces CH_2 groups into the samples. This would contribute to the spectral regions where the lipid fatty acyl chain CH_2 groups would also be seen. It is therefore required that further work is needed to understand the implications that paraformaldehyde has imposed on any conclusions that could be drawn about tumour sensitivity from changes within lipid intensities. It is unknown whether paraformaldehyde may interact differently with those sensitive and resistant cells, as permeability of the cells has already been previously discussed. Conversely, no prominent differences were observed at the phosphate bands following the addition of the chemotherapy agent gemcitabine. This indicates that the 1740cm^{-1} band may be more discriminative within the fingerprint region of the spectra.

Interestingly these data show that S-FTIR microspectroscopy can separate between resistant and sensitive, 2D cultured, clonal populations prior to the addition of the drug gemcitabine. Although it has been considered that some of these differences could be attributed to the differences between the actual populations of clones themselves, it has been described that differences within the 1740 cm^{-1} band can separate between multiresistant and sensitive cells (Gaigneaux, R. 2002) and that differences between the mechanisms of resistance to the drug that are inherent to each individual cell which might provide us with a different spectral characteristics for sensitive and resistant clones (Fryer, R.A. 2011; Bergman, A. M. 2002) leaving our results to look promising. This would have to be confirmed with further studies of differing cancer types and a wider range of chemotherapy agents.

Conclusions

To summarise, this work has presented a proof of concept, using a clonal lung model based around the previously reported work on lung cancer and gemcitabine. The experimental methods using clonal techniques have refined the study of the effects of chemotherapy agents on populations of cancer cells with vibrational spectroscopy. This work could be applied to examine a wider range of cancer treatments, such as radiotherapy and other non-chemotherapy based techniques. The methodology could also be applied to correlating cell spectra with apoptotic pathways within more uniform cell populations (Holman, H. 2000; Holman, H.Y.N. 2000). Cell studies with clonal populations could also be expanded to include lung models, applying the 3D systems previously discussed in this thesis to examine the effects that sensitivity could have on the spectra of cells grown in an environment with increased physiological relevance.

Tentatively, we can confirm that SFTIR was able to separate gemcitabine sensitive and resistant lung cells. To the vibrational spectroscopy community this conclusion points towards the expansion of clonal work, to identify if these changes are unique to lung cancer/this culture model. Broader ramifications of this work are also considered, that is, the conclusions here point towards a potential diagnostic tool that could support currently utilised techniques.

Chapter 8 Conclusions and Further Work

There is great demand for a complimentary diagnostic tool, that could support current pathological techniques, to improve the management of lung cancer. The disease is currently plagued by a poor prognosis, which has been largely attributed to the cancer being diagnosed at a late stage, by which time curative treatment may not be available. In order to address this problem, novel diagnostic tools could be used to compliment current diagnostic practices used within the clinic. This thesis aimed to examine 2 techniques, addressing some of the practical issues associated with both clinical and scientific application, with the purpose of leading towards better management of lung cancer.

The first experimental chapter (Chapter 3) is focused on the use of the SIFT-MS to quantify acetaldehyde release by lung cells. As a novel technique, SIFT-MS offers non-destructive and real-time analysis of VOCs given out by lung cells. This analysis could be used to identify a profile of cancerous lung cells that is different from non-cancerous lung cells. Acetaldehyde was identified by previous studies as a VOC of interest, in part because early studies had associated lung cancer cells with releasing higher amounts of the VOC (Sulé-Suso, J. 2009). It is also of interest because other studies had found conflicting results, that acetaldehyde levels in cell culture medium decreased in the presence of the lung cancer cell line CALU-1 (Filipiak,W. 2008). The chapter therefore had 3 main aims; firstly to widen the examination of the release of acetaldehyde in different lung types. Secondly, to improve upon the cell culture environment the cells were grown in, to a more physiological representation of a lung

tissue. Thirdly, to investigate the impact of using different cell culture mediums on the VOCs released by lung cell lines.

The study reiterated the findings from previous studies, that acetaldehyde is released above the quantity of that seen in the cell culture medium headspace (Sulé-Suso, J. 2009; Smith, D. 2003) within 3D cell culture models. The levels of AC were raised in 3D collagen models above those found in 2D models. This indicated that changes in the environment the cells are cultured in have ramifications on the acetaldehyde metabolism the cells will undergo. The same chapter continued to investigate how changes to this environment affected VOCs released by cells. This was done through changing the different types of culture medium cells were initially cultured in (in 2D, cell culture flasks) before being transferred to a 3D model and also by changing the base culture medium used to create the 3D collagen model.

Through changing the cell culture medium in the models, it has been found that the effect can be dramatic on the cell metabolism of acetaldehyde. The presence of DMEM cell culture medium causing the cells to produce higher levels of acetaldehyde than the Ham's F12 medium alternative. It is not yet clear why these changes are happening. It is suggesting that a component of the DMEM cell culture medium is contributing to some of the metabolical processes of the cell that are involved in acetaldehyde production. Further work therefore would lend itself to the investigation of some of the components that are known to have roles within mammals in this pathway and are present in different quantities' within the cell culture mediums. As already discussed in chapter 3, pyridoxal and L-threonine are obvious starting points for further work. The 2

components could be added to the cell culture medium or 3D collagen model and changes in the VOCs measured using the SIFT-MS.

Another immediate avenue for further work would also be to study how the different media and the subsequently added components (such as the L-threonine and Pyridoxal) affect the function of the ALDH enzymes present within the cells. As mentioned, this could be investigated using flow cytometry. The ALDEFLOUR ^{TM} Kit (Stemcell Technologies, 01700) allows for the study of ALDH (non-specifically). A comparison of ALDH activity and cell culture medium could be examined.

Chapter 3 has met the aims set out for the chapter having examined the release of acetaldehyde in differing lung types using a refined 3D collagen model using SIFT-MS, which has led to a publication (Rutter, A. V. 2013). The chapter has also gone some way to address the differences seen between previous studies on the release of acetaldehyde by lung cancer cells, pointing the research towards the contribution that cell culture medium has on the metabolism of cells. The chapter has also given further work a firm direction. That is, to understand the role of specific cell culture medium components on the VOCs released by lung cell lines. The chapter has also contributed well to the main aim of the thesis. It works towards the understanding of the metabolical pathways of lung cells that may help to identify useful VOCs given out by lung cancer cells using a clinically viable tool (the SIFT-MS).

The second experimental chapter, chapter 4, also used the novel technique SIFT-MS as a diagnostic tool. The chapter addresses the use of labelled glucose (labelled at ^{13}C) as

a marker for metabolism within the lung cell lines given its association with the Warhburg effect within the cancerous populations (Koppenol, W.H. 2011; Ngo, D.C. 2015), and also previous studies that have already explored the use of labelled glucose to identify changes in the VOCs in the breath of participants. This chapter also compliments chapter 3, leading on to another way of examining the metabolical effects of the components of cell culture medium we have already seen.

The first aim of the study was to establish a refined 3D collagen model for use with SIFT-MS analysis. The PBS based 3D collagen model allowed for the 3D structure needed to improve the physiological architecture of cell culture but lacked some of the components of cell culture medium that have been affecting the release of VOCs by the lung cells. This was demonstrated by production of a 3D model containing PBS and by the cell viability seen within the chapter.

The second aim of chapter 4 was to utilise labelled glucose for the study of VOCs produced by metabolical markers. The study identified no trend in the release of acetaldehyde between ^{12}C and ^{13}C glucose across all lung cell types. Acetaldehyde was found in lung cell samples to be below that of the PBS cell culture medium alone, implying there was a change in metabolism of the cells grown in the new 3D collagen model, but this was not identifiable using the ^{13}C labelled glucose. PCA of full scan data did show a difference between ^{12}C and ^{13}C glucose samples and so shows promise for the use of labelled compounds for the study of metabolical pathways using SIFT-MS, although some issues still need refinement as discussed in chapter 4 if this technique is to be used to its full potential.

Chapter 5 was also a dedicated chapter to using the novel tool SIFT-MS. The chapter aimed to establish a suitable methodology for the acquisition of breath samples for lung cancer patients. It also aimed to be able to separate these breath profiles from those taken from participants without lung cancer.

Chapter 5 found that establishing a suitable sampling method was a challenging task, each method (direct, bag and bottle) had its own challenge. Direct sampling methods may obviate the loss of any sample but are difficult to obtain from those patients with poor lung function or who are unable to attend clinics. FSM sampling is also a challenge for direct breath as a patient must provide a full exhalation for the desired scanning time. Bag and bottle sampling methods overcome this by allowing for large measuring times but have the downside of losing some of the sample and being difficult to store efficiently. Although chapter 5 demonstrates it is reasonable to still obtain useful data from these sampling methods, further work could be done to increase the efficiency of the materials. Overall bag and bottle sampling methods have proved useful, they are portable and cost effective mode of sample acquisition and storage. They also collect a full exhalation from the patient, which they can provide easily.

Future work for chapter 5 is therefore clear; the sampling methods can be refined further, creating sampling bags and bottles with increasingly sufficient seals. Also, the investigation of the storage temperature of these vessels could also improve the sampling efficiency. Reducing the temperature of the vessels to below -80°C, for example, would slow down the loss of VOCs. This could potentially decrease the overall

loss of VOCs on sampling and also lengthen the sampling time. Vessels would need to be returned to 37 °C upon sampling, but temperature alteration would be a cost efficient and fast avenue of sample storage to explore.

The second aim of chapter 5 was to distinguish between the breath of people with and without lung cancer. There were no clear differences between the profiles of those with and without lung cancer using the MUI analysis. This work could be revisited, in part with the refinement of the sampling method, but also to incorporate the FSM of each participant, that would give details on a broader amount of VOCs. The main separation within the FSM data showed that the differences that did occur between those patients with lung cancer and those without was acetonitrile; a VOC found in the breath of smokers (Abbott, S. M 2003; Španěl, P. 1996).

Although not an aim of the study, chapter 5 demonstrated the use of SIFT-MS to identify the smoking status of the participants involved. The amount of acetonitrile present in the breath of participants being correlated with the smoking history. This demonstrates the SIFT-MS and the bag sampling method's suitability as a tool to assess smoking status. This is clinically relevant as being able to accurately assess smoking status can provide help for the patient with regard to treatment advice and the assessment of the suitability of the patient for lung transplant.

Chapter 6 turned to the use of S-FTIR microspectroscopy as a tool to study lung cancer. The aim of the chapter was centred on establishing methodologies that increased the suitability of the cellular models for S-FTIR sampling. Firstly, through increasing the homogeneity of

our samples (where relevant) and also investigating if fundamental 3D cell culture practises, that is passage, affects the data acquired from S-FTIR microspectroscopy. The chapter also addressed the identification of the cells with the 3D collagen models and the effect of the presence of the 3D collagen model itself.

Chapter 6 demonstrated that producing clonal populations of cells does increase the homogeneity of the sample population compared to the parental counterparts. This is particularly useful and has been used in chapter 7 to assess the sensitivity of lung cancer cells to a chemotherapy agent, gemcitabine.

The chapter also demonstrated that early passages do not make a difference, however the ongoing passage of cells will mean a differentiation from the original parental body, which is to be expected. If studies were to incorporate cells grown over large amount of time and passaged regularly this would have to be a consideration. Findings here meant that later work is based on cells that are close in passage number to avoid any variance caused by this to be seen as differences in cell populations.

Chapter 6 also showed the challenges faced when working with 3D collagen models for S-FTIR analysis, although this challenge can also be applied to all forms of spectroscopy. DAPI provided confirmation of the location of cells within these tissues easily, however there were slight changes to the spectra produced from cells after being stained. This methodology needs to be further assessed to establish that the changes in spectra are definitely just due to noise. If not a refinement of the DAPI stain method itself could be changed to reduce any differences down. This could be done by reducing down the exposure

of the stain through time or concentration and to also look at the suspension fluid that the stain is delivered in.

Chapter 6 illustrates the use of an important methodology for the field of spectroscopy, the first experiment highlighting that differences seen within cellular populations could be due to general differences that could mask smaller experimental changes. In order for the cloning method to be justified the same chapter also illustrates the practicalities of using the clonal method and how many passages should be taken before a population. DAPI staining could be of use to a wide community, being an attractive method to be applied to a variety of regenerative medicine studies, where the confirmation of cell nuclei is important. The overall impact of the chapter is perhaps modest, but vital in the experimental set up of how we prepare cells for SFTIR spectroscopy.

Chapter 7 utilised the findings from chapter 6, incorporating the use of clonal populations to assess the sensitivity of lung cancer cells to the chemotherapy agent gemcitabine. The chapter's aims were to establish a biomarker of sensitivity in clonal populations of CALU-1 grown in 2D culture conditions. The second aim of the chapter was also to identify sensitivity and resistance to the drug prior to the addition of the drug.

The work in chapter 6 did show differences between sensitive and resistant clonal populations of cells. It is not straightforward to identify a biomarker of sensitivity from this work intrinsically, as there were other variables that needed to be accounted for such as the role of the fixative PFA used. Further work to assess the full extent of the effect of fixatives in drug dosed, clonal populations of cells needs to be explored. Although the results in this chapter are promising, showing differences between sensitive and resistant groups of cells,

further work to expand the study needs to be implemented before any main conclusions can be drawn. Firstly, the work needs to be expanded to assess different lung cancer and general cancer types to ensure the features seen here contributing to the differences in the spectra are not specific to the CALU-1 cell line alone. The work also needs to be expanded to include other chemotherapy agents used for the treatment of cancer.

The second aim of the chapter was clearly answered. The characterisation of drug sensitivity and resistance in cells prior to the addition of the drug was fulfilled by utilising the clonal methodology expanded in chapter 6. Differences among the control portions of clonal populations that were not exposed to the drug, clearly identifying profiles that are indicative of sensitivity. The clonal methodology also demonstrates that changes seen in the spectra are also due to differences in sensitivity and not due to other features caused through the application of the drug. This chapter lead to a publication on the findings and methodology used here on the identification of gemcitabine sensitivity in cells post drug application.

In conclusion, this thesis has answered a majority of the aims set out for each chapter. Future work is clearly outlined from each study on ways to improve the methodology where in some cases these aims have not been met in their entirety. The future direction of the research to improve the management of lung cancer as a whole is also outlined and this thesis has laid appropriate foundations for the continuation of this improvement. The potential of SIFT-MS as a novel tool to help diagnose lung cancer as a non-invasive and economical technique seems promising but still has much more work to establish trends in larger populations and also to refine the sampling techniques used. S-FTIR microspectroscopy also shows much promise in the *in vitro* study of cell characterisation. This technique could be used in support of pathological practises to identify cells that are cancerous. S-FTIR microspectroscopy also

has the potential to be used to support the identification of appropriate treatment for patients, characterising how cancerous population will respond to drugs.

Overall, this thesis has made a contribution to the methodological preparations that will be undertaken in both the fields of mass spectrometry and vibrational spectroscopy. It has also demonstrated the potential of two techniques that could support the current diagnostic practises that are currently used to diagnose lung cancer.

Appendices

Appendix 1. WHO Histological Classification of Tumours of The Lung

Benign epithelial tumours

Papillomas

Adenomas

Malignant epithelial tumours

Squamous cell carcinoma

Small cell carcinoma

Adenocarcinoma

Large cell carcinoma

Adenosquamous carcinoma

Sarcomatoid carcinoma

Carcinoid

Salivary gland tumours

Preinvasive lesions

Mesenchymal tumours

Lymphoproliferative tumours

Lymphoma

Lymphomatoid granulomatosis

Langerhans cell histiocytosis

Miscellaneous tumours

Hamartoma

Sclerosing haemangioma

Clear cell tumour

Germ cell tumours

Intrapulmonary thymoma

Melanoma

Metastatic tumours

Appendix 2. Stages of Lung Cancer

Small Cell Lung Cancer

Limited disease. Confined to the ipsilateral hemithorax

Extensive disease. Beyond ipsilateral hemithorax, which may include malignant pleural or pericardial effusion or haematogenous metastases.

Non Small Cell Lung Cancer (TNM)

Primary tumour (T)

Tx Primary tumour cannot be assessed, or the tumour is proven by the presence of malignant cells in sputum or bronchial washing but is not visualized by imaging or bronchoscopy

T0 No evidence of primary tumour

Tis Carcinoma in situ

T1 Tumour ≤ 3 cm in greatest dimension, surrounded by lung or visceral pleura, no bronchoscopic evidence of invasion more proximal than the lobar bronchus (not in the main bronchus); superficial spreading of tumour in the central airways (confined to the bronchial wall)

T1a Tumour ≤ 2 cm in the greatest dimension

T1b Tumour > 2 cm but ≤ 3 cm in the greatest dimension

T2 Tumour > 3 cm but ≤ 7 cm or tumour with any of the following:

- Invades visceral pleura
- Involves the main bronchus ≥ 2 cm distal to the carina
- Associated with atelectasis/obstructive pneumonitis extending to hilar region but not involving the entire lung

T2a Tumour > 3 cm but ≤ 5 cm in the greatest dimension

T2b Tumour > 5 cm but ≤ 7 cm in the greatest dimension

T3 Tumour > 7 cm or one that directly invades any of the following:

- Chest wall (including superior sulcus tumours), diaphragm, phrenic nerve, mediastinal pleura, or parietal pericardium;
- Or tumour in the main bronchus < 2 cm distal to the carina but without involvement of the carina
- Or associated atelectasis/obstructive pneumonitis of the entire lung or separate tumour nodule(s) in the same lobe

T4 Tumour of any size that invades any of the following: mediastinum, heart, great vessels, trachea, recurrent laryngeal nerve, oesophagus, vertebral body, or carina; or separate tumour nodule s) in a different ipsilateral lobe

Regional lymph nodes (N)

Nx Regional lymph nodes cannot be assessed

N0 No regional node metastasis

N1 Metastasis in ipsilateral peribronchial and/or ipsilateral hilar lymph nodes and intrapulmonary nodes, including involvement by direct extension

N2 Metastasis in the ipsilateral mediastinal and/or subcarinal lymph node(s)

N3 Metastasis in the contralateral mediastinal, contralateral hilar, ipsilateral or contralateral scalene, or supraclavicular lymph nodes

Distant metastasis (M)

Mx Distant metastasis cannot be assessed

M0 No distant metastasis

M1 Distant metastasis

M1a Separate tumour nodule(s) in a contralateral lobe; tumour with pleural nodules or malignant pleural (or pericardial) effusion

M1b Distant metastasis

Anatomical Stage

Stage	T	N	M
IA	T1a	N0	M0
	T1b	N0	M0
IB	T2a	N0	M0
IIA	T1a	N1	M0
	T1b	N1	M0
	T2a	N1	M0
	T2b	N0	M0
IIB	T2b	N1	M0
	T3	N0	M0
IIIA	T1	N2	M0
	T2	N2	M0
	T3	N1	M0
	T3	N2	M0
	T4	N0	M0
	T4	N1	M0
IIIB	T4	N2	M0
	T1	N3	M0
	T2	N3	M0
	T3	N3	M0
	T4	N3	M0
IV	Any T	Any N	M1a or M1b

Appendix 3. Typical Operating Conditions of the SIFT-MS

Parameter	Symbol	Typical value	Unit
Flow tube (reaction) length	l	50	mm
End correction factor	ε	20	mm
Flow tube diameter	d_t	10	mm
Injection orifice diameter	O_2	1.0-2.0	mm
Ion sampling orifice diameter	O_3	0.3	mm
Reaction time	t	5×10^{-4}	s
Bulk velocity	υ_g	10^4	$cm.s^{-1}$
Precursor ion velocity	υ_i	1.5×10^4	$cm.s^{-1}$
Carrier gas flow rate	Φ_C	11.0 820	$Torr.l.s^{-1}$ ml/min
Sample flow rate	$\Phi_{A,M}$	0.32 24	$Torr.l.s^{-1}$ ml/min
Helium number density	[He]	3×10^{16}	cm^{-3}
Flow tube pressure	P_g	1.0	Torr
Ion source pressure		0.5	Torr
Precursor ion filter pressure		10^{-4}	Torr
Downstream mass spectrometer pressure		10^{-4}	Torr
Gas temperature	T_g	300	K

Table adapted from (254 Smith, D. 2011)

Appendix 4. A List of Media Components (Lonza and Sigma)

DMEM High Glucose w/o L3Glutamine w/ Sodium Pyruvate

1119-34-2	L-Arginine Monohydrochloride	C6H14N4O2.HCL	84.00 mg/l
73-22-3	L-Tryptophan	C11H12N2O2	16.00 mg/l
72-19-5	L-Threonine	C4H9NO3	95.00 mg/l
61-90-5	L-Leucine	C6H13NO2	105.00 mg/l
56-45-1	L-Serine	C3H7NO3	42.00 mg/l
30925-07-6	L-Cystine Dihydrochloride	C6H12N2O4S2.2HCL	62.60 mg/l
72-18-4	L-Valine	C5H11NO2	94.00 mg/l
56-40-6	Glycine	C2H5NO2	30.00 mg/l
73-32-5	L-Isoleucine	C6H13NO2	105.00 mg/l
69847-45-6	L-Tyrosine Disodium Salt Dihydrate	C9H11N03+2Na+2H2O	103.79 mg/l
71-00-1	L-Histidine Monohydrochloride monohydrate	C6H9N3O2	42.00 mg/l
63-91-2	L-Phenyalanine	HO2CCH(NH2)CH2C6H	66.00 mg/l
63-68-3	L-Methionine	C5H11NO2S	30.00 mg/l
657-27-2	L-Lysine Monohydrochloride	C6H14N2O2.HCL	146.00 mg/l
7487-88-9	Magnesium Sulfate Anhydrous	MgSO4	97.67000 mg/l
7647-14-5	Sodium Chloride	NaCl	6400.00000 mg/l
10043-52-4	Calcium Chloride Dihydrate	CaCl2	265.00000 mg/l
7558-80-7	Sodium Phosphate Monobasic Anhydrous	NaH2PO4	109.00000 mg/l
7447-40-7	Potassium Chloride	KCL	400.00000 mg/l
50-99-7	D-Glucose Anhydrous	C6H12O6	4500.00000 mg/l
7782-61-8	Ferric Nitrate Nonahydrate	Fe(NO3)3•9H2O	0.10000 mg/l
67-48-1	Choline Chloride	C5H14NO.Cl	4.00000 mg/l
137-08-6	D-Ca Pantothenate	C9H17NO5	4.00000 mg/l
59-30-3	Folic Acid	C19H19N7O6	4.00000 mg/l
87-89-8	Myo-inositol	C6H12O6	7.20000 mg/l
98-92-0	Nicotinamide (Nicotinic Acid Amide)	C6H6N2O	4.00000 mg/l
65-22-5	Pyridoxal Hydrochloride	C8H9NO3.HCl	4.00000 mg/l
83-88-5	Riboflavin	C17H20N4O6	0.40000 mg/l
67-03-8	Thiamine Hydrochloride	C12H17N4OS+Cl-.HCl	4.00000 mg/l
34487-61-1	Phenol Red Sodium Slat	C19H13NaO5S	15.90000 mg/l
113-24-6	Sodium Pyruvate	C3H3NaO3	110.00000 mg/l
144-55-8	Sodium Bicarbonate	NaHCO3	3,700.00 mg/l

Ham's F-12 Medium w/ L-Glutamine

Lonza

Description	Chemical Formula	Concentration		Molarity	
		g/L	mg/L	mM	uM
Calcium Chloride Anhydrous	CaCl2	3.330E-02	33.300	0.300	300.027
Cupric Sulfate Pentahydrate	CuSO4 • 5H2O	2.500E-06	2.500E-03	1.001E-05	0.010
Dextrose	C6H12O6	1.802	1.802E+03	10.000	1.000E+04
Ferrous Sulfate Heptahydrate	FeSO4 • 7H2O	8.300E-04	0.830	2.986E-03	2.986
Potassium Chloride	KCl	0.224	223.650	3.000	3.000E+03
Sodium Bicarbonate	NaHCO3	1.176	1.176E+03	13.998	1.400E+04
Sodium Chloride	NaCl	7.599	7.599E+03	130.031	1.300E+05
Sodium Phosphate, Dibasic Anhydrous	Na2HPO4	0.142	142.020	1.000	1.000E+03
Zinc Sulfate Heptahydrate	ZnSO4 • 7H2O	8.600E-04	0.860	2.991E-03	2.991
L-Alanine	HO2CCH(NH2)CH3	8.910E-03	8.910	0.100	100.011
L-Arginine Monohydrochloride	C6H14N4O2 • HCl	0.211	210.700	1.000	1.000E+03
L-Asparagine Monohydrate	NH2COCH2CH(NH2)COOH • H2O	1.501E-02	15.010	9.998E-02	99.980
L-Aspartic Acid	HO2CCH(NH2)CH2CO2H	1.331E-02	13.310	0.100	100.000
L-Cysteine Monohydrochloride Monohydrate	C3H7NO2S • HCl • H2O	3.512E-02	35.120	0.200	200.000
L-Glutamic Acid	C5H9NO4	1.471E-02	14.710	0.100	100.000
L-Glutamine	C5H10N2O3	0.146	146.200	1.000	1.000E+03
Glycine	HO2CCH2NH2	7.510E-03	7.510	0.100	100.040
L-Histidine Monohydrochloride Monohydrate	C6H9N3O2 • HCl • H2O	2.096E-02	20.960	0.100	100.000
L-Isoleucine	HO2CCH(NH2)CH(CH3)CH2CH3	3.940E-03	3.940	3.004E-02	30.037
L-Leucine	HO2CCH(NH2)CH2CH(CH3)2	1.312E-02	13.120	0.100	100.023
L-Lysine Monohydrochloride	C6H14N2O2 • HCl	3.654E-02	36.540	0.200	200.055
L-Methionine	HO2CCH(NH2)CH2CH2SCH3	4.480E-03	4.480	3.003E-02	30.027
L-Phenylalanine	HO2CCH(NH2)CH2C6H5	4.960E-03	4.960	3.003E-02	30.026
L-Proline	C5H9NO2	3.453E-02	34.530	0.300	299.922
L-Serine	HO2CCH(NH2)CH2OH	1.051E-02	10.510	0.100	100.010
L-Threonine	HO2CCH(NH2)CH(OH)CH3	1.191E-02	11.910	9.998E-02	99.983
L-Tryptophan	C11H12N2O2	2.040E-03	2.040	9.989E-03	9.989
L-Valine	HO2CCH(NH2)CH(CH3)2	1.171E-02	11.710	0.100	100.000
D-Biotin (Vitamin H)	C10H16N2O3S	7.000E-06	7.000E-03	2.865E-05	0.029
D-Calcium Pantothenate (Vitamin B5)	C18H32CaN2O10	2.400E-04	0.240	5.036E-04	0.504
Choline Chloride	HOCH2CH2N(CH3)3Cl	1.396E-02	13.960	9.998E-02	99.979
Cyanocobalamin (Vitamin B12)	C63H88CoN14O14P	1.360E-03	1.360	1.003E-03	1.003
Folic Acid	C19H19N7O6	1.320E-03	1.320	2.990E-03	2.990
I-Inositol	C6H12O6	1.800E-02	18.000	9.989E-02	99.889
DL-α-lipoic acid (thioctic acid)	C8H14O2S2	2.100E-04	0.210	1.018E-03	1.018
Niacinamide (Nicotinamide)	C6H6N2O	3.700E-05	3.700E-02	3.030E-04	0.303
Pyridoxine Monohydrochloride	C8H11NO3	6.200E-05	6.200E-02	3.016E-04	0.302
Riboflavin (Vitamin B2)	C17H20N4O6	3.800E-05	3.800E-02	1.010E-04	0.101
Thiamine Monohydrochloride (Vitamin B1)	C12H18N4OSCl2	3.400E-04	0.340	1.008E-03	1.008
Thymidine	C10H14N2O5	7.300E-04	0.730	3.014E-03	3.014
Phenol Red	C19H14O5S	1.242E-03	1.242	3.300E-03	3.300
Pyruvic Acid Sodium Salt	CH3COCO2Na	0.110	110.000	1.000	999.636
Putrescine Dihydrochloride	NH2(CH2)4NH2 • 2HCl	1.600E-04	0.160	9.933E-04	0.993
L-Tyrosine Disodium Salt, Dihydrate	C9H9NO3Na2 • 2H2O	7.842E-03	7.842	3.002E-02	30.024
Linoleic Acid Methyl Ester	C19H34O2	8.800E-05	8.800E-02	2.988E-04	0.299
Hypoxanthine Disodium Salt	C5H2N4ONa2	5.460E-03	5.460	3.031E-02	30.315
Magnesium Chloride, Anhydrous	MgCl2	5.719E-02	57.190	0.601	600.672

Appendix 5. Table of ADH and ALDH information

Enzyme	Activator	Inhibitor	Metabolite	Occurrence DMEM	Occurrence Hams
ADH	Sulfhydryl activating reagents Mercaptoethanol Dithiothreitol Cysteine Heavy metal chelating agents	Heavy metals and -SH reagents Thiourea Purine and pyrimidine derivatives Chloroethanol and fluoroethanol N-alkylmaleimides Iodoacetamide 1,10-phenanthroline 8-hydroxyquinoline Beta-NAD analogs		L-Cysteine hydrochloride-H2O, L-Cystine 2HCl	L-Cysteine Monohydrochloride Monohydrate
Enzyme	**Enzyme Specifics/ where effect is/ details**	**Inhibitor**	**Metabolite**	**Occurrence DMEM**	**Occurrence Hams**
ALDHs	ALDH 1 & 3	Ampal (4-amino-4-methyl-2-pentyne-1-al)	Thioampal		
	ALDH 2	Benomyl	MBT		
	ALDH 2	Citrala	Neral and geranial		

	NAD+ ALDH 3	Chloral hydratea	Chloral hydrate		
		Chlorpropamide analogs NPI-1 API-1	NPI-1		
	esterase catalase anti-dipsotropic Confers sensitivity to cyclophosphamide-resistant cells. Inhibits dopamine β-hydroxylase; displays copper chelation activity; inhibits carboxylesterase and cholinesterase Inhibits several other dehydrogenase enzymes. Interacts with alcohol in system to form a toxic metabolite, Tryptophane metabolites in the kynurenine pathway seem to have the potential for ALDH2 specific inhibition.	Coprine	1-Amino cyclopropanol	L-Tryptophan	L-Tryptophan
		Cyanamide	HNO		
		Daidzin	Daidzin		
		CVT-10216	CVT-10216		
		DEABa	DEAB		
		DPABa	DPAB		
		Disulfiram	Disulfiram		
		DDTC-SO DDTC-SO2 DETC-SO DETC-SO2			
		Gossypol	Gossypol		
		Kynurenine Tryptophan metabolites	KA		
		3-HK 3-HAA			

	ALDH DTT but not GSH (ALDH2) Activated by CYP2E1 in liver microsomes; irreversible inhibitor of monoaminoxidase	Molinate	Molinate		
		Molinate sulfoxide Molinate sulfone			
		Nitroglycerina	$NO3^-$		
		Pargylinea	Propiolaldehyde		

Appendix 6. Table of suppliers for media and components

General Culture Components	Supplier and Code
DMEM High Glucose	Biosera, LM-D1112
Ham's F12	Lonza, BE12-615F
Fetal Bovine Serum	
Fetal Bovine Serum (South America Origin)	LabTech, FCS-SA/500
Antibiotic Antimycotic Solution	100x, Sigma Aldrich, A5955
L - Glutamine	200nM, Sigma Aldrich, G7513
Hepes Buffer Solution	1M, Sigma Aldrich, H0887
Non-Essential Amino Acids	100X, Sigma Aldrich, M7145
Sodium Pyruvate Solution	100mM, Sigma Aldrich, S8636
Powdered glucose	Sigma Aldrich, G7021
Trypsin-EDTA Solution	10x, Sigma Aldrich, T4174
Dulbecco's Phosphate Buffered Saline	1x, Gibco, 14190
Hank's Balanced Salt Solution	1x, Gibco, 14175-046

References

ABBOTT, S.M., ELDER, J.B., ŠPANĚL, P. and SMITH, D., 2003. Quantification of acetonitrile in exhaled breath and urinary headspace using selected ion flow tube mass spectrometry. *International Journal of Mass Spectrometry,* **228**(2), pp. 655-665.

ADAMS, N.G. and SMITH, D., 1976. The selected ion flow tube (SIFT); A technique for studying ion-neutral reactions. *International Journal of Mass Spectrometry and Ion Physics,* **21**(3–4), pp. 349-359.

AKTIPIS, C. and NESSE, R.M., 2013. Evolutionary foundations for cancer biology. *Evolutionary applications,* **6**(1), pp. 144-159.

ALLARDYCE, R.A., LANGFORD, V.S., HILL, A.L. and MURDOCH, D.R., 2006. Detection of volatile metabolites produced by bacterial growth in blood culture media by selected ion flow tube mass spectrometry (SIFT-MS). *Journal of microbiological methods,* **65**(2), pp. 361-365.

AMANN, A. and SMITH, D., 2013. *Volatile biomarkers: non-invasive diagnosis in physiology and medicine.* Newnes.

AMANN, A., CORRADI, M., MAZZONE, P. and MUTTI, A., 2011. Lung cancer biomarkers in exhaled breath. *Expert review of molecular diagnostics JID - 101120777,* , pp. 207-217.

ANDERSON, I.C., MARI, S.E., BRODERICK, R.J., MARI, B.P. and SHIPP, M.A., 2000. The Angiogenic Factor Interleukin 8 Is Induced in Non-Small Cell Lung Cancer/Pulmonary Fibroblast Cocultures. *Cancer research,* **60**(2), pp. 269-272.

AVWIORO.GODWIN, 2011. Histochemical Uses of Haematoxylin - A Review. *JPCS,* **1**, pp. 24-34.

BACH, P.B., MIRKIN, J.N., OLIVER, T.K., AZZOLI, C.G., BERRY, D.A., BRAWLEY, O.W., BYERS, T., COLDITZ, G.A., GOULD, M.K. and JETT, J.R., 2012. Benefits and harms of CT screening for lung cancer: a systematic review. *Jama,* **307**(22), pp. 2418-2429.

BADAWY, A.A., BANO, S. and STEPTOE, A., 2011. Tryptophan in alcoholism treatment I: kynurenine metabolites inhibit the rat liver mitochondrial low Km aldehyde dehydrogenase activity, elevate blood acetaldehyde concentration and induce aversion to alcohol. *Alcohol and Alcoholism (Oxford, Oxfordshire),* **46**(6), pp. 651-660.

BADAWY, A.A.B. and MORGAN, C.J., 2007. Tryptophan metabolites as potent inhibitors of aldehyde dehydrogenase activity and potential alcoholism-aversion therapeutic agents, *International Congress Series* 2007, Elsevier, pp. 344-351.

BAKER, R.R. and DIXON, M., 2006. The retention of tobacco smoke constituents in the human respiratory tract. *Inhalation toxicology,* **18**(4), pp. 255-294.

BAKER, M.J., GAZI, E., BROWN, M.D., SHANKS, J.H., CLARKE, N.W. and GARDNER, P., 2009. Investigating FTIR based histopathology for the diagnosis of prostate cancer. *Journal of Biophotonics,* **2**(1-2), pp. 104-113.

BARTH, A. and HARIS, P.I., 2009. Biological and Biomedical Infrared Spectrscopy. *Advances in Biomedical Spectroscopy,* IOS, **2**, pp. 317.

BELL, E. 2014. Organotypic and Histiotypic Models of Engineered Tissues, Lanza. R., Langer. R., Vacanti, J. P. *Principles of Cells and Tissue Engineering, Elsevier,* pp. 188.

BELLISOLA, G., DELLA PERUTA, M., VEZZALINI, M., MORATTI, E., VACCARI, L., BIRARDA, G., PICCININI, M., CINQUE, G. and SORIO, C., 2010. Tracking infrared signatures of drugs in cancer cells by Fourier transform microspectroscopy. *Analyst,* **135**(12), pp. 3077-3086.

BERGMAN, A.M., PINEDO, H.M. and PETERS, G.J., 2002. Determinants of resistance to 2', 2'-difluorodeoxycytidine (gemcitabine). *Drug Resistance Updates,* **5**(1), pp. 19-33.

BIRD, B., ROMEO, M., LAVER, N. and DIEM, M., 2009. Spectral detection of micro-metastases in lymph node histo-pathology. *Journal of Biophotonics,* **2**(1-2), pp. 37-46.

BLUMENTHAL, R.D. and GOLDENBERG, D.M., 2007. Methods and goals for the use of in vitro and in vivo chemosensitivity testing. *Molecular biotechnology,* **35**(2), pp. 185-197.

BOFFETTA, P. and NYBERG, F., 2003. Contribution of environmental factors to cancer risk. *British medical bulletin,* **68**(1), pp. 71-94.

BRANDENBURG, K. and SEYDEL, U., 2002. Vibrational Spectroscopy of Carbohydrates and Glycoconjugates. Handbook of Vibrational Spectroscopy. *J.M Chalmers and P.R Griffiths. Chichester, UK., John Wiley & Sons, Ltd.* **5**, pp. 3481-3507.

BRONSTED, J.N 1923. The individual thermodynamic properties of ions. *Journal of the American Chemical Society,* **45**(12), pp. 2898-2910.

BUSZEWSKI, B., ULANOWSKA, A., LIGOR, T., JACKOWSKI, M., KŁODZIŃSKA, E. and SZELIGA, J., 2008. Identification of volatile organic compounds secreted from cancer tissues and bacterial cultures. *Journal of Chromatography B,* **868**(1–2), pp. 88-94.

CANCER.ORG, 2016, Targeted therapy drugs for non-small cell lung cancer. Available: http://www.cancer.org/cancer/lungcancer-non-smallcell/detailedguide/non-small-cell-lung-cancer-treating-targeted-therapies# [01/01, 2016].

CANCER RESEARCH UK, 2015, Lung Cancer Statistics. Available: http://www.cancerresearchuk.org/health-professional/cancer-statistics/statistics-by-cancer-type/lung-cancer#heading-Zero [08/30, 2015].

CARR, G.L., 1999. High-resolution microspectroscopy and sub-nanosecond time-resolved spectroscopy with the synchrotron infrared source. *Vibrational Spectroscopy,* **19**(1), pp. 53-60.

CARROLL, W., LENNEY, W., WANG, T., ŠPANĚL, P., ALCOCK, A. and SMITH, D., 2005. Detection of volatile compounds emitted by Pseudomonas aeruginosa using selected ion flow tube mass spectrometry. *Pediatric pulmonology,* **39**(5), pp. 452-456.

CHANG, J.C., WOOTEN, E.C., TSIMELZON, A., HILSENBECK, S.G., GUTIERREZ, M.C., ELLEDGE, R., MOHSIN, S., OSBORNE, C.K., CHAMNESS, G.C. and ALLRED, D.C., 2003. Gene expression profiling

for the prediction of therapeutic response to docetaxel in patients with breast cancer. *The Lancet,* **362**(9381), pp. 362-369.

CHEN, X., XU, F., WANG, Y., PAN, Y., LU, D., WANG, P., YING, K., CHEN, E. and ZHANG, W., 2007. A study of the volatile organic compounds exhaled by lung cancer cells in vitro for breath diagnosis. *Cancer,* **110**(4), pp. 835-844.

CLAY, M.R., TABOR, M., OWEN, J.H., CAREY, T.E., BRADFORD, C.R., WOLF, G.T., WICHA, M.S. and PRINCE, M.E., 2010. Single-marker identification of head and neck squamous cell carcinoma cancer stem cells with aldehyde dehydrogenase. *Head & neck,* **32**(9), pp. 1195-1201.

COLLINS, L., HAINES, C., PERKEL, R. and ENCK, R., 2007. Lung cancer: diagnosis and management. *Am Fam Physician,* **75**(1), pp. 56-63.

CREE, I.A., 2009. Chemosensitivity and chemoresistance testing in ovarian cancer. *Current opinion in obstetrics & gynecology,* **21**(1), pp. 39-43.

CROKER, A.K., GOODALE, D., CHU, J., POSTENKA, C., HEDLEY, B.D., HESS, D.A. and ALLAN, A.L., 2009. High aldehyde dehydrogenase and expression of cancer stem cell markers selects for breast cancer cells with enhanced malignant and metastatic ability. *Journal of Cellular and Molecular Medicine,* **13**(8b), pp. 2236-2252.

DALERBA, P., DYLLA, S.J., PARK, I.K., LIU, R., WANG, X., CHO, R.W., HOEY, T., GURNEY, A., HUANG, E.H., SIMEONE, D.M., SHELTON, A.A., PARMIANI, G., CASTELLI, C. and CLARKE, M.F., 2007. Phenotypic characterization of human colorectal cancer stem cells. *Proceedings of the National Academy of Sciences of the United States of America,* **104**(24), pp. 10158-10163.

DAVIES, S., ŠPANĚL, P. and SMITH, D., 1997. Quantitative analysis of ammonia on the breath of patients in end-stage renal failure. *Kidney international,* **52**(1), pp. 223-228.

DERENNE, A., VERDONCK, M. and GOORMAGHTIGH, E., 2012. The effect of anticancer drugs on seven cell lines monitored by FTIR spectroscopy. *Analyst,* **137**(14), pp. 3255-3264.

DI GIAMBATTISTA, L., GRIMALDI, P., GAUDENZI, S., POZZI, D., GRANDI, M., MORRONE, S., SILVESTRI, I. and CONGIU CASTELLANO, A., 2010. UVB radiation induced effects on cells studied by FTIR spectroscopy. *Eur Biophys J,* **39**(6), pp. 929-934.

DIEM, M., ROMEO, M., MATTHÄUS, C., MILJKOVIC, M., MILLER, L. and LASCH, P., 2004. Comparison of Fourier transform infrared (FTIR) spectra of individual cells acquired using synchrotron and conventional sources. *Infrared Physics & Technology,* **45**(5), pp. 331-338.

DRAUX, F., GOBINET, C., SULÉ-SUSO, J., MANFAIT, M., JEANNESSON, P. and SOCKALINGUM, G.D., 2011. Raman imaging of single living cells: probing effects of non-cytotoxic doses of an anti-cancer drug. *Analyst,* **136**(13), pp. 2718-2725.

DRAUX, F., JEANNESSON, P., GOBINET, C., SULÉ-SUSO, J., PIJANKA, J., SANDT, C., DUMAS, P., MANFAIT, M. and SOCKALINGUM, G.D., 2009. IR spectroscopy reveals effect of non-cytotoxic doses of anti-tumour drug on cancer cells. *Analytical & Bioanalytical Chemistry,* **395**(7), pp. 2293.

ENDERBY, B., LENNEY, W., BRADY, M., EMMETT, C., ŠPANĚL, P. and SMITH, D., 2009. Concentrations of some metabolites in the breath of healthy children aged 7–18 years measured

using selected ion flow tube mass spectrometry (SIFT-MS). *Journal of breath research,* **3**(3), pp. 036001.

ENDERBY, B., SMITH, D., CARROLL, W. and LENNEY, W., 2009. Hydrogen cyanide as a biomarker for Pseudomonas aeruginosa in the breath of children with cystic fibrosis. *Pediatric pulmonology,* **44**(2), pp. 142-147.

EZZATI, M. and LOPEZ, A.D., 2003. Estimates of global mortality attributable to smoking in 2000. *The Lancet,* **362**(9387), pp. 847-852.

FAN, T., LANE, A.N., HIGASHI, R.M., FARAG, M.A., GAO, H., BOUSAMRA, M. and MILLER, D.M., 2009. Altered regulation of metabolic pathways in human lung cancer discerned by (13) C stable isotope-resolved metabolomics (SIRM). *Mol Cancer,* **8**(10.1186), pp. 1476-4598.

FILIPIAK, W., SPONRING, A., FILIPIAK, A., AGER, C., SCHUBERT, J., MIEKISCH, W., AMANN, A. and TROPPMAIR, J., 2010. TD-GC-MS analysis of volatile metabolites of human lung cancer and normal cells in vitro. *Cancer epidemiology, biomarkers & prevention : a publication of the American Association for Cancer Research, cosponsored by the American Society of Preventive Oncology JID - 9200608,* **19**(1), pp. 182-195.

FILIPIAK, W., SPONRING, A., MIKOVINY, T., AGER, C., SCHUBERT, J., MIEKISCH, W., AMANN, A. and TROPPMAIR, J., 2008. Release of volatile organic compounds (VOCs) from the lung cancer cell line CALU-1 in vitro. *Cancer cell international JID - 101139795 PMC - PMC2639533 OID - NLM: PMC2639533 EDAT- 2008/11/26 09:00 MHDA- 2008/11/26 09:01 CRDT- 2008/11/26 09:00 PHST- 2008/09/29 [received] PHST- 2008/11/24 [accepted] PHST- 2008/11/24 [aheadofprint] AID - 1(TRUNCATED),* **8**(1), pp. 17.

FISHER, A.B., 1984. Intermediary metabolism of the lung. *Environmental health perspectives,* **55**, pp. 149-158.

FISHER, S.E., HARRIS, A.T., KHANNA, N. and SULÉ-SUSO, J., 2011. Vibrational Spectroscopy: What Does the Clinician Need? In: D. MOSS, ed, *Biomedical Applications of Synchrotron Infrared Microspectroscopy.A Practical Approach.* 1st edn. pp. 3-28.

FORSYTH, N.R., EVANS, A.P., SHAY, J.W. and WRIGHT, W.E., 2003. Developmental differences in the immortalization of lung fibroblasts by telomerase. *Aging Cell,* **2**(5), pp. 235-243.

FRENCH, C.A., 2009. Chapter 2 - Respiratory Tract. *Cytology (Third Edition).* Philadelphia: W.B. Saunders, pp. 65-103.

FRIEDRICH, M.J., 2003. Studying Cancer in 3 Dimensions. *JAMA: The Journal of the American Medical Association,* **290**(15), pp. 1977-1979.

FRISCH, S.M. and SCREATON, R.A., 2001. Anoikis mechanisms. *Current opinion in cell biology JID - 8913428,* **13**(5), pp. 555-562.

FRYER, R.A., BARLETT, B., GALUSTIAN, C. and DALGLEISH, A.G., 2011. Mechanisms underlying gemcitabine resistance in pancreatic cancer and sensitisation by the iMiD lenalidomide. *Anticancer Research,* **31**(11), pp. 3747-3756.

GAIGNEAUX, A., RUYSSCHAERT, J. and GOORMAGHTIGH, E., 2002. Infrared spectroscopy as a tool for discrimination between sensitive and multiresistant K562 cells. *European Journal of Biochemistry,* **269**(7), pp. 1968-1973.

GASPARRI, F. and MUZIO, M., 2003. Monitoring of apoptosis of HL60 cells by Fourier-transform infrared spectroscopy. *Biochem.J,* **369**, pp. 239-248.

GASPER, R., DEWELLE, J., KISS, R., MIJATOVIC, T. and GOORMAGHTIGH, E., 2009. IR spectroscopy as a new tool for evidencing antitumor drug signatures. *Biochimica et Biophysica Acta (BBA)-Biomembranes,* **1788**(6), pp. 1263-1270.

GAUGLITZ, G. and MOORE, D.S., 2014. *Handbook of Spectroscopy, 4 Volume Set.* John Wiley & Sons.

GILCHRIST, F.J., RAZAVI, C., WEBB, A.K., JONES, A.M., ŠPANĚL, P., SMITH, D. and LENNEY, W., 2012. An investigation of suitable bag materials for the collection and storage of breath samples containing hydrogen cyanide. *Journal of breath research,* **6**(3), pp. 036004.

GKIOZOS, I., CHARPIDOU, A. and SYRIGOS, K., 2007. Developments in the treatment of non-small cell lung cancer. *Anticancer Research,* **27**(4C), pp. 2823-2827.

GORDON, S.M., SZIDON, J.P., KROTOSZYNSKI, B.K., GIBBONS, R.D. and O'NEILL, H.J., 1985. Volatile organic compounds in exhaled air from patients with lung cancer. *Clinical chemistry,* **31**(8), pp. 1278-1282.

GRAHAM, D., EVANS, D., ALPERT, L., KLEIN, P., EVANS, D., OPEKUN, A. and BOUTTON, T., 1987. Campylobacter pylori detected noninvasively by the 13 C-urea breath test. *The Lancet,* **329**(8543), pp. 1174-1177.

GRIFFITHS, P.R., 2002. Introduction to Vibrational Spectroscopy. *Handbook of vibrational spectroscopy.* J. M. Chalmers and P. R. Griffiths. Chichester, UK. John Wiley & sons, **1**, pp. 33-43.

GRIFFITHS, P.R. and HASETH, J.A.D., 2007. *Fourier Transform Infrared Spectrometry.* 2nd edn. Hoboken, New Jersey: Wiley & Sons.

GUO, R. and REN, J., 2010. Alcohol and acetaldehyde in public health: from marvel to menace. *International journal of environmental research and public health,* **7**(4), pp. 1285-1301.

HANSEL, A., JORDAN, A., HOLZINGER, R., PRAZELLER, P., VOGEL, W. and LINDINGER, W., 1995. Proton transfer reaction mass spectrometry: on-line trace gas analysis at the ppb level. *International Journal of Mass Spectrometry and Ion Processes,* **149**, pp. 609-619.

HODGKIN, D.C., 1950. X-ray analysis and protein structure. *Cold Spring Harbor symposia on quantitative biology,* **14**, pp. 65-78.

HOLMAN, H.Y.N., MARTIN, M.C., BLAKELY, E.A., BJORNSTAD, K. and MCKINNEY, W.R., 2000. IR spectroscopic characteristics of cell cycle and cell death probed by synchrotron radiation based Fourier transform IR spectromicroscopy. *Biopolymers,* **57**(6), pp. 329-335.

HONOKI, K., FUJII, H., KUBO, A., KIDO, A., MORI, T., TANAKA, Y. and TSUJIUCHI, T., 2010. Possible involvement of stem-like populations with elevated ALDH1 in sarcomas for chemotherapeutic drug resistance. *Oncology reports,* **24**(2), pp. 501-505.

IUPAC, 1997. Compendium of Chemical Terminology, 2nd ed. (the "Gold Book"). Compiled by A. D. McNaught and A. Wilkinson. Blackwell Scientific Publications, Oxford. XML on-line corrected version: http://goldbook.iupac.org (2006-) created by M. Nic, J. Jirat, B. Kosata; updates compiled by A. Jenkins. ISBN 0-9678550-9-8. doi:10.1351/goldbook.

JAMIN, N., DUMAS, P., MONCUIT, J., FRIDMAN, W.H., TEILLAUD, J.L., CARR, G.L. and WILLIAMS, G.P., 1998. Highly resolved chemical imaging of living cells by using synchrotron infrared microspectrometry. *Proceedings of the National Academy of Sciences of the United States of America,* **95**(9), pp. 4837-4840.

JELSKI, W. and SZMITKOWSKI, M., 2008. Alcohol dehydrogenase (ADH) and aldehyde dehydrogenase (ALDH) in the cancer diseases. *Clinica Chimica Acta,* **395**(1), pp. 1-5.

JEMAL, A., BRAY, F., CENTER, M.M., FERLAY, J., WARD, E. and FORMAN, D., 2011. Global cancer statistics. *CA: A Cancer Journal for Clinicians,* **61**(2), pp. 69-90.

JONES, A.M., HANSON, I.M., ARMSTRONG, G.R. and O'DRISCOLL, B.R., 2001. Value and accuracy of cytology in addition to histology in the diagnosis of lung cancer at flexible bronchoscopy. *Respiratory medicine,* **95**(5), pp. 374-378.

KACURAKOVA, M. and MATHLOUTHI, M. 1996. “FTIR and laser-Raman spectra of oligosaccharides in water: characterisation of glycosidic bond.” Carbohydr Res 284(2), pp. 145-57.

KALAPOS, M.P., 2003. On the mammalian acetone metabolism: from chemistry to clinical implications. *Biochimica et Biophysica Acta (BBA)-General Subjects,* **1621**(2), pp. 122-139.

KENDALL, C., ISABELLE, M., BAZANT-HEGEMARK, F., HUTCHINGS, J., ORR, L., BABRAH, J., BAKER, R. and STONE, N., 2009. Vibrational spectroscopy: a clinical tool for cancer diagnostics. *Analyst,* **134**(6), pp. 1029-1045.

KERESZTURY, G., 2002. Raman Spectroscopy: Theory. Handbooks of Vibrational Spectroscopy. J. M. Chalmers and P. R. Griffiths. Chichester, UK. John Wiley & sons, **1**, pp. 33-43.

KIM, M.P., FLEMING, J.B., WANG, H., ABBRUZZESE, J.L., CHOI, W., KOPETZ, S., MCCONKEY, D.J., EVANS, D.B. and GALLICK, G.E., 2011. ALDH activity selectively defines an enhanced tumor-initiating cell population relative to CD133 expression in human pancreatic adenocarcinoma. *PloS one,* **6**(6), pp. e20636.

KIM, J.W. and DANG, C.V., 2006. Cancer's molecular sweet tooth and the Warburg effect. *Cancer research,* **66**(18), pp. 8927-8930.

KOPPAKA, V., THOMPSON, D.C., CHEN, Y., ELLERMANN, M., NICOLAOU, K.C., JUVONEN, R.O., PETERSEN, D., DEITRICH, R.A., HURLEY, T.D. and VASILIOU, V., 2012. Aldehyde dehydrogenase inhibitors: a comprehensive review of the pharmacology, mechanism of action, substrate specificity, and clinical application. *Pharmacological reviews,* **64**(3), pp. 520-539.

KOPPENOL, W.H., BOUNDS, P.L. and DANG, C.V., 2011. Otto Warburg's contributions to current concepts of cancer metabolism. *Nature Reviews Cancer,* **11**(5), pp. 325-337.

KRAFFT, C., CODRICH, D., PELIZZO, G. and SERGO, V., 2008. Raman and FTIR imaging of lung tissue: Methodology for control samples. *Vibrational Spectroscopy,* **46**(2), pp. 141-149.

KRISHNA, C., SOCKALINGUM, G., BHAT, R., VENTEO, L., KUSHTAGI, P., PLUOT, M. and MANFAIT, M., 2007. FTIR and Raman microspectroscopy of normal, benign, and malignant formalin-fixed ovarian tissues. *Anal Bioanal Chem,* **387**(5), pp. 1649-1656.

LACROIX, M., MOSORA, F., PONTUS, M., LEFEBVRE, P., LUYCKZ, A. and LOPEZ-HABIB, G., 1973. Glucose naturally labeled with carbon-13: use for metabolic studies in man. *Science (New York, N.Y.),* **181**(4098), pp. 445-446.

LAM, W., WHITE, N. and CHAN-YEUNG, M., 2004. Lung cancer epidemiology and risk factors in Asia and Africa. *Int J Tuberc Lung Dis,* **8**(9), pp. 1045-1057.

LANGER, C.J., BESSE, B., GUALBERTO, A., BRAMBILLA, E. and SORIA, J., 2010. The Evolving Role of Histology in the Management of Advanced Non–Small-Cell Lung Cancer. *Journal of Clinical Oncology,* **28**(36), pp. 5311-5320.

LEE, C.H., SINGLA, A. and LEE, Y., 2001. Biomedical applications of collagen. *International journal of pharmaceutics,* **221**(1), pp. 1-22.

LEE, K.Y. and MOONEY, D.J., 2001. Hydrogels for tissue engineering. *Chemical reviews,* **101**(7), pp. 1869-1880.

LEE, K.M., CHOI, K.H. and OUELLETTE, M.M., 2004. Use of exogenous hTERT to immortalize primary human cells. *Cytotechnology,* **45**(1-2), pp. 33-38.

LEWIS, R.N.A.H. and MCELHANEY, R.N., 2006; 2001. Vibrational Spectroscopy of Lipids. *Handbook of Vibrational Spectroscopy.* John Wiley & Sons, Ltd, .

LIU, K.Z. and MANTSCH, H.H., 2001. Apoptosis-induced structural changes in leukemia cells identified by IR spectroscopy. *Journal of Molecular Structure,* **565**, pp. 299-304.

LY, E., PIOT, O., WOLTHUIS, R., DURLACH, A., BERNARD, P. and MANFAIT, M., 2008. Combination of FTIR spectral imaging and chemometrics for tumour detection from paraffin-embedded biopsies. *Analyst,* **133**(2), pp. 197-205.

MA, S., CHAN, K.W., LEE, T.K., TANG, K.H., WO, J.Y., ZHENG, B.J. and GUAN, X.Y., 2008. Aldehyde dehydrogenase discriminates the CD133 liver cancer stem cell populations. *Molecular cancer research : MCR,* **6**(7), pp. 1146-1153.

MACHANA, S., WEERAPREEYAKUL, N., BARUSRUX, S., THUMANU, K. and TANTHANUCH, W., 2012. FTIR microspectroscopy discriminates anticancer action on human leukemic cells by extracts of Pinus kesiya; Cratoxylum formosum ssp. pruniflorum and melphalan. *Talanta,* **93**, pp. 371-382.

MACKAY, J., 2004. *The tabacco atlas.* WHO.

MARCSISIN, E.J.S., UTTERO, C.M., MAZUR, A.I., MILJKOVIĆ, M., BIRD, B. and DIEM, M., 2012. Noise adjusted principal component reconstruction to optimize infrared microspectroscopy of individual live cells. *Analyst,* **137**(13), pp. 2958-2964.

MAZZONE, P.J., 2012. Exhaled breath volatile organic compound biomarkers in lung cancer. *Journal of breath research,* **6**(2), pp. 027106.

MAZZONE, P.J., 2008. Analysis of Volatile Organic Compounds in the Exhaled Breath for the Diagnosis of Lung Cancer. *Journal of Thoracic Oncology,* **3**(7), pp. 774.

MILLER, L.M. and SMITH, R.J., 2005. Synchrotrons versus globars, point-detectors versus focal plane arrays: Selecting the best source and detector for specific infrared microspectroscopy and imaging applications. *Vibrational Spectroscopy,* **38**(1–2), pp. 237-240.

MOHLENHOFF, B., ROMEO, M., DIEM, M. and WOOD, B.R., 2005. Mie-type scattering and non-Beer-Lambert absorption behavior of human cells in infrared microspectroscopy. *Biophysical journal,* **88**(5), pp. 3635-3640.

MOLINA, J.R., YANG, P., CASSIVI, S.D., SCHILD, S.E. and ADJEI, A.A., 2008. Non-small cell lung cancer: epidemiology, risk factors, treatment, and survivorship, *Mayo Clinic Proceedings* 2008, Elsevier, pp. 584-594.

MOREB, J.S., BAKER, H.V., CHANG, L.J., AMAYA, M., LOPEZ, M.C., OSTMARK, B. and CHOU, W., 2008. ALDH isozymes downregulation affects cell growth, cell motility and gene expression in lung cancer cells. *Molecular cancer,* **7**, pp. 87-4598.

MORENO-AROTZENA, O., MEIER, J.G., AMO, C.D. and GARCIA-AZNAR, J.M., 2015. Characterization of Fibrin and Collagen Gels for Engineering Wound Healing Models. *Materials,* **8**(4), pp. 1636-1651.

MOVASAGHI, Z., REHMAN, S. and UR REHMAN, D.I., 2008. Fourier Transform Infrared (FTIR) Spectroscopy of Biological Tissues. *Applied Spectroscopy Reviews,* **43**(2), pp. 134-179.

MOYSAN, E., BASTIAT, G. and BENOIT, J., 2012. Gemcitabine versus modified gemcitabine: a review of several promising chemical modifications. *Molecular pharmaceutics,* **10**(2), pp. 430-444.

NATIONAL CANCER INSTITUTE, 27/07/2015, 2015-last update, Acetaldehyde (Code C44328) [Homepage of National Cancer Institute Thesaurus], [Online]. Available: https://ncit.nci.nih.gov/ncitbrowser/ConceptReport.jsp?dictionary=NCI_Thesaurus&code=C44328&ns=NCI_Thesaurus [01/09/2015, 2015].

NGO, D.C., VERVERIS, K., TORTORELLA, S.M. and KARAGIANNIS, T.C., 2015. Introduction to the molecular basis of cancer metabolism and the Warburg effect. *Molecular biology reports,* **42**(4), pp. 819-823.

NATIONAL INSTITUTE OF HEATH AND CARE EXCELLENCE, 2011. The diagnosis and treatment of lung cancer (update). *National Collaborating Centre for Cancer,* pp. 8, 51-106.

Ó FAOLÁIN, E., HUNTER, M.B., BYRNE, J.M., KELEHAN, P., MCNAMARA, M., BYRNE, H.J. and LYNG, F.M., 2005. A study examining the effects of tissue processing on human tissue sections using vibrational spectroscopy. *Vibrational Spectroscopy,* **38**(1–2), pp. 121-127.

OGAWA, H., GOMI, T. and FUJIOKA, M., 2000. Serine hydroxymethyltransferase and threonine aldolase: are they identical? *The international journal of biochemistry & cell biology,* **32**(3), pp. 289-301.

O'NEILL, H.J., GORDON, S.M., O'NEILL, M.H., GIBBONS, R.D. and SZIDON, J.P., 1988. A computerized classification technique for screening for the presence of breath biomarkers in lung cancer. *Clinical chemistry,* **34**(8), pp. 1613-1618.

OSTROFF, R.M., BIGBEE, W.L., FRANKLIN, W., GOLD, L., MEHAN, M., MILLER, Y.E., PASS, H.I., ROM, W.N., SIEGFRIED, J.M. and STEWART, A., 2010. Unlocking biomarker discovery: large scale application of aptamer proteomic technology for early detection of lung cancer. *PloS one,* **5**(12), pp. e15003.

P. ŠPANĚL AND, D.S., 2008. Quantification of trace levels of the potential cancer biomarkers formaldehyde, acetaldehyde and propanol in breath by SIFT-MS. *Journal of Breath Research,* **2**(4), pp. 046003.

PAUL, W., 1993. Electromagnetic traps for charged and neutral particles. Aalam Al-Zarra, (27), 18-31.

PETERSEN, M.C., LAZAR, J., JACOB, H.J. and WAKATSUKI, T., 2007. Tissue engineering: a new frontier in physiological genomics. *Physiological genomics,* **32**(1), pp. 28-32.

PHILLIPS, M., CATANEO, R.N., CUMMIN, A.R., GAGLIARDI, A.J., GLEESON, K., GREENBERG, J., MAXFIELD, R.A. and ROM, W.N., 2003. Detection of lung cancer with volatile markers in the breath. *Chest JID - 0231335,* **123**(6), pp. 2115-2123.

PHILLIPS, M., BOEHMER, J.P., CATANEO, R.N., CHEEMA, T., EISEN, H.J., FALLON, J.T., FISHER, P.E., GASS, A., GREENBERG, J. and KOBASHIGAWA, J., 2004. Heart allograft rejection: detection with breath alkanes in low levels (the HARDBALL study). *The Journal of heart and lung transplantation,* **23**(6), pp. 701-708.

PHILLIPS, M., GLEESON, K., HUGHES, J.M.B., GREENBERG, J., CATANEO, R.N., BAKER, L. and MCVAY, W.P., 1999. Volatile organic compounds in breath as markers of lung cancer: a cross-sectional study. *The Lancet,* **353**(9168), pp. 1930-1933.

PIJANKA, J.K., KOHLER, A., YANG, Y., DUMAS, P., CHIO-SRICHAN, S., MANFAIT, M., SOCKALINGUM, G.D. and SULE-SUSO, J., 2009. Spectroscopic signatures of single, isolated cancer cell nuclei using synchrotron infrared microscopy. *Analyst,* **134**(6), pp. 1176-1181.

PIJANKA, J., SOCKALINGUM, G.D., KOHLER, A., YANG, Y., DRAUX, F., PARKES, G., LAM, K., COLLINS, D., DUMAS, P., SANDT, C., VAN PITTIUS, D.,G., DOUCE, G., MANFAIT, M., UNTEREINER, V. and SULE-SUSO, J., 2010. Synchrotron-based FTIR spectra of stained single cells. Towards a clinical application in pathology. *Laboratory investigation; a journal of technical methods and pathology,* **90**(5), pp. 797-807.

POLI, D., CARBOGNANI, P., CORRADI, M., GOLDONI, M., ACAMPA, O., BALBI, B., BIANCHI, L., RUSCA, M. and MUTTI, A., 2005. Exhaled volatile organic compounds in patients with non-small cell lung cancer: cross sectional and nested short-term follow-up study. *Respiratory research,* **6**, pp. 71.

QUARONI, L. and CASSON, A.G., 2009. Characterization of Barrett esophagus and esophageal adenocarcinoma by Fourier-transform infrared microscopy. *Analyst,* **134**(6), pp. 1240-1246.

RECK, M., HEIGENER, D.F., MOK, T., SORIA, J. and RABE, K.F., 2013. Management of non-small-cell lung cancer: recent developments. *The Lancet,* **382**(9893), pp. 709-719.

REKHTMAN, N., BRANDT, S.M., SIGEL, C.S., FRIEDLANDER, M.A., RIELY, G.J., TRAVIS, W.D., ZAKOWSKI, M.F. and MOREIRA, A.L., 2011. Suitability of Thoracic Cytology for New Therapeutic Paradigms in Non-small Cell Lung Carcinoma: High Accuracy of Tumor Subtyping and Feasibility of EGFR and KRAS Molecular Testing. *Journal of Thoracic Oncology,* **6**(3), pp. 451-458 10.1097/JTO.0b013e31820517a3.

RICHARD DOLL and A. BRADFORD HILL, 1956. Lung Cancer and Other Causes of Death in Relation to Smoking. *BMJ,* **2**(5001), pp. 1071-1081.

RIVEROS-ROSAS, H., JULIAN-SANCHEZ, A. and PIÑA, E., 1997. Enzymology of ethanol and acetaldehyde metabolism in mammals. *Archives of Medical Research,* **28**, pp. 453-470.

ROBERT, J., VEKRIS, A., POURQUIER, P. and BONNET, J., 2004. Predicting drug response based on gene expression. *Critical reviews in oncology/hematology,* **51**(3), pp. 205-227.

ROMEO, M. and DIEM, M., 2005. Correction of dispersive line shape artifact observed in diffuse reflection infrared spectroscopy and absorption/reflection (transflection) infrared micro-spectroscopy. *Vibrational Spectroscopy,* **38**(1), pp. 129-132.

RONNOV-JESSEN, L., PETERSEN, O.W. and BISSELL, M.J., 1996. Cellular changes involved in conversion of normal to malignant breast: importance of the stromal reaction. *Physiological Reviews,* **76**(1), pp. 69-125.

RUTTER, A.V., CHIPPENDALE, T., YANG, Y., ŠPANĚL, P., SMITH, D. and SULÉ-SUSO, J., 2013. Quantification by SIFT-MS of acetaldehyde released by lung cells in a 3D model. *Analyst,* **138**(1), pp. 91-95.

SAMSON, D.J., SEIDENFELD, J., ZIEGLER, K. and ARONSON, N., 2004. Chemotherapy Sensitivity and Resistance Assays: A Systematic Review. *Journal of Clinical Oncology,* **22**(17), pp. 3618-3630.

SCHAEFER-PROKOP, C. and PROKOP, M., 2002. New imaging techniques in the treatment guidelines for lung cancer. *The European respiratory journal.Supplement JID - 8910681,* **19**(35), pp. 71S-83S.

SCHRAG, D., GAREWAL, H.S., BURSTEIN, H.J., SAMSON, D.J., VON HOFF, D.D., SOMERFIELD, M.R. and FOR THE ASCO WORKING GROUP ON CHEMOTHERAPY SENSITIVITY AND RESISTANCE ASSAYS, 2004. American Society of Clinical Oncology Technology Assessment: Chemotherapy Sensitivity and Resistance Assays. *Journal of Clinical Oncology,* **22**(17), pp. 3631-3638.

SCHREVENS, L., LORENT, N., DOOMS, C. and VANSTEENKISTE, J., 2004. The Role of PET Scan in Diagnosis, Staging, and Management of Non-Small Cell Lung Cancer. *The oncologist,* **9**(6), pp. 633-643.

SCOTTER, J.M., ALLARDYCE, R.A., LANGFORD, V.S., HILL, A. and MURDOCH, D.R., 2006. The rapid evaluation of bacterial growth in blood cultures by selected ion flow tube–mass spectrometry

(SIFT-MS) and comparison with the BacT/ALERT automated blood culture system. *Journal of microbiological methods,* **65**(3), pp. 628-631.

SEITZ, H.K. and STICKEL, F., 2007. Molecular mechanisms of alcohol-mediated carcinogenesis. *Nature Reviews Cancer,* **7**(8), pp. 599-612.

SENTHILMOHAN, S.T., MILLIGAN, D.B., MCEWAN, M.J., FREEMAN, C.G. and WILSON, P.F., 2000. Quantitative analysis of trace gases of breath during exercise using the new SIFT–MS technique. *Redox Report,* **5**(2-3), pp. 151-153.

SIEGEL, R., NAISHADHAM, D. and JEMAL, A., 2013. Cancer statistics, 2013. *CA: A Cancer Journal for Clinicians,* **63**(1), pp. 11-30.

SILKOFF, P.E., CARLSON, M., BOURKE, T., KATIAL, R., ÖGREN, E. and SZEFLER, S.J., 2004. The Aerocrine exhaled nitric oxide monitoring system NIOX is cleared by the US Food and Drug Administration for monitoring therapy in asthma. *Journal of allergy and clinical immunology,* **114**(5), pp. 1241-1256.

SMALLEY, K.S.M., LIONI, M. and HERLYN, M., 2006. Life Isn't Flat: Taking Cancer Biology to the Next Dimension. *In Vitro Cellular & Developmental Biology.Animal,* **42**(8/9), pp. pp. 242-247.

SMITH, D. and ŠPANĚL, P., 2015. Pitfalls in the analysis of volatile breath biomarkers: suggested solutions and SIFT–MS quantification of single metabolites. *Journal of breath research,* **9**(2), pp. 022001.

SMITH, D. and ŠPANĚL, P., 2011. Ambient analysis of trace compounds in gaseous media by SIFT-MS. *Analyst,* **136**(10), pp. 2009-2032.

SMITH, D., ŠPANĚL, P., ENDERBY, B., LENNEY, W., TURNER, C. and DAVIES, S.J., 2010a. Isoprene levels in the exhaled breath of 200 healthy pupils within the age range 7–18 years studied using SIFT-MS. *Journal of breath research,* **4**(1), pp. 017101.

SMITH, D., ŠPANĚL, P., HERBIG, J. and BEAUCHAMP, J., 2014. Mass spectrometry for real-time quantitative breath analysis. *Journal of breath research,* **8**(2), pp. 027101.

SMITH, D., ŠPANĚL, P., HOLLAND, T.A., AL SINGARI, W. and ELDER, J.B., 1999. Selected ion flow tube mass spectrometry of urine headspace. *Rapid communications in mass spectrometry,* **13**(8), pp. 724-729.

SMITH, D., ŠPANĚL, P. and SULÉ-SUSO, J., 2010b. Advantages of breath testing for the early diagnosis of lung cancer. *Expert review of molecular diagnostics JID - 101120777,* **10**(3), pp. 255.

SMITH, D., WANG, T., SULÉ-SUSO, J. and ŠPANĚL P, E.H.,A., 2003. Quantification of acetaldehyde released by lung cancer cells in vitro using selected ion flow tube mass spectrometry. *Rapid communications in mass spectrometry : RCM JID - 8802365,* **17**(8), pp. 845-850.

SMITH, D., 1992. The ion chemistry of interstellar clouds. *Chemical reviews,* **92**(7), pp. 1473-1485.

SMITH, D. and ADAMS, N., 1980. Elementary plasma reactions of environmental interest. In: S. VEPREK and M. VENUGOPALAN, eds, *Plasma Chemistry I.* Springer Berlin / Heidelberg, pp. 1-43.

SMITH, D., CHIPPENDALE, T.W.E. and ŠPANĚL, P., 2011. Selected ion flow tube, SIFT, studies of the reactions of H3O+, NO+ and O2+ with some biologically active isobaric compounds in preparation for SIFT-MS analyses. *International Journal of Mass Spectrometry,* **303**(2–3), pp. 81-89.

SMITH, D. and ŠPANĚL, P., 2005. Selected ion flow tube mass spectrometry (SIFT-MS) for on-line trace gas analysis. *Mass spectrometry reviews,* **24**(5), pp. 661-700.

ŠPANĚL, P., DAVIES, S. and SMITH, D., 1999. Quantification of breath isoprene using the selected ion flow tube mass spectrometric analytical method. *Rapid communications in mass spectrometry,* **13**(17), pp. 1733-1738.

ŠPANĚL, P., DRYAHINA, K., REJŠKOVÁ, A., CHIPPENDALE, T.W. and SMITH, D., 2011. Breath acetone concentration; biological variability and the influence of diet. *Physiological Measurement,* **32**(8), pp. N23.

ŠPANĚL, P., DRYAHINA, K. and SMITH, D., 2007. Acetone, ammonia and hydrogen cyanide in exhaled breath of several volunteers aged 4–83 years. *Journal of breath research,* **1**(1), pp. 011001.

ŠPANĚL, P. and SMITH, D., 2011. Progress in SIFT-MS: Breath analysis and other applications. *Mass spectrometry reviews,* **30**(2), pp. 236-267.

ŠPANĚL, P., ROLFE, P., RAJAN, B. and SMITH, D., 1996. The selected ion flow tube (SIFT)--a novel technique for biological monitoring. *The Annals of Occupational Hygiene,* **40**(6), pp. 615-626.

ŠPANĚL, P., SMITH, D., HOLLAND, T.A., HOLLAND, T.A., SINGARY, W. and ELDER, J.B., 1999. Analysis of formaldehyde in the headspace of urine from bladder and prostate cancer patients using selected ion flow tube mass spectrometry. *Rapid communications in mass spectrometry : RCM JID - 8802365,* **13**(14), pp. 1354-1359.

SPONRING, A., FILIPIAK, W., MIKOVINY, T., AGER, C., SCHUBERT, J., MIEKISCH, W., AMANN, A. and TROPPMAIR, J., January 2009. Release of Volatile Organic Compounds from the Lung Cancer Cell Line NCI-H2087 In Vitro. *Anticancer Research,* **29**(1), pp. 419-426.

STORER, M.K., HIBBARD-MELLES, K., DAVIS, B. and SCOTTER, J., 2011. Detection of volatile compounds produced by microbial growth in urine by selected ion flow tube mass spectrometry (SIFT-MS). *Journal of microbiological methods,* **87**(1), pp. 111-113.

SULÉ-SUSO, J., SKINGSLEY, D., SOCKALINGUM, G., KOHLER, A., KEGELAER, G., MANFAIT, M. and EL HAJ, A., 2005. FT-IR microspectroscopy as a tool to assess lung cancer cells response to chemotherapy. *Vibrational spectroscopy,* **38**(1), pp. 179-184.

SULÉ-SUSO, J., PYSANENKO, A., ŠPANĚL, P. and SMITH, D., 2009. Quantification of acetaldehyde and carbon dioxide in the headspace of malignant and non-malignant lung cells in vitro by SIFT-MS. *Analyst,* **134**(12),.

TABISH, S.A., 2007. Building a healthy world for tomorrow. *International journal of health sciences,* **1**(1), pp. IX-X.

TANEI, T., MORIMOTO, K., SHIMAZU, K., KIM, S.J., TANJI, Y., TAGUCHI, T., TAMAKI, Y. and NOGUCHI, S., 2009. Association of breast cancer stem cells identified by aldehyde dehydrogenase

1 expression with resistance to sequential Paclitaxel and epirubicin-based chemotherapy for breast cancers. *Clinical cancer research : an official journal of the American Association for Cancer Research,* **15**(12), pp. 4234-4241.

TODARO, M., IOVINO, F., ETERNO, V., CAMMARERI, P., GAMBARA, G., ESPINA, V., GULOTTA, G., DIELI, F., GIORDANO, S., DE MARIA, R. and STASSI, G., 2010. Tumorigenic and metastatic activity of human thyroid cancer stem cells. *Cancer research,* **70**(21), pp. 8874-8885.

TRAVO, A., DESPLAT, V., BARRON, E., POYCHICOT-COUSTAU, E., GUILLON, J., DÉLÉRIS, G. and FORFAR, I., 2012. Basis of a FTIR spectroscopy methodology for automated evaluation of Akt kinase inhibitor on leukemic cell lines used as model. *Analytical and bioanalytical chemistry,* **404**(6-7), pp. 1733-1743.

TURNER, C., ŠPANĚL, P. and SMITH, D., 2006. A longitudinal study of ammonia, acetone and propanol in the exhaled breath of 30 subjects using selected ion flow tube mass spectrometry, SIFT-MS. *Physiological Measurement,* **27**(4), pp. 321.

TURNER, C., WALTON, C., HOASHI, S. and EVANS, M., 2009. Breath acetone concentration decreases with blood glucose concentration in type I diabetes mellitus patients during hypoglycaemic clamps. *Journal of breath research,* **3**(4), pp. 046004.

UCAR, D., COGLE, C.R., ZUCALI, J.R., OSTMARK, B., SCOTT, E.W., ZORI, R., GRAY, B.A. and MOREB, J.S., 2009. Aldehyde dehydrogenase activity as a functional marker for lung cancer. *Chemico-biological interactions,* **178**(1), pp. 48-55.

VAN DEN HOOGEN, C., VAN DER HORST, G., CHEUNG, H., BUIJS, J.T., LIPPITT, J.M., GUZMAN-RAMIREZ, N., HAMDY, F.C., EATON, C.L., THALMANN, G.N., CECCHINI, M.G., PELGER, R.C. and VAN DER PLUIJM, G., 2010. High aldehyde dehydrogenase activity identifies tumor-initiating and metastasis-initiating cells in human prostate cancer. *Cancer research,* **70**(12), pp. 5163-5173.

VAN'T WESTEINDE, S.C. and VAN KLAVEREN, R.J., 2011. Screening and early detection of lung cancer. *Cancer journal (Sudbury, Mass.),* **17**(1), pp. 3-10.

VILENO, B., JENEY, S., SIENKIEWICZ, A., MARCOUX, P., MILLER, L. and FORRÓ, L., 2010. Evidence of lipid peroxidation and protein phosphorylation in cells upon oxidative stress photo-generated by fullerols. *Biophysical chemistry,* **152**(1), pp. 164-169.

WANG, L., PARK, P., ZHANG, H., LA MARCA, F. and LIN, C., 2011. Prospective identification of tumorigenic osteosarcoma cancer stem cells in OS99-1 cells based on high aldehyde dehydrogenase activity. *International Journal of Cancer,* **128**(2), pp. 294-303.

WANG, H.P., WANG, H.-. and HUANG, Y.-., 1997. Microscopic FTIR studies of lung cancer cells in pleural fluid. *Science of The Total Environment,* **204**(3), pp. 283-287.

WANG, M., HAN, C. and YIN, S., 2009. Substrate specificity of human and yeast aldehyde dehydrogenases. *Chemico-biological interactions,* **178**(1–3), pp. 36-39.

WARBURG, O., 1924. Über den stoffwechsel der carcinomzelle. *Naturwissenschaften,* **12**(50), pp. 1131-1137.

WARBURG, O., 1956. On the origin of cancer cells. *Science (New York, N.Y.),* **123**(3191), pp. 309-314.

WARDWELL JR, N.R. and MASSION, P.P., 2005. Novel Strategies for the Early Detection and Prevention of Lung Cancer. *Seminars in oncology,* **32**(3), pp. 259-268.

WEAVER, V.M., PETERSEN, O.W., WANG, F., LARABELL, C.A., BRIAND, P., DAMSKY, C. and BISSELL, M.J., 1997. Reversion of the malignant phenotype of human breast cells in three-dimensional culture and in vivo by integrin blocking antibodies. *The Journal of cell biology,* **137**(1), pp. 231-245.

WOLTHAUS, J.W.H., VAN.HERK, M., MULLER, S. H., BELDERBOS, J.S.A., LEBESQUE, J.V., DE.BOIS, J.A., ROSSI, M.M.G. and DAMEN, E.M.F., 2005. Fusion of respiration-correlated PET and CT scans: correlated lung tumour motion in anatomical and functional scan. *Physics in Medicine and Biology,* **50**(7), pp. 1569.

XU, F., BURG, K. and BURG, K.L.J., 2007. Three-dimensional polymeric systems for cancer cell studies. *Cytotechnology JID - 8807027 PMC - PMC2267509 OID - NLM: PMC2267509 EDAT- 2008/11/13 09:00 MHDA- 2008/11/13 09:01 CRDT- 2008/11/13 09:00 PHST- 2006/09/21 [received] PHST- 2007/02/27 [accepted] PHST- 2007/07/31 [aheadofprint] AID - 10.1007/s10616(TRUNCATED),* **54**(3), pp. 135-143.

YANG, Y., SULÉ-SUSO, J., SOCKALINGUM, G.D., KEGELAER, G., MANFAIT, M. and EL HAJ, A.J., 2005. Study of tumor cell invasion by Fourier transform infrared microspectroscopy. *Biopolymers,* **78**(6), pp. 311-317.

YANO, K., OHOSHIMA, S., GOTOU, Y., KUMAIDO, K., MORIGUCHI, T. and KATAYAMA, H., 2000. Direct Measurement of Human Lung Cancerous and Noncancerous Tissues by Fourier Transform Infrared Microscopy: Can an Infrared Microscope Be Used as a Clinical Tool? *Analytical Biochemistry,* **287**(2), pp. 218-225.

YAZDI, H.M., MACDONALD, L.L. and HICKEY, N.M., 1987. Thoracic fine needle aspiration biopsy versus fine needle cutting biopsy. A comparative study of 40 patients. *Acta cytologica JID - 0370307,* **32**(5), pp. 635-640.

ZARCONE, D., TILDEN, A.B., FRIEDMAN, H.M. and GROSSI, C.E., 1987. Human leukemia-derived cell lines and clones as models for mechanistic analysis of natural killer cell-mediated cytotoxicity. *Cancer research,* **47**(10), pp. 2674-2682.

ZELIG, U., KAPELUSHNIK, J., MOREH, R., MOREDECHAI, S. and NATHAN, I., 2009. Diagnosis of cell death by means of infrared spectroscopy. *Biophysical journal,* (97), pp. 2107-2114.

ZHOU, J., WANG, Z., SUN, S., LIU, M. and ZHANG, H., 2001. A rapid method for detecting conformational changes during differentiation and apoptosis of HL60 cells by Fourier-transform infrared spectroscopy. *Biotechnology and applied biochemistry,* **33**(2), pp. 127-132.